RECORD COPY
C.1

RETAIN HARDCOPY

MICROFICHE

SANDIA REPORT
SAND94–1117 • UC–1302, 1303
Unlimited Release
Printed November 1995

SANDIA NATIONAL
LABORATORIES
TECHNICAL LIBRARY

Test Results Industrial Solar Technology Parabolic Trough Solar Collector

Vernon E. Dudley
EG&G MSI
Albuquerque, NM 87119

Lindsey R. Evans, Chauncey W. Matthews
Solar Thermal Test Department
Sandia National Laboratories
Albuquerque, NM 87185

Prepared by
Sandia National Laboratories
Albuquerque, New Mexico 87185 and Livermore, California 94550
for the United States Department of Energy
under Contract DE-AC04-94AL85000

Approved for public release; distribution is unlimited.

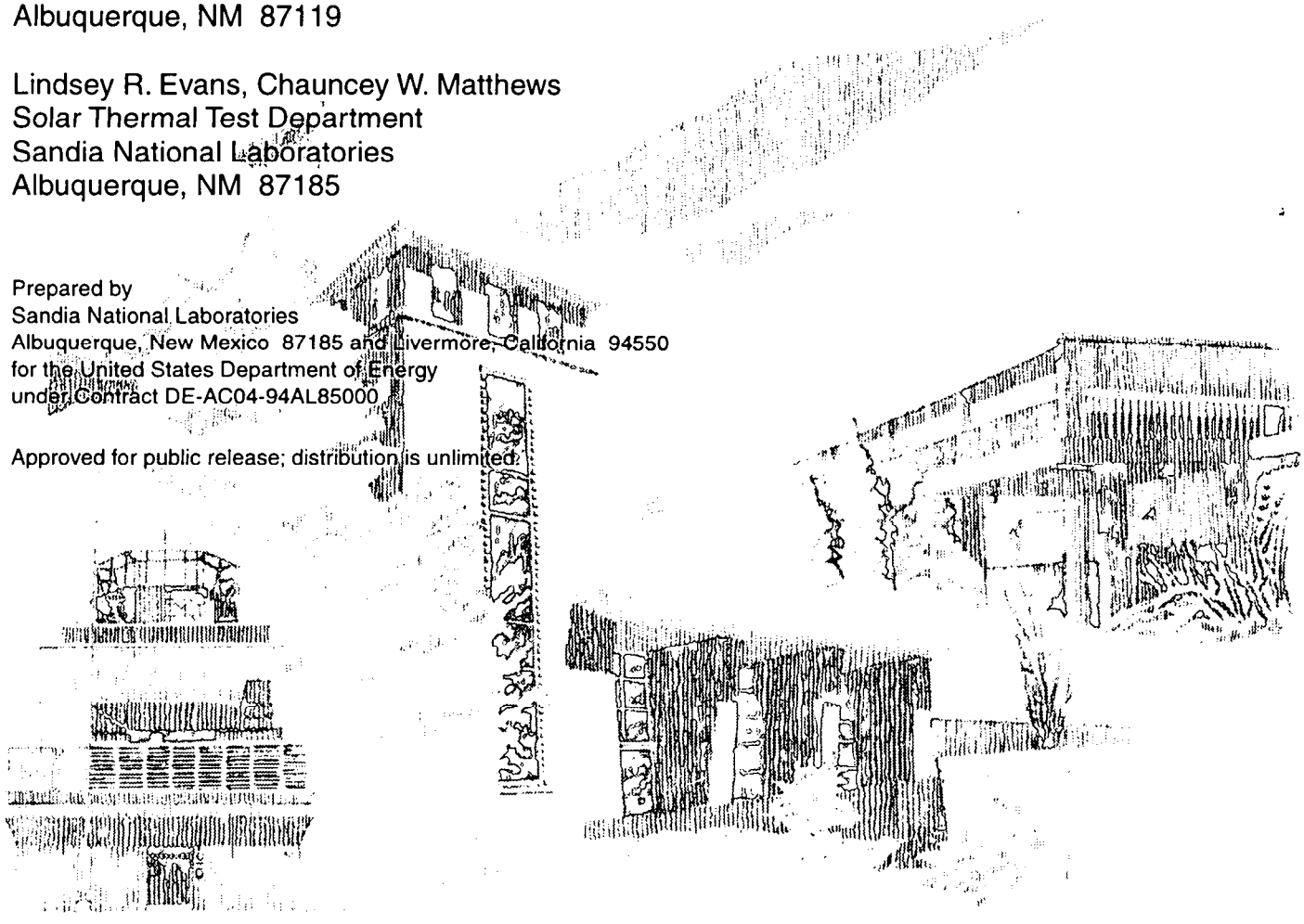

SF2900Q(8-81)

140 p. in Various Pagings

Issued by Sandia National Laboratories, operated for the United States Department of Energy by Sandia Corporation.
NOTICE: This report was prepared as an account of work sponsored by an agency of the United States Government. Neither the United States Government nor any agency thereof, nor any of their employees, nor any of their contractors, subcontractors, or their employees, makes any warranty, express or implied, or assumes any legal liability or responsibility for the accuracy, completeness, or usefulness of any information, apparatus, product, or process disclosed, or represents that its use would not infringe privately owned rights. Reference herein to any specific commercial product, process, or service by trade name, trademark, manufacturer, or otherwise, does not necessarily constitute or imply its endorsement, recommendation, or favoring by the United States Government, any agency thereof or any of their contractors or subcontractors. The views and opinions expressed herein do not necessarily state or reflect those of the United States Government, any agency thereof or any of their contractors.

Printed in the United States of America. This report has been reproduced directly from the best available copy.

Available to DOE and DOE contractors from
Office of Scientific and Technical Information
PO Box 62
Oak Ridge, TN 37831

Prices available from (615) 576-8401, FTS 626-8401

Available to the public from
National Technical Information Service
US Department of Commerce
5285 Port Royal Rd
Springfield, VA 22161

NTIS price codes
Printed copy: A04
Microfiche copy: A01

SAND94-1117
Unlimited Release
Printed November 1995

Distribution Category
UC 1302, 1303

Test Results
Industrial Solar Technology
Parabolic Trough Solar Collector

Vernon E. Dudley
E G & G MSI
Albuquerque, New Mexico 87119

Lindsey R. Evans
Chauncey W. Matthews
Solar Thermal Test Department
Sandia National Laboratories
Albuquerque, New Mexico 87185

Abstract

Sandia National Laboratories and Industrial Solar Technology are cost-sharing development of advanced parabolic trough technology. As part of this effort, several configurations of an IST solar collector were tested to determine the collector efficiency and thermal losses with black chrome and black nickel receiver selective coatings, combined with aluminized film and silver film reflectors, using standard Pyrex® and anti-reflective coated Pyrex® glass receiver envelopes.

The development effort has been successful, producing an advanced collector with 77% optical efficiency, using silver-film reflectors, a black nickel receiver coating, and a solgel anti-reflective glass receiver envelope.

For each receiver configuration, performance equations were empirically derived relating collector efficiency and thermal losses to the operating temperature. Finally, equations were derived showing collector performance as a function of input insolation value, incident angle, and operating temperature.

Contents

Tables

Summary of Test Results

Introduction

The Sandia National Laboratories and Industrial Solar Technology (IST) are cost-sharing a series of component developments, tests and analytical models to characterize the performance of the IST parabolic trough solar collector over the complete range of operating temperatures and incident angles. Fields of these collectors are currently installed at Aurora and Brighton, Co and at Tehachapi, Calif., supplying energy for domestic hot water. The Sandia tests were also designed to measure progress in the cost-shared development of an advanced design receiver assembly, using a black nickel selective coating and a solgel anti-reflective coated glass envelope. The test effort was part of the Department of Energy Industrial Heat Program and the Solar Thermal Electric Program.

The IST collector module tested at Sandia was the smallest portion of the complete collector that could be operated independently, consisting of a single mirror module, receiver, and the drive system. As tested, the mirror aperture width was 2.3 m and the length was 6.1 m. A complete IST collector would include several rows of collectors driven by a single drive system. Each row usually has two or three of the mirror modules on each side of the drive wheel, with four to six rows moved by cables from a single drive motor and tracking system. Figure 1 is a photograph of an IST collector; Figure 2 shows the IST collector field at Brighton, Co.

Two different reflector assemblies were delivered for testing: one using a 3M SA-85 aluminized film reflector, and another using 3M ECP-305 silver film reflector material. Shortly after testing began, the aluminized reflector was discovered to have been damaged. Since this reflector was unable to focus all the light on the receiver, and was not field repairable, it was removed. The silver film reflector was used for most of the tests covered by this report.

Two different receiver selective coatings -- black chrome and black nickel -- were tested. The black chrome receivers are currently used in the operational collector fields; the black nickel is a proposed receiver that may have a longer lifetime and better optical properties than the black chrome version. Black chrome selective coatings have been used for a number of years on both concentrating and non-concentrating solar collectors. The coating is applied by an electroplating process, which must be very carefully controlled for a reasonable coating lifetime at high operating temperatures.

Two different receiver glass envelopes were also tested: a conventional borosilicate Pyrex® glass, and a solgel anti-reflective coated Pyrex® glass.

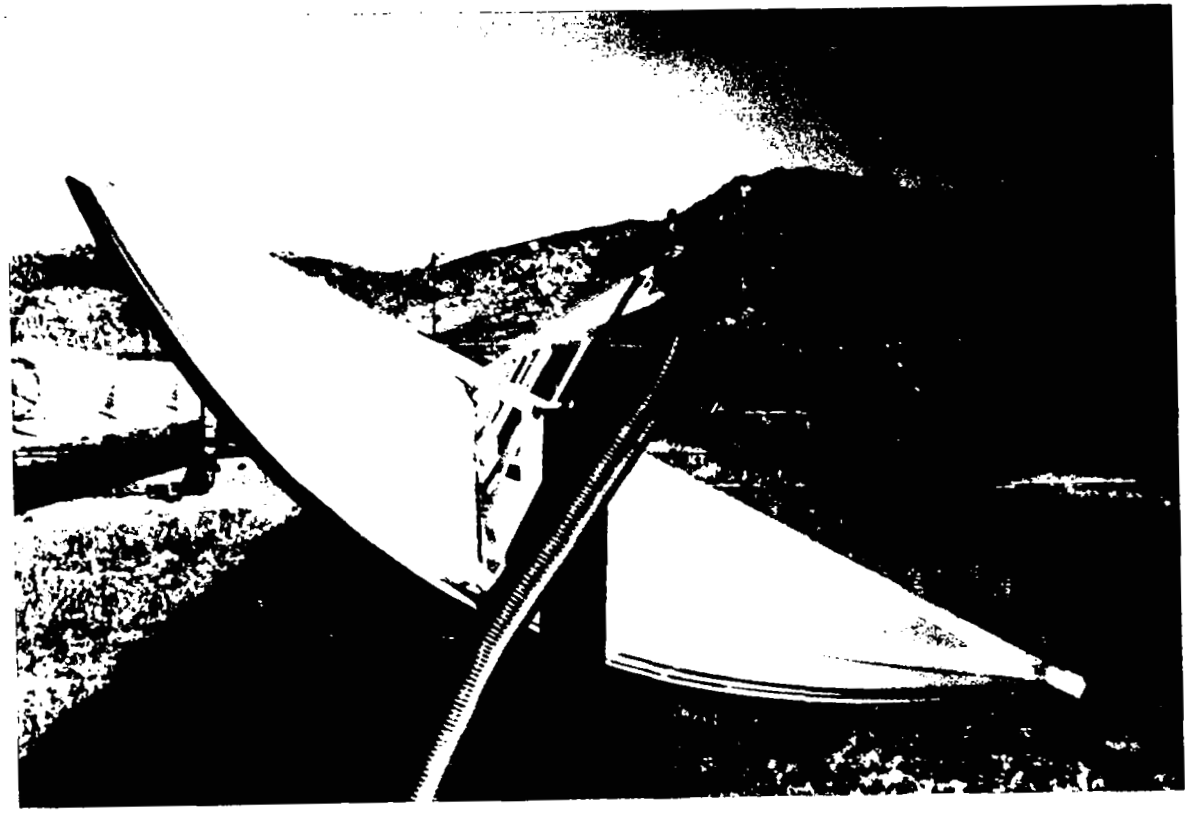

Figure 1. Row of IST Collector Modules

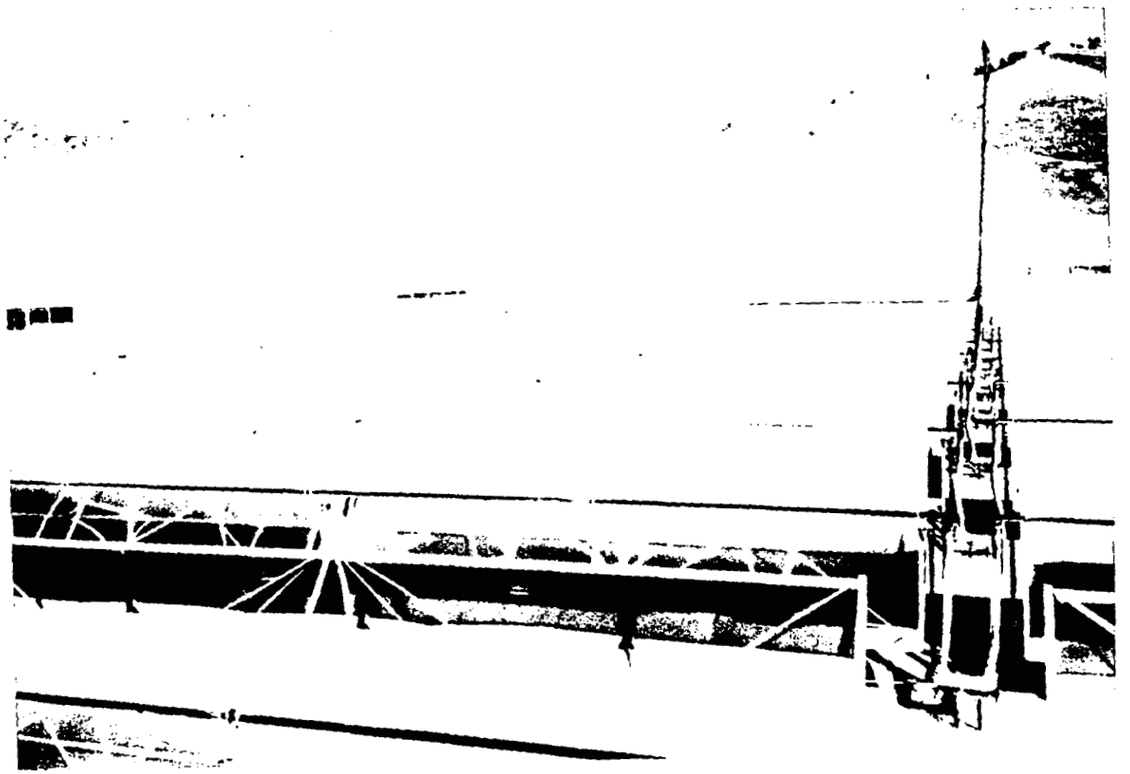

Figure 2. IST Collector Field at Tehachapi, CA.

Test Results

Figure 3 summarizes the efficiency test results for the black chrome and black nickel receivers, with both plain glass and anti-reflective glass envelopes. Optical property measurements of the receiver surfaces confirmed that the black nickel receiver had a higher absorptivity than the black chrome, which leads directly to the improved optical efficiency observed during the test series. Similarly, the solgel anti-reflective coated receiver glass transmitted more concentrated light to the receiver, again improving the optical efficiency for both receiver types. Optical efficiency points were obtained using cold water as the heat-transfer fluid, prior to connecting the receiver to the oil system. All elevated temperature testing was done with Dow Corning's Syltherm® 800 silicone oil as the heat-transfer fluid.

Figure 4 shows the measured thermal losses from the black chrome and black nickel receivers. The measured emissivity of the two receiver surfaces was similar, but the glass envelopes were different. The presence of the anti-reflective solgel coating on the black nickel glass envelope was not expected to change the glass properties for infra-red heat radiation, and nearly identical measured thermal losses were measured for the two receivers. All thermal loss testing was done with Syltherm® oil as the heat-transfer fluid.

Change in collector performance for a range of solar beam incident angles was measured with both glass types and both receiver coatings, at both positive and negative incident angles. The tests did not detect any change in incident angle modifier with the two different receivers, and essentially no difference between positive and negative incident angles. All the measured incident angle performance data is summarized in Figure 5. All incident angle testing was done with cold water at near ambient air temperatures to minimize any errors due to thermal losses from the receiver assembly. Incident angle test data were corrected for end loss to compensate for the short length of the test collector.

The equations shown in the Figures were obtained from a least-squares regression analysis of the measured data points. The complete sets of measured data are in Appendix D. The error bars on the data points are the expected worst-case uncertainty resulting from instrument bias, measurement errors, and thermal stability of the test system. A discussion of the test errors is in Appendix F.

A theoretical heat-transfer computer model of the IST collector was constructed (see Appendix E) using the measured physical parameters of the system. Calculated heat gain and heat loss using this theoretical model are in reasonable agreement with the actual test results. This indicates that the theoretical model might be useful for calculating the performance of other collectors that differ slightly from the tested equipment.

Performance Equations

The operating efficiency data and equations shown in the previous figures are valid only for a narrow range of insolation values near those existing during the tests.. The thermal losses shown are valid only for an essentially zero value of incident direct insolation on the receiver. These

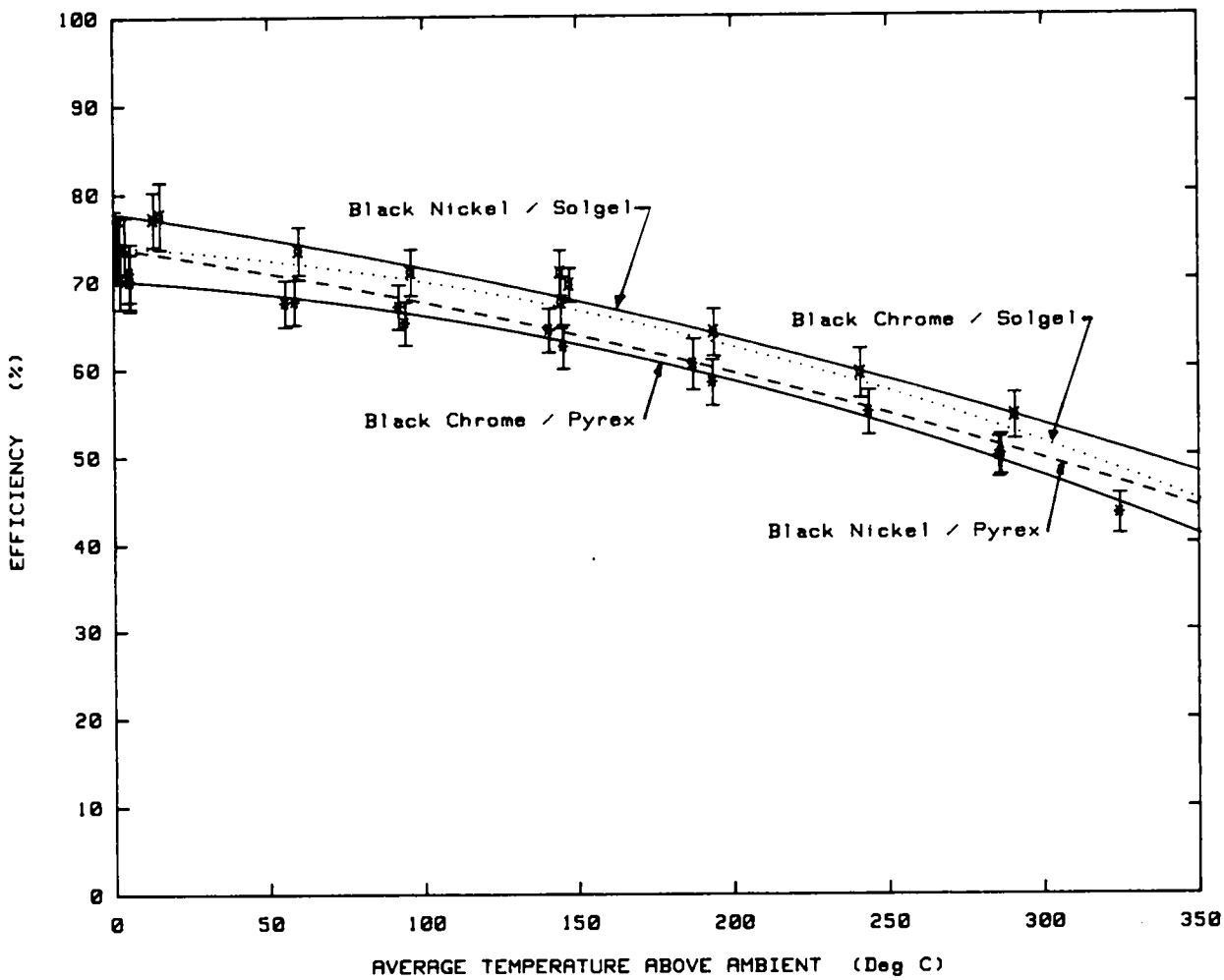

Figure 3. Efficiency Comparison - Black Nickel and Black Chrome Receivers

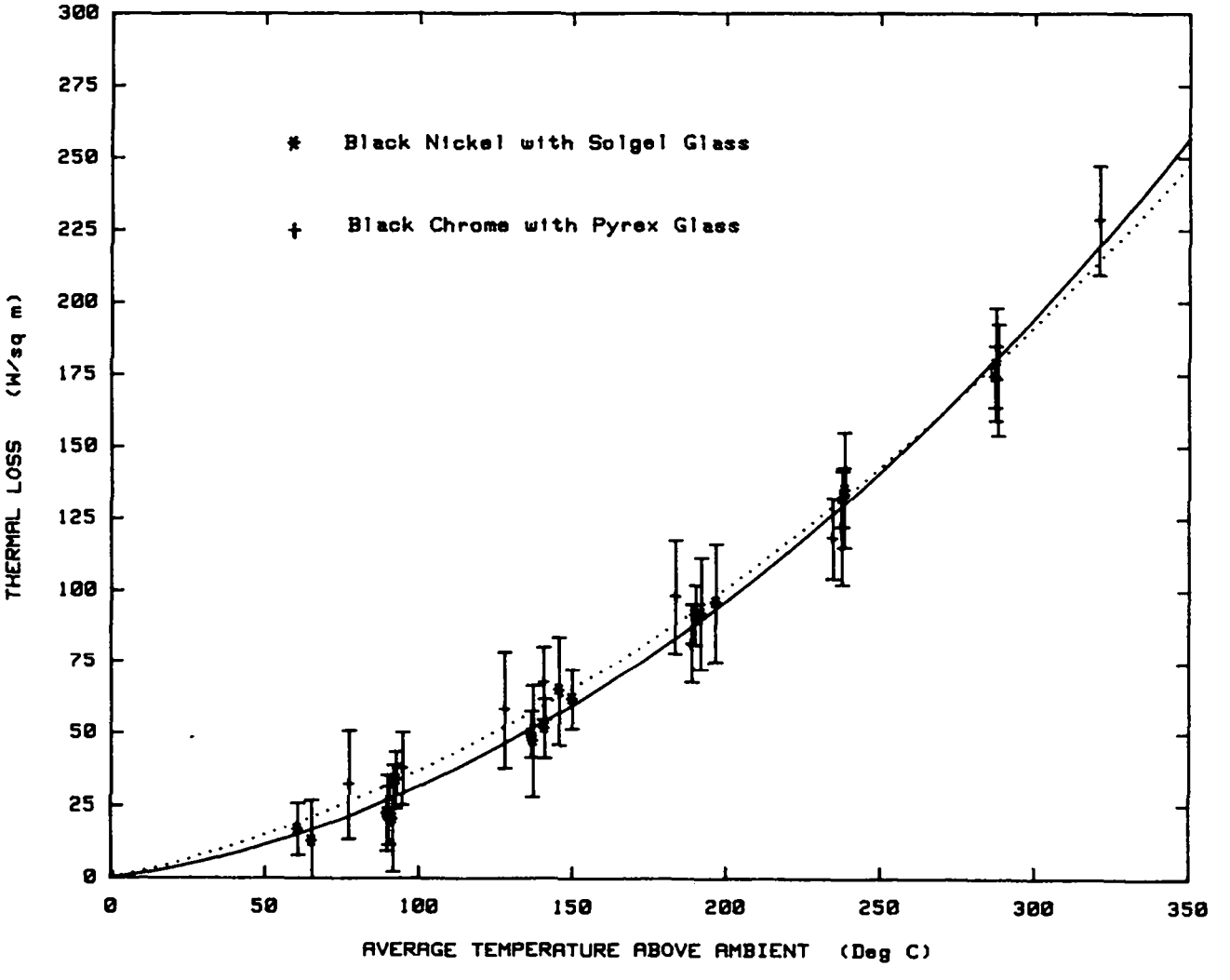

Figure 4. Thermal Loss Comparison of Black Chrome and Black Nickel Receivers

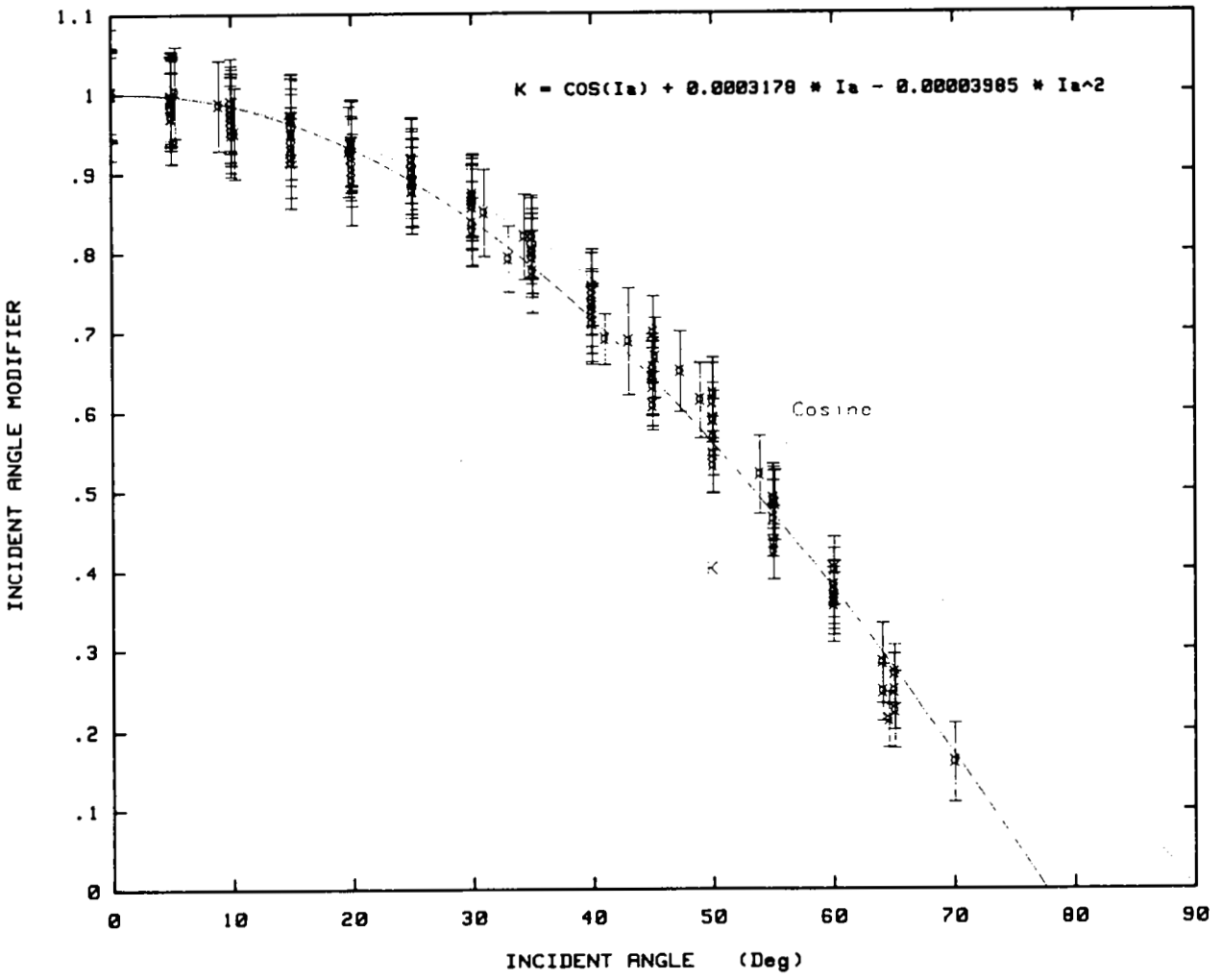

Figure 5. IST Incident Angle Modifier for All Receivers

equations will not correctly predict collector performance when insolation differs by hundreds of W/m^2 from the Sandia test conditions, as happens daily in an operational solar field. The efficiency equation can be extended as outlined in Appendix C to cover the complete range of expected solar irradiance. Figure 6 shows a plot of the final performance equation for several levels of insolation, using the black nickel receiver with a solgel anti-reflective glass envelope. Incident angle was zero for the curves in Figure 6.

Collector performance will decrease with increasing incident angle. Figure 7 shows the same collector as Figure 6, but now for an incident angle of 50 degrees, which would occur at noon in mid-December for a North-South field of these collectors. High incident angles combined with low insolation values also occur during early morning and late afternoon hours for a collector field that is oriented East-West.

Figure 8 illustrates the same performance equation as Figures 6 & 7, but shows the complete range of possible operating temperatures and insolation values for a zero incident angle. A performance equation in this form has been shown to correctly predict the all-day, steady-state output from a single collector module, and from a small collector field (Ref. 1 and 2). We believe the equation can also be successfully used with larger solar installations (See Ref. 3).

The general shape of Figure 8, and the equation used to draw the figure, shows that collector efficiency varies in a hyperbolic fashion with changing values of insolation; and as a quadratic polynomial with changes in operating temperature. The performance equations shown for efficiency and incident angle modifier are not exact physical models of the collector, but instead are empirical fits to the experimental test data. The first term in the performance equation represents the approximate optical efficiency of the collector. Some experience with the Acurex collector (Ref. 2) indicates that the optical efficiency term can be varied slightly to account for accumulated soiling of the collector mirrors and receiver glass.

It is possible to read an expected collector efficiency for a given insolation and operating temperature from a graph such as Figures 6, 7, and 8, but not very accurately, and a new graph would be needed for each different incident angle. A more practical way to use this data is to solve the equations (1) to (5) shown in below in Table 1 for each operating parameter set of interest. Note that the incident angle modifier K is the same for all the receiver variations. Also note that the equations are valid only for steady-state conditions, and include only the collector itself -- thermal losses from interconnecting piping must be considered separately. If the collector field is increasing or decreasing in temperature, a separate calculation is necessary to account for heat being stored in (or removed from) the mass of oil and pipe in the field.

The equations below summarize the test performance of the IST collector, and should apply to any temperature between ambient and 350°C, at any insolation level from 100 to 1100 W/m^2, and at any incident angle from 0 to 70 degrees.

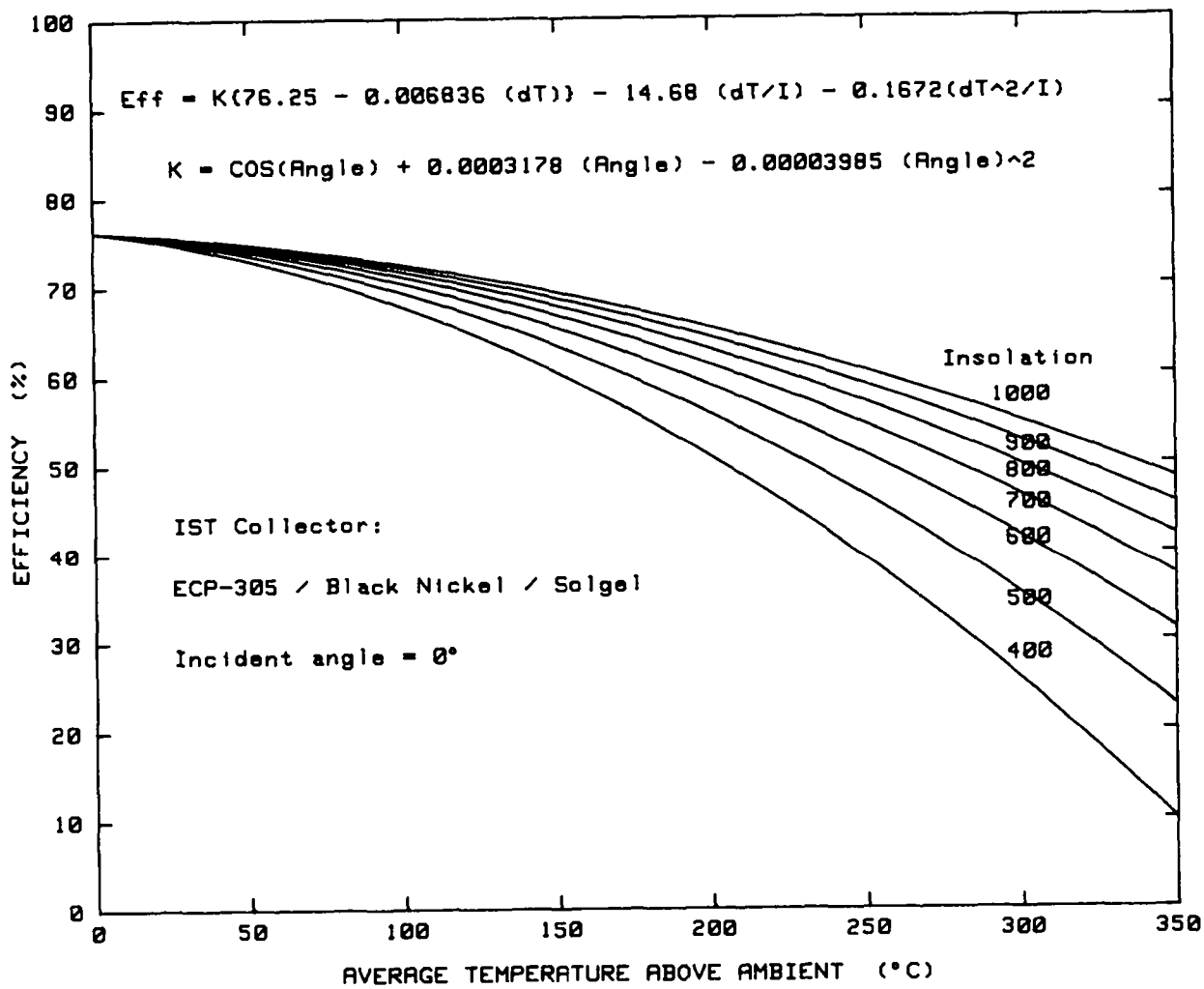

Figure 6. IST Collector vs Temp & Insolation at Zero Incident Angle

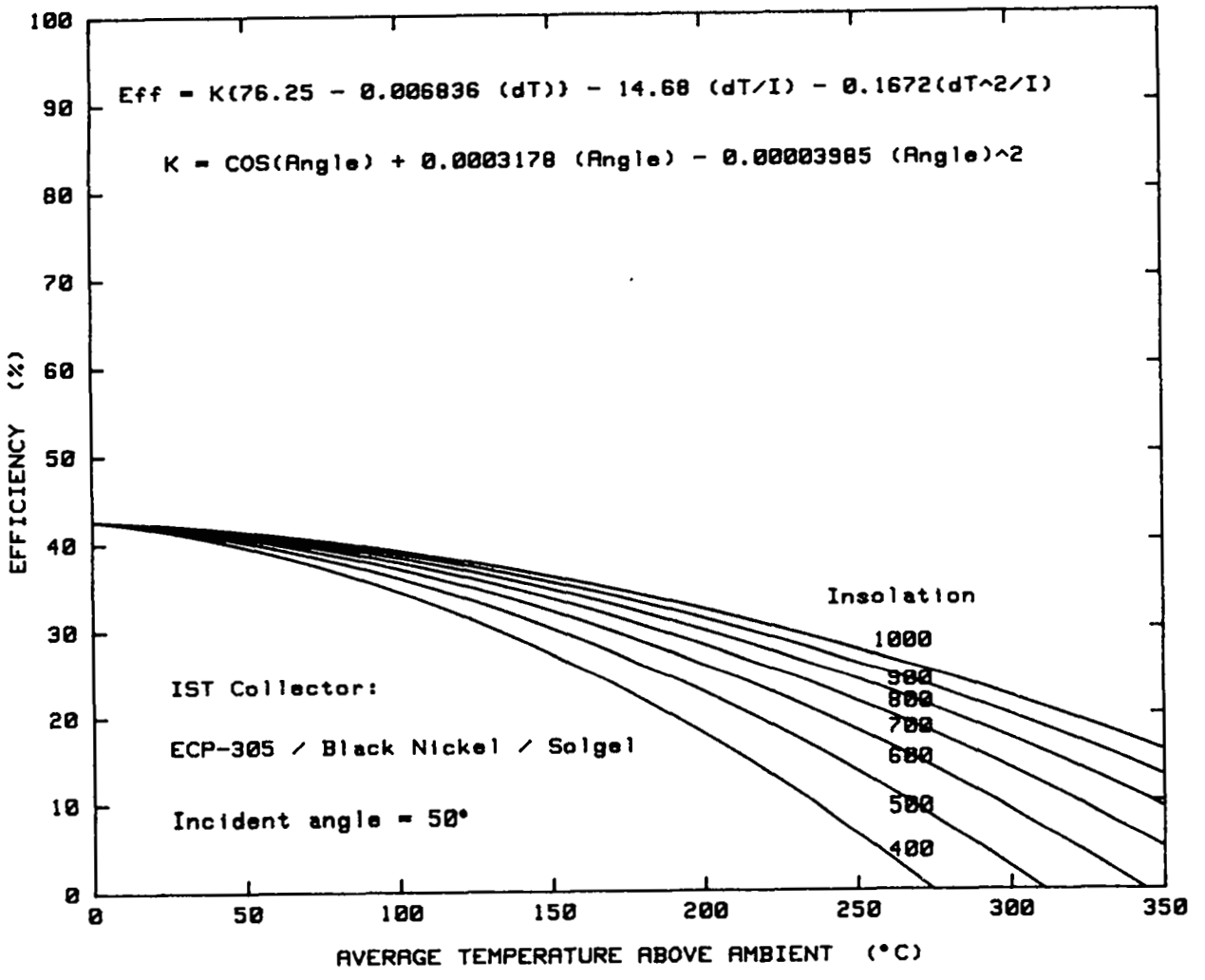

Figure 7. IST Collector vs Temp & Insolation at 50 Deg Incident Angle

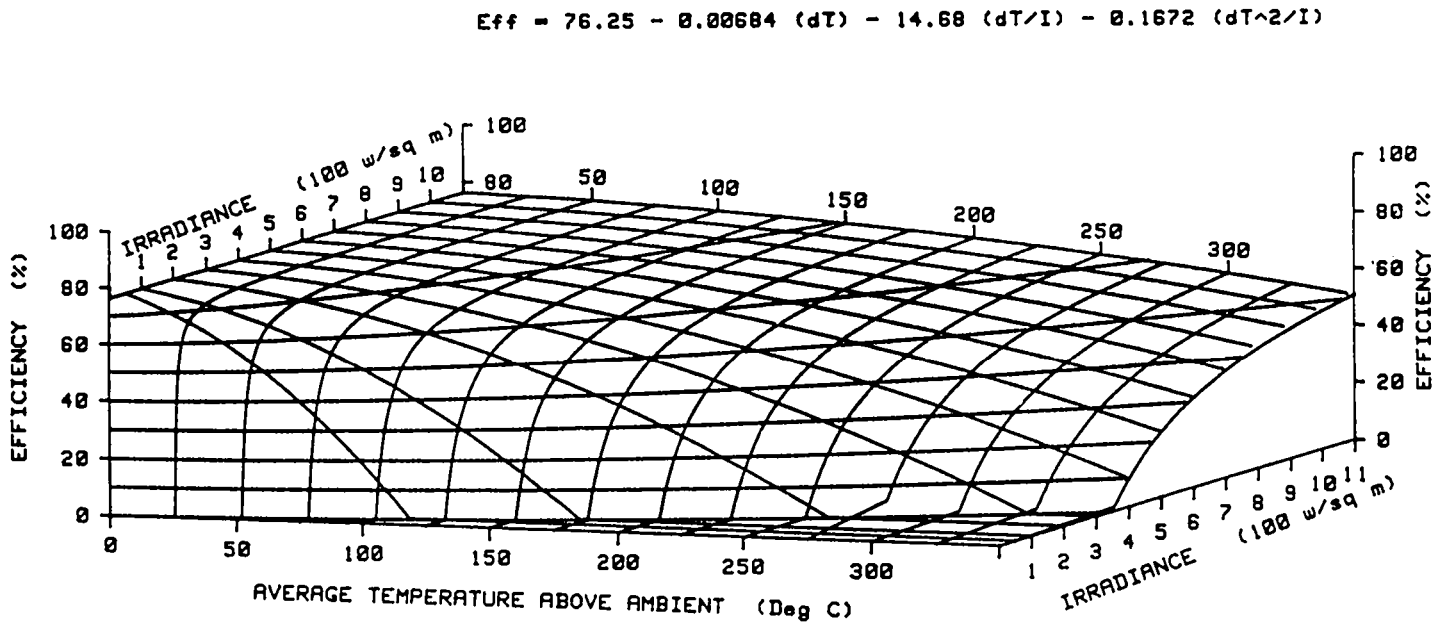

Figure 8. IST - ECP-305/Black Nickel/Solgel Receiver at Zero Incident Angle

Table 1

IST Collector Performance Equations For Silver Film Reflector

Black Nickel selective absorber, Solgel receiver glass

$$\eta = K\{76.25 - 0.006836(\Delta T)\} - 14.68(\Delta T/I) - 0.1672(\Delta T^2/I) \quad (1)$$

Black Nickel selective absorber, Pyrex receiver glass

$$\eta = K\{72.36 - 006836(\Delta T)\} - 14.68(\Delta T/I) - 0.1672(\Delta T^2/I) \quad (2)$$

Black chrome selective absorber, Solgel receiver glass

$$\eta = K\{74.52 - 0.009764(\Delta T)\} - 23.26(\Delta T/I) - 0.1355(\Delta T^2/I) \quad (3)$$

Black chrome selective absorber, Pyrex receiver glass

$$\eta = K\{70.75 - 0.01028(\Delta T)\} - 23.27(\Delta T/I) - 0.1355(\Delta T^2/I) \quad (4)$$

Incident Angle Modifier, K

$$K = \cos(Ia) + 0.0003178(Ia) - 0.00003985(Ia)^2 \quad (5)$$

In Table 1 performance equations (1) through (5):

η	=	Collector efficiency, in percent
K	=	Incident angle modifier
I	=	Incident direct normal solar irradiance, W/m^2
ΔT	=	Avg. receiver fluid temperature above ambient air temperature, °C
Ia	=	Solar beam incident angle, in degrees

References

Dudley, V. E., and Workhoven, R. M., 1982. SAND81-0984, Performance Testing of the Solar Kinetics T-700 Solar Collector. Albuquerque, N.M, Sandia National Laboratories.

Cameron, C. P., and Dudley, V. E., 1985. SAND85-2316, Acurex Solar Corporation Modular Industrial Solar Retrofit Qualification Test Results. Albuquerque, N. M, Sandia National Laboratories.

Lippke, F.,1995. SAND95-1293. Simulation of the Part-Load Behavior of a 30 Mwe SEGS Plant. Albuquerque, N. M, Sandia National Laboratories.

APPENDIX A

IST COLLECTOR TEST ARTICLE

Intentionally Left Blank

IST Parabolic Trough Solar Collector Test Article

In a field installation, an IST collector system may have 4 to 6 rows of mirror modules, all driven by cables from a single drive motor and tracking system. Each row would typically have 2 to 3 mirror modules on each side of the drive wheel. For testing at Sandia Laboratories, only a single mirror module was used, with a control/tracking system and drive motor. The mirror module was about 2.3 m wide by 6.1 m long, providing a net mirror aperture of 13.2 m^2. The mirror module was constructed with a welded aluminum angle framework supporting a 1 mm thick aluminum mirror sheet. The reflector surface was either 3M SA-85 aluminized acrylic film, or 3M ECP-305 silvered acrylic film bonded to the aluminum backing sheet.

Concentrated light from the mirror assembly is focused on the receiver, which is a steel tube surrounded by a glass envelope. Two different receiver glass envelopes were tested; one was conventional borosilicate Pyrex glass, the other had a solgel anti-reflective coating on both surfaces. The glass protects the selective surface coating on the steel receiver, and also serves to reduce convection and conduction thermal losses from the heated tube. The space between the receiver surface and the glass envelope was not sealed, and contained air at atmospheric pressure.

Two different receiver selective coatings were tested on the IST collector: black chrome and black nickel. Black chrome is an electroplated coating, which is not recommended for long term use much above about 300 °C, and depending on the process control used in the plating process, sometimes changes in color and selective properties in use. Black nickel is an electroplated chemical conversion coating, which is being evaluated as a possible alternative to black chrome.

The 6 m long receiver module was made up of two 3 m steel receiver tubes and glass envelopes. The receiver was modified from the normal configuration by inserting a 31.75 mm diameter closed-end plug tube inside the steel receiver in order to reduce the flow area and increase fluid velocities. This change was necessary because the heat transfer fluid flow rates available for testing were less than those normally used in a field installation.

The collector's sun-tracking system is manufactured by IST under a license from Honeywell. The tracker/controller is a microprocessor based optical system; sensing concentrated light at the receiver tube.

Table A-1

IST Parabolic Trough Solar Collector

Manufacturer:	Industrial Solar Technology Corporation 4420 McIntyre Street Golden, CO 80403
Operating Temperature:	100-300 °C
Module size:	2.3 m x 6.1 m (as tested at Sandia)
Rim Angle:	72 degrees
Reflectors:	Second-surface silvered acrylic film, 3M ECP-305 Solar reflectivity : 0.93 Second surface aluminized acrylic film, 3M SA-85. Solar reflectivity: 0.83
Aperture Area:	13.2 m^2 (as tested at Sandia)
Focal Length:	76.2 cm
Concentration Ratio:	45 (Reflector width/absorber diameter)
Receiver:	Absorber diameter: 51 mm length: 6.1 m Pyrex® glass envelope: 75 mm diameter Solgel anti-reflective coated: Transmittance: 0.96 Plain glass, no AR coating: Transmittance: 0.91 Black chrome selective surface Absorptance: 0.94 Emittance: 0.25 @ 300°C 0.10 @ 100°C Black nickel selective surface Absorptance: 0.97 Emittance: 0.30 @ 300°C 0.14 @ 100°C
Sun Tracking:	Optical, viewing reflected light at the receiver.
Tracking Drive System:	230 v, 3 ∅, 850 rpm drive motor Jack screw driving cables to move collectors.

APPENDIX B

TEST FACILITY DESCRIPTION

Intentionally Left Blank

Test Facility Description

AZTRAK Azimuth Tracking Platform

During testing of a linear-cylindrical parabolic trough solar collector, one of the performance parameters that must be measured is the peak efficiency of the collector at zero incident angle. When the collector is mounted with a fixed East-West orientation of the trough rotational axis, zero incident angle occurs only once each day, at solar noon. If the trough rotational axis has some other orientation, such as North-South, a zero incident angle may not occur at all on some days of the year.

Because of the limited times that zero incident angles are available, completing a test series with a fixed collector orientation can be a frustrating experience. Some past tests have dragged on for months while waiting for a few days when no clouds were present during the times zero incident angles were also available. Since each test must be repeated at several different temperatures (usually 4-6) to define the operating curve, considerable wasted time is inevitable.

Another important operating parameter is the collector's performance over a range of incident angles, usually 0-60 degrees. Sufficient data to define this parameter can be even more frustrating than peak performance, since clear skies and stable insolation must be available over at least an entire half-day in order to complete the test.

The remaining parameter that must be measured is thermal loss from the collector's receiver as a function of operating temperature. Thermal loss should be measured with zero insolation incident on the receiver. Even though the collector is defocused such that no concentrated light from the reflector assembly falls on the receiver, some heat gain will still result if the direct beam from the sun can reach the receiver surface. The heat gain from unconcentrated sunlight is small, but can significantly change measured heat loss. To obtain a true measure of receiver thermal loss, the receiver must be shaded from direct sunlight.

Because the receiver exchanges infra-red energy with any object in view, it is also not possible to aim the reflector assembly at the ground in order to shade the receiver from sunlight. The ground temperature is considerably higher than the sky temperature to which the receiver is normally exposed, which would again lead to an error in a thermal loss measurement. For the same reason, it is not possible to cover the receiver with some sort of shadow shield without changing the thermal loss properties of the receiver.

Zero incident insolation is easy if the test is done at night; otherwise it is usually difficult or impossible to accomplish during daylight hours when the test collector has a fixed orientation. The reflector structure never seems to be in the right place to shadow the receiver from incident sunlight.

All the test difficulties mentioned above can be avoided if the solar collector is on a two-axis sun-tracking mount. Since linear-cylindrical parabolic trough concentrating collectors already have a solar elevation tracking capability, only an azimuth-tracking platform is needed to complete a

two-axis system. The AZTRAK rotating platform, located at the Solar Thermal Test Facility, Sandia National Laboratories, is an azimuth-tracking platform with unique capabilities for testing solar collectors.

The AZTRAK platform is microcomputer controlled, and can position a collector at zero incident angle at any hour of any day of the year. In addition, the platform can track so that that any given incident angle from 0-90 degrees can be maintained for as long as necessary to obtain test data. During thermal loss testing, the collector can be aimed at the sky away from the sun, thus shading the receiver, while the platform tracks the sun to maintain the receiver shading.

The AZTRAK platform incorporates provisions for electrical power to an installed collector, heat-transfer fluid flow to and from the receiver, and a large variety of instrumentation lines for test instrumentation. The platform is hydraulically driven from local or remote manual control stations, or by the tracking microcomputer. Provisions are included for automatic defocusing of the test collector and rotation away from the sun upon an overtemperature condition or if heat-transfer fluid flow is lost.

The platform construction is large square steel beams, welded into a rectangular assembly. The platform's collector mounting surface is 4m (13.1 ft) wide and 13m (42.6 ft) long. It is designed to support a collector weighing up to 3600 kg (8000 lb.) with a mirror aperture up to 50 sq. m (538 sq ft), with a center of pressure 1.8m (6 ft) above the top surface of the platform. Sun tracking operation is possible in winds up to 13.4 m/sec (30 mph), and the platform is designed to support the collector in winds up to 40 m/sec (90 mph). Platform rotation is 115 degrees in either direction from true South.

Heat Transfer Fluid Supply System

Two heat-transfer fluid supply systems are available for solar collector testing on the AZTRAK platform. Domestic cold water is used for optical efficiency and incident angle testing; a specially designed hot-oil supply system is used for the elevated temperature tests.

Domestic cold water has often been used directly into the collector inlet, with only a flow-control valve needed. During the present test series, we found that the water supply pressure varied randomly due to unknown causes; producing variations in fluid flow rates, and subsequent unacceptable receiver temperature changes. The water supply also contained numerous air bubbles, which also contributed to unstable flow and erratic flowmeter operation. The automatic flow-control valve was unable to maintain a constant flow rate, so a portable pump cart was used to supply water to the collector.

Essential components of the water pump cart are a 1135 liter (300 gallon) water tank, a multi-stage centrifugal pump, and a pressure-control valve. Water was delivered from the pump at 1 mPa (150 psi), and was throttled by a pressure regulator to about 0.7 mPa (100 psi) at 23 L/min (6 gpm) into the collector. Water flow output from the collector was regulated by an automatic flow-control valve, then dumped to the surface. We found that both the inlet pressure regulator and the output flow regulator were required for the most stable flow rates. A garden hose served to keep the water tank filled. The large water tank allowed the air bubbles to separate from the

water before reaching the pump. This simple system delivered extremely stable water flow rates and temperatures and was largely responsible for the excellent optical efficiency and incident angle data obtained.

The hot-oil fluid system was specifically designed for solar collector testing after considerable experience with the shortcomings of other oil systems. Vital components are a 190 liter (50 gal) oil tank, centrifugal pump and drive motor, a 40 kW electric oil heater, a water-cooled heat exchanger, an oil filter, flow meters, and several control valves. Operation of the oil system is remotely controlled from the nearby data-acquisition trailer. At present, the system uses Dow Corning's Syltherm® 800 silicone-based heat-transfer fluid; other heat-transfer oils are compatible with the system and could be used if desired. Water cannot be used in this fluid-supply system.

In operation, the oil system pumps oil from the supply tank through the heater and heat-exchanger, out through the solar collector being tested, and return to the supply tank. Both automatic and manual temperature and flow control systems are provided; as well as local and remote temperature and pressure indicators. Oil is supplied to the collector inlet at temperatures from 50 to 400°C, as selected by the operator. Oil pressure at the pump outlet is about 1 mPa (150 psi), and is throttled to about 0.7 mPa (100 psi) at the system outlet. Fluid flow rates from 4 to 57 L/min (1-15 gpm) are available. Figure B-1 shows a flow diagram of the high-temperature fluid loop.

Several of the fluid system's operating characteristics may appear excessive to those not familiar with the difficulties of solar collector testing. For example, the 20 hp fluid pump is quite large, considering that only 40-50 L/min fluid flow is needed through the collector under test. The pump actually pumps about 230 L/min (60 gpm) at a pressure approaching 1 mPa. Most of the fluid flow does not go out to the test collector, but is returned to the supply tank after passing through the heating and cooling heat exchangers. One objective of the high flow-rate through the heater, cooling heat-exchanger, and supply tank is to keep the fluid supply extremely well stirred and uniform in bulk fluid temperature. Close temperature control is also facilitated; since the fluid temperature seen by the heater controller is always an accurate measure of bulk fluid temperature throughout the system. Collector input temperature regulation to 0.1°C is routinely achieved.

Another objective of the large fluid pump is obtaining a highly stable fluid flow-rate through the collector. The fluid flow-control valves throttle the 1 mPa pump pressure to about 140 kPa at the collector inlet. Fluid flow stability to less than 0.2 L/min is easily achieved. Constant fluid flow is ultimately a major factor in temperature stability of the test collector.

Fluid temperature control over a wide temperature range by using either a fluid heater or cooler alone is inherently more difficult than using both together. For example, at a low operating temperature, the temperature controller will have difficulty getting small amounts of heat from the large electric heater. Thermal losses will be low, resulting in very slow correction rates as the temperature setpoint is overshot by the controller. The problem is a very high rate of response to a temperature below the setpoint, and a very slow rate of response to a temperature above the setpoint.

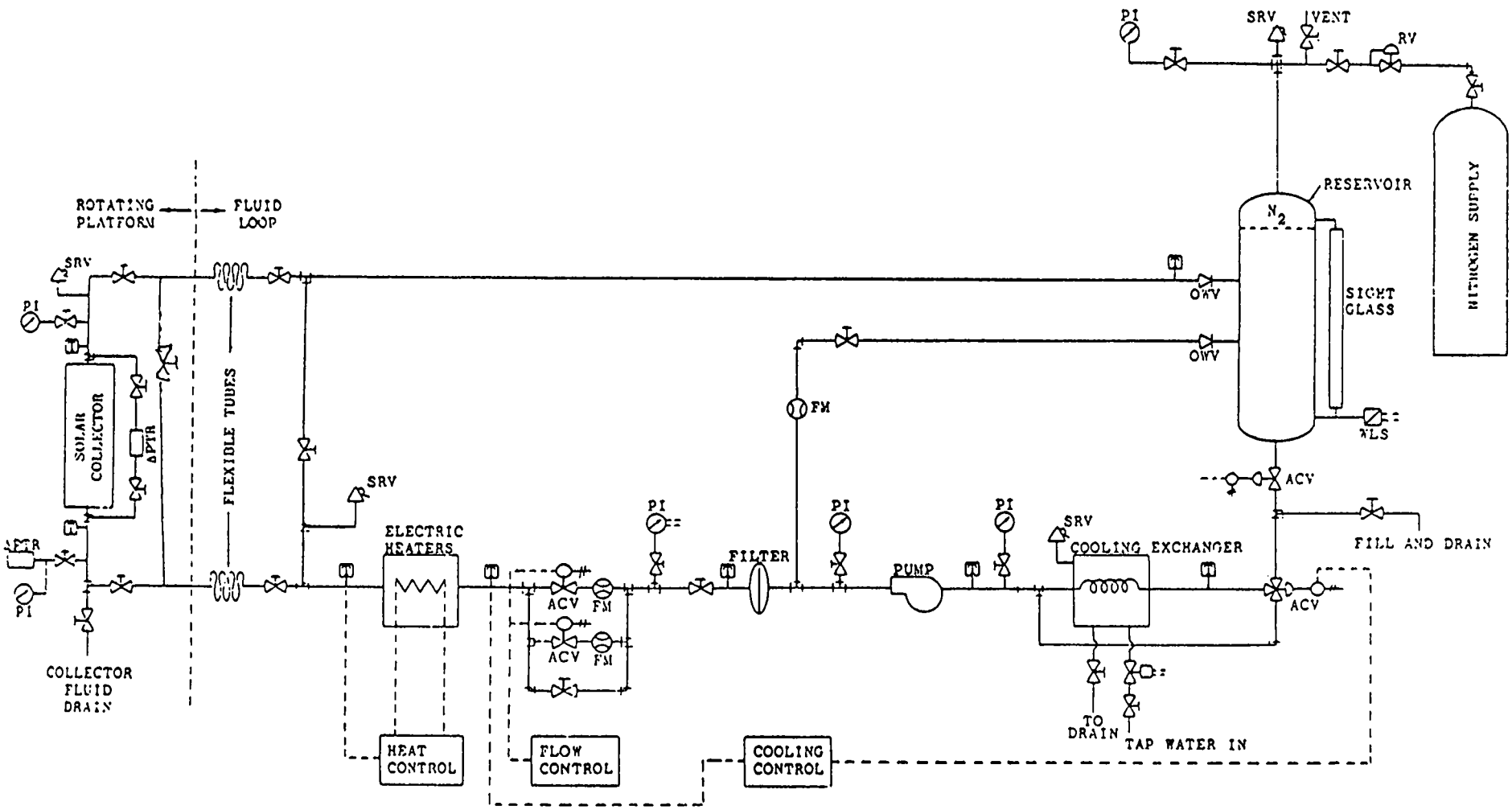

Figure B-1. Schematic of High Temperature Fluid Suppy Loop

At the highest operating temperatures, the control problem is reversed. Only a very small amount of cooling will be needed, as thermal losses from the entire heated system may dissipate most of the heat input. The cooling controller may find it impossible to open the cooling water valve by a small enough amount to achieve the required small amount of fluid cooling.

The temperature control scheme incorporated into this high temperature fluid loop is the nearly continuous use of simultaneous heating and cooling. For a given operating temperature, the fluid loop and the collector are first allowed to reach a rough state of temperature equilibrium under automatic control. The control system is set such that the cooling heat exchanger is always dissipating slightly more heat than is produced by the collector being tested. The cooling control is then placed under manual control so that the amount of cooling cannot change. The fluid flow-rate controller is also switched to manual control to improve flow stability. This procedure leaves the heater temperature as the only variable in the system. The heater is thus forced to always operate near the middle of its control range, with a continuous requirement for added heat. Some experience with the fluid loop is needed by the test operator, in order to judge the amount of cooling to use at various operating temperatures.

Examples of the fluid flow and temperature stability achieved can be seen in the test results section of this report.

References

Solar Thermal Test Facility, 1992. NSSTF OP #038, *Operating Procedure for AZTRAK Rotating Platform.* Albuquerque, NM: Sandia National Laboratories, Div. 6215.

Solar Thermal Test Facility, 1992. NSSTF OP #039 *Operating Procedure for High Temperature Fluid Loop.* Albuquerque, NM: Sandia National Laboratories, Div. 6215.

APPENDIX B

Test Instrumentation

Data Acquisition System

The data acquisition system used was based upon a Hewlett Packard 9845B desktop computer. Instrumentation channels were scanned with an HP3497A data acquisition unit, and the analog signals were then measured with an HP3456A digital voltmeter. The accuracy of the voltmeter is better than 0.01%. Voltage measurements were converted to engineering units, recorded on a hard disk, and selected data items were printed and displayed for the test operator. Each day's data file was later transferred to floppy disk for permanent archive. Data was normally measured and recorded at 15 - 20 second intervals during a test.

Table B-1 lists the test data items included in the data files, the transducer used to measure the item, and the data acquisition system channel numbers used for the measurements.

Heat Transfer Fluid Flow

Both domestic water and Dow Corning's Syltherm®-800 were used as heat transfer fluids. Fluid flow was measured by two Flow Technology turbine flow meters installed near the collector fluid inlet. Flow Technology Pulse Rate Converters were used to convert the voltage pulses from the flow meters to a 0-5 volt signal , which was then read by the data acquisition system. When high temperature Syltherm®-800 oil was being used, an additional two flow meters measured the oil flow leaving the fluid loop skid. Calibration of these flow meters was performed by Flow Technology immediately before beginning the test series, and their calibration was confirmed to be within 1% by timing and weighing the flow into a 30 gal bucket during the water tests.

Fluid Property Calculations

Equations for the properties of water were obtained by polynomial fits to data from Keenan & Keyes (Ref. 1). Sufficient terms were included to provide agreement within 0.2% over the range of temperatures used.

Equations for the properties of Syltherm®-800 heat transfer fluid were supplied by Dow Corning (Ref. 2). Accuracy of these equations is not specified. Density, specific heat, viscosity, and Reynolds number were calculated for each flow measurement data point. All the calculated data was recorded as part of the collected test data.

Temperature

Performance data was measured using type T thermocouples. To obtain the best accuracy possible, a number of type T thermocouples were compared by Sandia's Standards Lab; two pairs were selected from the lot which were within 0.1°C over the temperature range 0 to 400 °C. These two pairs were used to determine the input and output temperatures of the heat transfer fluid. An additional thermocouple was installed at the flow meters for temperature input to fluid property calculations.

Tracking Angle

Tracking angle is the rotation angle of the collector's aim point above the local horizon that is necessary to focus on the sun. Collector elevation tracking angle was measured with a Lucas Shaevitz mass-balance inclinometer mounted on the collector. The resolution of the inclinometer is 0.1 arc second. Linearity of the instrument is 0.05%.

The azimuth tracking angle of the AZTRAK platform (which determines the azimuth angle of the collector rotational axis) is controlled by a microcomputer as required by an individual test objective. The angle was measured by a 10-bit BEI optical shaft encoder, which has a resolution of 0.35 degrees. Calculated azimuth and elevation of the sun, calculated tracking and incident angles, and measured collector positions were included in the data files.

Weather data

Solar energy input to the collector was measured with an Eppley Normal Incidence Pyrheliometer calibrated against a Kendall secondary standard, active cavity radiometer. Accuracy of the pyrheliometer is 1 - 2%, including uncorrected temperature effects. Wind speed and direction at the test site was measured by a Weathertronics instrument, located at 10 m elevation about 30 m west of the installed collector. Ambient air temperature was measured with a type T thermocouple in a shaded enclosure.

References

Keenan, J H., Keys, F. G., Hill, J. G., Moore, J. G. 1978. *Steam Tables*. New York: Wiley-Interscience.

Properties of Syltherm 800 Heat Transfer Liquid. Midland, Michigan: Dow Corning Corporation, 1985.

APPENDIX B

Table B-1

DATA MENU FOR IST ON AZTRAK PLATFORM

Menu #	Chan #	S/C #	Transdu	Description		(Units)
401				Test system number		(#5, IST trough on Aztrak)
402			Clock	Date of test		(Menu revised 29 Nov 93)
403			Clock	Mountain Standard Time		(HH:MM:SS)
404			Calc	Site Solar time		(HH:MM:SS)
405			Calc	Collector solar time		(HH:MM:SS)
406	021	S01C01	NIP	Direct normal insolation		(W/m^2)
407	372	S23C12	TCamb	Ambient air temperature		(Deg C)
408	023	S01C03	WS100	Wind speed		(m/s)
409	024	S01C04	WD100	Wind direction		(degrees CW from North)
410	305	S20C05	AZ100	Platform Azimuth		(Degrees from South, +East, -West)
411	306	S20C06	FT100	Collector flow #1		(L/min)
412	307	S20C07	FT101	Collector flow #2		(L/min)
413	308	S20C08	FIC 1A	Fluid loop high flow		(L/min)
414	309	S20C09	FIC 1B	Fluid loop Low flow		(L/min)
415	310	S20C10	IN100	Inclinometer Voltage		(Volts)
416	311	S20C11	IN100	Collector elevation Inclinometer		(Deg above horizon)
417	312	S20C12	PDI 6	Collector delta pressure		(kPa)
418	313	S20C13	PI3	Collector Inlet pressure		(kPa)
419	314	S20C14	Manual	Water / Oil Test?		1 = Water, 0 = Oil
420	315	S20C15	Spare			
421	316		Calc.	Mass Flow #2		(kg/hr)
422	317		Calc.	Efficiency (#470) corrected for end loss		(%)
423	318	S20C18	TC1/10	Collector Diff. Delta-T Volts #1	(TC 01/TC 10)	(mv)
424	319	S20C19	TC2/09	Collector Diff. Delta-T Volts #2	(TC 02/TC 09)	(mv)
425	360	S23C00	TC001	Collector inlet temperature #1		(Deg C)
426	361	S23C01	TC002	Collector inlet temperature #2		(Deg C)
427	362	S23C02	TC003	Spare T-Type Thermocouple #3		(Deg C)
428	363	S23C03	TC004	Spare T-Type Thermocouple #4		(Deg C)
429	364	S23C04	TC005	Spare T-Type Thermocouple #5		(Deg C)
430	365	S23C05	TC006	Spare T-Type Thermocouple #6		(Deg C)
431	366	S23C06	TC007	Spare T-Type Thermocouple #7		(Deg C)
432	367	S23C07	TC008	Flowmeter temperature		(Deg C)
433	368	S23C08	TC009	Collector Outlet temperature #2		(Deg C)
434	369	S23C09	TC010	Collector Outlet temperature #1		(Deg C)
435			Calc.	Average Receiver Temperature	(TC #1)	(Deg C)
436			Calc.	Average Receiver Temp above ambient	(TC #1)	(Deg C)
437			Calc.	Solar azimuth		(Degrees from South, +East, -West)
438			Calc.	Solar elevation		(degrees above horizon)
439			Calc.	Solar Incident angle		(degrees from normal)
440			Calc.	Solar tracking angle		(degrees above horizon)
441			Calc.	Collector delta-T	(Diff. dT #1)	(TC 01/10)(Deg C)
442			Calc.	Collector delta-T	(Sub. dT #1)	(TC 01/10)(Deg C)
443			Calc.	Mass flow #1	(@ Flowmeter temp)	(kg/hr)
444			Calc.	Heat gain (Flow #1)	(Diff. dT #1)	(TC 01/10)(W/m^2)

Table B-1 (Continued)

DATA MENU FOR IST ON AZTRAK PLATFORM

Menu #	Chan #	Slot #	Transdu	Description			(Units)
445			Calc.	Heat gain (Flow #1)	(Sub. dT #1)	(TC 01/10	(W/m^2)
446			Calc.	Efficiency (Flow #1)	(Diff. dT #1)	(TC 01/10)	(%)
447			Calc.	Efficiency (Flow #1)	(Sub. dT #1)	(TC 01/10)	(%)
448			Calc	Density of Heat Transfer Fluid			kg/m^3)
449			Calc.	Specific Heat of Heat Transfer Fluid			(J/kg °C)
450			Calc.	Viscosity of Heat Transfer Fluid			(N sec/m^2)
451			Calc.	Reynolds Number, Collector HTF flow			(Thousands)
452			Calc.	Mirror Aperture of Collector under test			(m^2)
453	380	S24	Calc.	Cosine of Incident Angle			
454	381	S24	Calc.	Absolute value of Incident Angle			(Deg)
455	382	S24	Calc.	Efficiency (Flow #1)	(Sub. dT #2)	(TC 02/09)	(%)
456	383	S24	Calc.	Efficiency (Flow #2)	(Sub. dT #1)	(TC 01/10)	(%)
457	384	S24		Spare			
458	385	S24	Calc.	Heat Gain (Flow #2)	(Sub. dT #1)	(TC 01/10)	(W/m^2)
459	386	S24	Calc.	Heat Gain (Flow #1)	(Sub. dT #2)	(TC 02/09)	(W/m^2)
460	387	S24		Spare			
461	388	S24	TC019	Collector Outlet Temp - K TC # 9			(Deg C)
462	389	S24	TC020	Syltherm tank Sight Gage TC - Bottom			(Deg C)
463	390	S24	TC021	Syltherm tank Sight Gage TC - Mid			(Deg C)
464	391	S24	TC022	Loop Cooling Water - Output temp			(Deg C)
465			Calc.	Collector delta-T	(Diff. dT #2)	(TC 02/09)	(Deg C)
466			Calc.	Collector delta-T	(Sub. dT #2)	(TC 02/09)	(Deg C)
467			Calc.	Heat gain (Flow #2)	(Diff. dT #2)	(TC 02/09)	(W/m^2)
468			Calc.	Heat gain (Flow #2)	(Sub. dT #2)	(TC 02/09)	(W/m^2)
469			Calc.	Efficiency (Flow #2)	(Diff. dT #2)	(TC 02/09)	(%)
470			Calc.	Efficiency (Flow #2)	(Sub. dT #2)	(TC 02/09)	(%)
471			Calc.	Tracking Error - (#440 - # 416)			(Deg)
472			Calc.	Efficiency (#447, corrected for end loss)			(%)

Intentionally Left Blank

APPENDIX C

TEST PLAN

Intentionally Left Blank

TEST PROCEDURES

The operating characteristics of a concentrating parabolic trough solar collector can be determined with only a few selected tests. These are:

- Measure peak efficiency at near-ambient-air temperature.
- Measure peak efficiency at several elevated temperatures.
- Measure receiver thermal loss as a function of temperature.
- Measure collector performance as a function of incident angle.

Peak efficiency of a concentrating solar collector can be determined only when the solar beam incident angle is zero. For single-axis tracking devices such as the IST parabolic trough collector, zero incident angles usually occur only once per day if the rotational axis is oriented East-West; or twice per day if the axis is oriented North-South. To allow continuous testing at any desired incident angle, the test collector was mounted on the AZTRAK rotating platform. For details on this device, see Appendix B.

All the calculations for heat gain or loss from an operating hot fluid system assume that the system in thermal equilibrium -- constant fluid flow-rate, and constant input and output temperatures. If equilibrium has not been established, then heat is either being stored in the mass of the system, or heat is being extracted from the system. In either case, calculations of heat gain or loss will be inaccurate. Because of the absolute necessity for highly stable flow and temperatures, a special hot-fluid supply source was used for the IST collector tests. For details on the Sandia high-temperature fluid loop, see Appendix B.

Even with a stable temperature source, long operating times are still necessary before all parts of the heated system are at their equilibrium temperatures. Time to reach temperature stability was longer than normal for the IST collector as installed for testing because an inner plug tube had to be inserted inside the receiver tube. The internal plug was necessary to restrict flow to a small annulus in order to achieve acceptable Reynolds numbers with the fluid flow-rates that are available from the test fluid loop. The internal plug was filled with the heat transfer fluid, but was closed at one end; so the internal fluid mass was heated only by conduction from the outer annulus. After about an hour at a given temperature setpoint, the system would stabilize to variations on the order of 0.1 °C. Heat gain/loss measurements were then deemed stable enough to be believed, and a data set was recorded for a time equal to about three collector time-constants.

Peak Efficiency Measurements

Measurements of zero-incident-angle efficiency were made with the heat-transfer fluid at approximately ambient-air temperature, and at approximately 50 °C intervals up to 300 °C. Data was continuously recorded at 15-20 sec intervals while the system was in operation. In order to establish temperature stability, the system was operated at each fixed temperature until the stability objectives below were attained. Achieving this level of temperature stability usually required an hour or more. Operation was then continued at stable temperatures and flow rates to

obtain a reportable data point. Each data point listed in the data tables in Appendix D and shown in the performance figures is the mean of all data measured over a time span of about three collector time-constants. For examples of collected data sets, see Figures 1-3 in Appendix F. The objective of each data set was to obtain stability of all variables that could cause significant changes in the desired measurements. The stability objectives were:

- Fluid temperatures constant to about 0.1 °C.
- Fluid flow-rate constant to about 0.2 L/min.
- Insolation constant to about 1%.

Performance measurements made within the system stability limits listed above produce data that is repeatable from day to day, with the magnitude of instability induced errors that are less than those produced by the instruments in the data acquisition system. The same stability criterion was applied to all data measurements made on the collector under test.

The near-ambient-air temperature measurement using cold water was used to define the approximate optical efficiency of the collector. The higher-temperature efficiency measurements document the decrease in efficiency caused by increasing thermal losses as the operating temperature is increased. Data from all of the efficiency measurements were used in a least-squares curve fit to obtain a performance equation of efficiency vs. temperature under bright sunshine, zero incident angle, stable temperature and flow conditions. The equation fitted to the data is normally a second order polynomial, which is not an exact physical model of the collector, but will correctly represent the measured performance data.

$$\eta = A + B\,(dT) + C\,(dT)^2 \qquad (1)$$

Where:

η = Efficiency of collector
A = Optical efficiency of collector
B = Coefficient for linear term
C = Coefficient for non-linear term
dT = Average receiver fluid temperature above ambient air temperature

Procedure for Efficiency Measurement (Elevated Temperature)

The objective of these tests was documenting changes in efficiency as operating temperature increases. Inlet temperature to the collector was set to a constant value, such that the output temperature would approximate the desired test temperature. The exact temperature achieved was not important; but temperature stability was extremely important during these tests.

Heat-transfer fluid flow was set to a constant value (usually the maximum obtainable for these tests). As for temperature, the exact flow-rate value was not very important; but flow stability was extremely important, because any change in fluid flow-rate would also cause changes in collector temperatures.

For the series of peak efficiency measurements, it is highly desirable for all the measurements to be made at the same level of solar irradiance. If the individual efficiency test points are obtained with a solar irradiance that differs more than about 100 W/m^2 between points, data extrapolation to other operational conditions will be less accurate. The solar irradiance levels during the efficiency tests should also be as high as are available at the test site, and constant in level to about 1% during an individual test point. This last requirement essentially eliminates very-early-morning and late-afternoon efficiency tests. These hours are more profitably used for thermal loss testing.

Procedure for Efficiency Measurement (Near-Ambient-Air Temperature)

The objective of this test was determination of approximate optical efficiency for the IST collector. True optical efficiency could be measured only if thermal losses from the collector system could be reduced to zero. Zero thermal loss probably cannot be achieved during an in-focus test of a real solar collector. However, a reasonable attempt can be made by operating the system at a low temperature as close as possible to the ambient air temperature.

Since the oil-supply fluid loop could not be operated at temperatures much below 60 °C, another source of heat-transfer fluid was needed. City water from local supply mains was used; see Appendix B for a description of the water supply system. Note that water flow was restricted to the collector only; no water was introduced into the oil supply system.

Ideally, water flow through the system would be adjusted such that the average temperature of the collector's receiver was approximately equal to local ambient air temperature. Because of the limited flow-rates and temperatures of the available water, this was not always possible. We used the closest approximation obtainable.

Two test results were needed from the tests performed with cool water:

1. Peak efficiency at zero incident angle.
2. Efficiency variation with incident angles up to about 60 degrees.

Given a cloud-free sky; data satisfying both test criteria can be obtained during a single test day.

Incident Angle Modifier Tests

The object of the incident angle modifier test was to document changes in operating efficiency as a function of incident angle. Measured efficiency of a parabolic trough collector decreases as the solar beam incident angle increases; with collector efficiency at a maximum only when the incident angle is zero. The decrease in collector efficiency with increasing incident angle is nearly proportional to the cosine of the incident angle. Efficiency data was usually measured at five degree intervals from zero to 60 degrees incident angle. The AZTRAK rotating platform was used to maintain each selected constant incident angle for as long as necessary to obtain stable data. The incident angle modifier K was defined as the ratio of the measured efficiency at a given

incident angle to the measured efficiency at a zero incident angle. A regression analysis of the data was then used to obtain an equation of the form:

$$K = \cos(A) - B(A) - C(A)^2 \quad (2)$$

Where:

K = Incident angle modifier, value ranges from 0 to 1
A = Solar beam incident angle (0 to 60 degrees)
B = Coefficient for linear term
C = Coefficient for non-linear term

As noted in the previous section, incident angle data was measured with cold water as the heat-transfer fluid, in conjunction with testing for optical efficiency.

If the collector and the sun-tracking system were perfectly symmetrical, the incident angle modifier would be the same for both positive and negative incident angles. As installed at Sandia for testing, the IST collector module was not exactly symmetrical because of a small shadowed area at one end of the receiver caused by the cable drive wheel. With zero or positive incident angles, the drive wheel shadow was not on the reflector. At negative incident angles, the shadow became a larger and larger fraction of the illuminated receiver length as the angle increased. This non-symmetrical behavior was peculiar to the test installation, and was not representative of a full collector field. Because of the drive wheel's open construction, the resulting shadow was not very dense, and was not expected to have a major effect.

When a beam of sunlight falls on a collector mirror at other than zero incident angle, the reflected beam will not fully illuminate the length of the receiver. The non-illuminated length 'x' is dependent on the reflector focal length 'f' and the incident angle 'Ia' of the sunlight:

$$x = f \tan(Ia) \quad (3)$$

The missing sunlight is usually called 'end loss', and is one of the factors that reduce the efficiency of a row of parabolic trough collectors with increasing incident angle. A row of IST collectors in a field installation would be 4 to 6 times the 6.1 meter length of the test collector module, resulting in an end loss of about 1-2% at high incident angles. However, during an incident angle performance test of a single 6 m module, the end loss of the test module would be on the order of 21% at 60 degree incident angles. When calculating collector efficiency for the incident angle tests in this report, end loss was corrected such that the collector appeared to be of infinite length.

Incident angle test data obtained is shown in Appendix D.

Thermal Loss Tests

The objective of the thermal loss test series was determination of steady-state heat losses from the collector receiver as a function of operating temperature. Good thermal loss data is more difficult to obtain than heat gain (efficiency) data, because the fluid temperature change through the collector receiver is smaller by as much as an order of magnitude. But the measuring instrument

errors, temperature instabilities and flow variations remain about the same, therefore the possible errors in the thermal loss measurements are larger.

The three components of thermal loss (conduction, convection and radiation losses) are changed in different ways depending on the receiver's configuration and operating conditions. When a vacuum is present in the annulus between the receiver surface and the glass envelope, conduction and convection across the annulus are effectively eliminated. When air is introduced into the vacuum space, measured losses increase significantly as conduction and convection begin to transfer heat to the glass envelope. Radiation loss from the heated receiver's metal surface to the glass envelope is not changed very much by the presence of air in the annulus. The IST collector design tested does not incorporate a vacuum receiver, although such a receiver is being designed for future use.

Since the glass receiver envelope is opaque to the infra-red radiation from the receiver surface, all three loss components serve to transfer heat from the receiver surface to the glass envelope. A second loss series then transfers heat by convection and conduction from the glass to the ambient air, and by radiation to the sky. Presence of an anti-reflective coating on the receiver glass will change the amount of concentrated visible light passing through the glass during in-focus operation. The coating should not normally change the thermal loss characteristics of the receiver.

Surface temperature of the glass is significantly lower than the receiver's metal surface. If the glass envelope is removed, conduction and convection losses to the ambient air will be greatly enhanced, and wind effects will be much larger. (See Ref. 4, SAND94-1884) Radiation losses will also increase when the glass is removed because the higher temperature metal surfaces now radiate directly to the sky.

Thermal loss from radiation effects is a problem for solar collector testing, because radiation loss is not necessarily dependent on ambient air temperature in the same way as conduction and convection losses. Some of the heat radiated by the collector's receiver is focused back in the direction the reflector is aimed, so temperature of the aim point becomes a factor in the radiation loss.

The temperature of the ground surface or other nearby objects is certain to be different (usually higher) than the sky temperature. Since the collector is always aimed at the sky when in operation, only a sky aim-point is suitable for reasonably accurate test results. The effective sky temperature is also changed by the presence of clouds; thermal loss tests made with an overcast sky show lower losses than those made with a clear sky. For our test purposes, the sky temperature was unknown, but is probably always lower than the ambient air temperature around the collector. A true measure of receiver thermal loss with zero contribution due to direct or scattered light absorption by the receiver can be obtained by aiming the reflector at a clear sky, at night. Other tests have also shown that an approximately equivalent thermal loss value occurs during more normal daylight hours when the receiver is shaded from direct sunlight and the reflector is aimed at a clear sky. (See Ref. 1, SAND 83-0984).

The receiver must be shaded from direct sunlight because the receiver surface would absorb energy equivalent to that from a non-concentrating collector with an aperture area equal to that of the receiver surface. This small amount of absorbed energy is not negligible when compared to the receiver thermal loss. Receiver shading must be done in such a way that there is no change in the receiver's view angle to the sky, or radiation losses will be changed.

The measured temperature drop across the receiver can be quite small during some loss tests (less than one degree C for the IST receiver). A test operator may therefore wish to reduce fluid flow rates from normal in-focus flow values in order to increase the delta-temperature. However, changing fluid flow will introduce another measurement error, because fluid pressure drop across the receiver is converted to heat, which tends to cancel some part of the thermal loss. Therefore, for minimum thermal loss measurement error, the same fluid flow rates used for efficiency testing should also be used during loss tests. In this respect, the IST tests at Sandia do not exactly reproduce thermal losses of this collector in a field installation, because fluid flow rate was not exactly the same, and receiver configuration was not the same (added plug tube inside the receiver). Both these receiver changes could change fluid pressure drop through the receiver.

Thermal loss from the IST collector receiver was measured at approximately the same temperatures used for peak efficiency measurements. As in all the tests, an exact value of temperature was not important; stability of fluid temperature and flow rate were the most important criteria for the test. The following test conditions were established for the loss tests:

- Clear or nearly clear sky.
- Collector defocused.
- Receiver shaded, reflector aimed at the sky.
- Losses measured at approx. 50 °C intervals, 60-300 °C.
- At each temperature, the system was operated until temperatures were stable to within about 0.1 °C over a measurement period equal to about three receiver time constants. At least one hour was usually required to achieve temperature stability.

Upon completion of the thermal loss tests, the measured data is used in a least-squares regression analysis to obtain a second-order-polynomial curve fit to the data. As for the efficiency data, the equation obtained is not an exact physical model of the receiver, but is an empirical fit to the experimental data.

$$Q_L = A + B\,(dT) + C\,(dT)^2 \qquad (4)$$

Where:

Q_L = Thermal loss from receiver, W/m^2 of aperture area
A = Constant, normally approximately zero
B = Coefficient for linear term
C = Coefficient for non-linear term
dT = Average receiver fluid temperature above ambient air temperature, °C

Test Data Analysis

Figure C-1 illustrates some of the factors that result in the operating heat gain (or efficiency) of a solar collector. By measuring collector efficiency at a low enough temperature, thermal losses will be reduced to zero (or at least a very small value), and we can determine the approximate optical efficiency. At any given higher operating temperature, we should be able to measure total thermal losses, subtract these losses from the heat gain at optical efficiency, and end up with the operating heat gain at the new temperature. Or alternatively, we should be able to measure heat gain (efficiency) at some high temperature, and derive the losses by the decrease in heat gain from that expected at optical efficiency. We will soon find out that the real collector is not that simple.

Figure C-2 shows what actually happens when we make some loss measurements. Measured thermal loss in Figure C-2 is that measured with the receiver shaded, at approximately zero incident sunlight. The "in-focus" curve is derived by calculating the heat gain difference between the operating efficiency and the measured optical efficiency. In Figure C-2, the in-focus loss resulted from tests at an average value of 960 W/m^2 insolation. Tests at other insolation values result in different in-focus loss curves. Tests that were done over a large range of incident solar irradiance have shown that the operating thermal loss scales approximately linearly between zero and 1000 W/m^2 insolation. (See Ref. 1)

During a thermal loss test, the receiver is shaded from direct sunlight, and the receiver surfaces are slightly cooler than the heat-transfer oil inside the receiver pipe. When the collector is in focus, the receiver surfaces are hotter than the oil inside the receiver. The surface temperature differences scale approximately linearly with the value of incident insolation, and since thermal losses depend on the surface temperature, this is the cause of the in-focus loss differences outlined above. We can take advantage of linear loss scaling with insolation to calculate the performance of the collector at any value of insolation. For example, the in-focus thermal loss at 480 W/m^2 insolation would be half way between the out-of-focus curve and the 960 W/m^2 in-focus curve in Figure C-2. For an accurate prediction of total solar field heat output, solar irradiance changes must be considered, since insolation changes by about a factor of three on nearly every day the field is in operation.

Table C-1 below shows a sample calculation of collector heat gain and efficiency at 300 °C and 960 W/m^2 insolation, first using the in-focus loss equation from Figure C-2, and then the equation from measured loss at zero insolation. The calculation was then repeated for 480 and 300 W/m^2 insolation. Since 480 W/m^2 insolation is half way between the two loss curves in Figure C-2, in-focus loss was also calculated as exactly half way between the two curves.

The table illustrates that collector heat gain and efficiency change with insolation even if the receiver surface temperatures are not considered. With a constant thermal loss at any given temperature, and a decreasing heat gain with decreasing insolation, collector efficiency must fall with decreasing insolation. In either case, there is some relatively low value of insolation where the heat gained in focus is equal to the ongoing thermal loss, and the collector efficiency is zero. Changes in surface temperature with insolation just operate to lower the efficiency below what would otherwise be expected from out-of-focus, zero insolation, measured thermal losses.

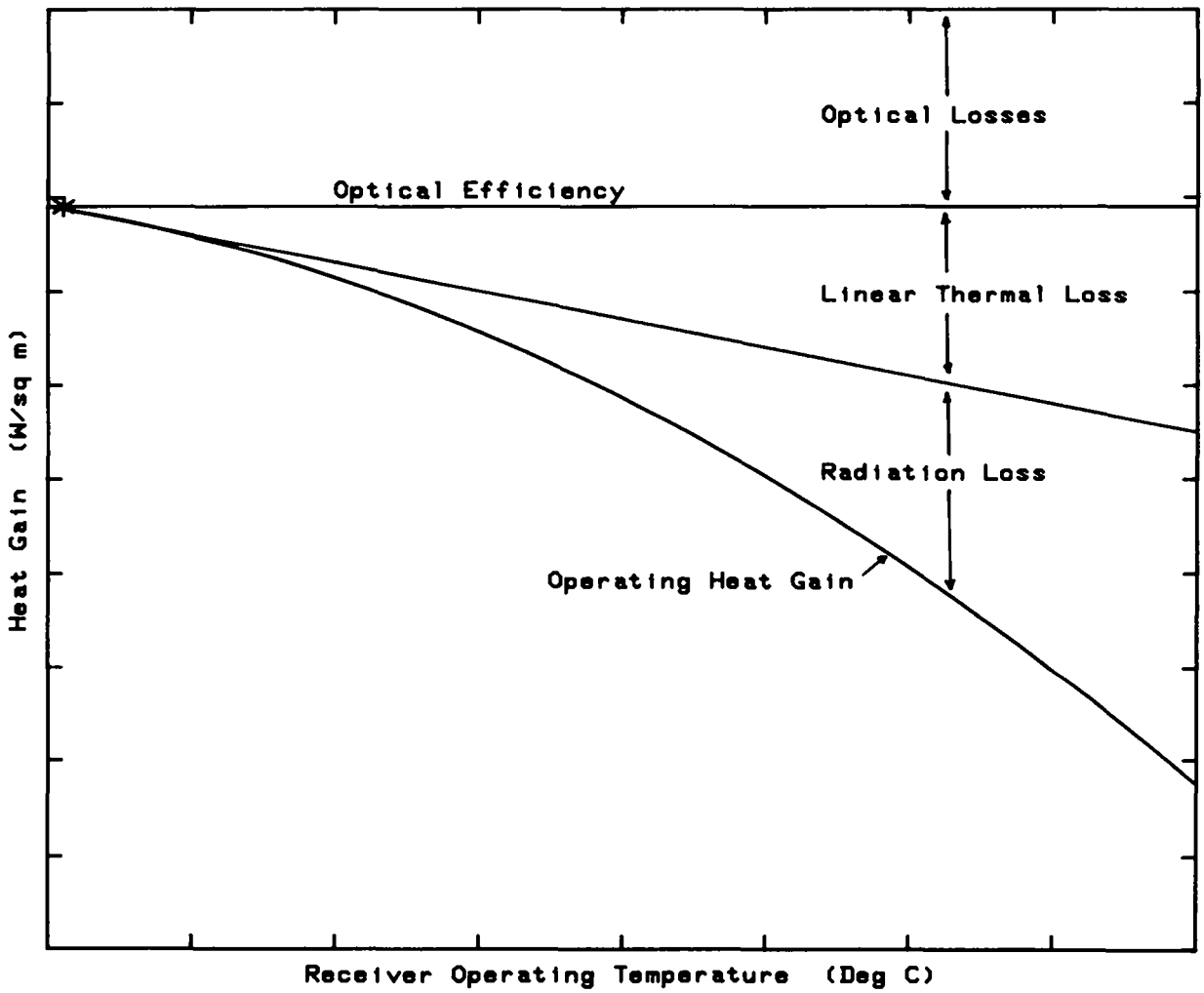

Figure C-1. Ideal Receiver Heat Gain and Losses

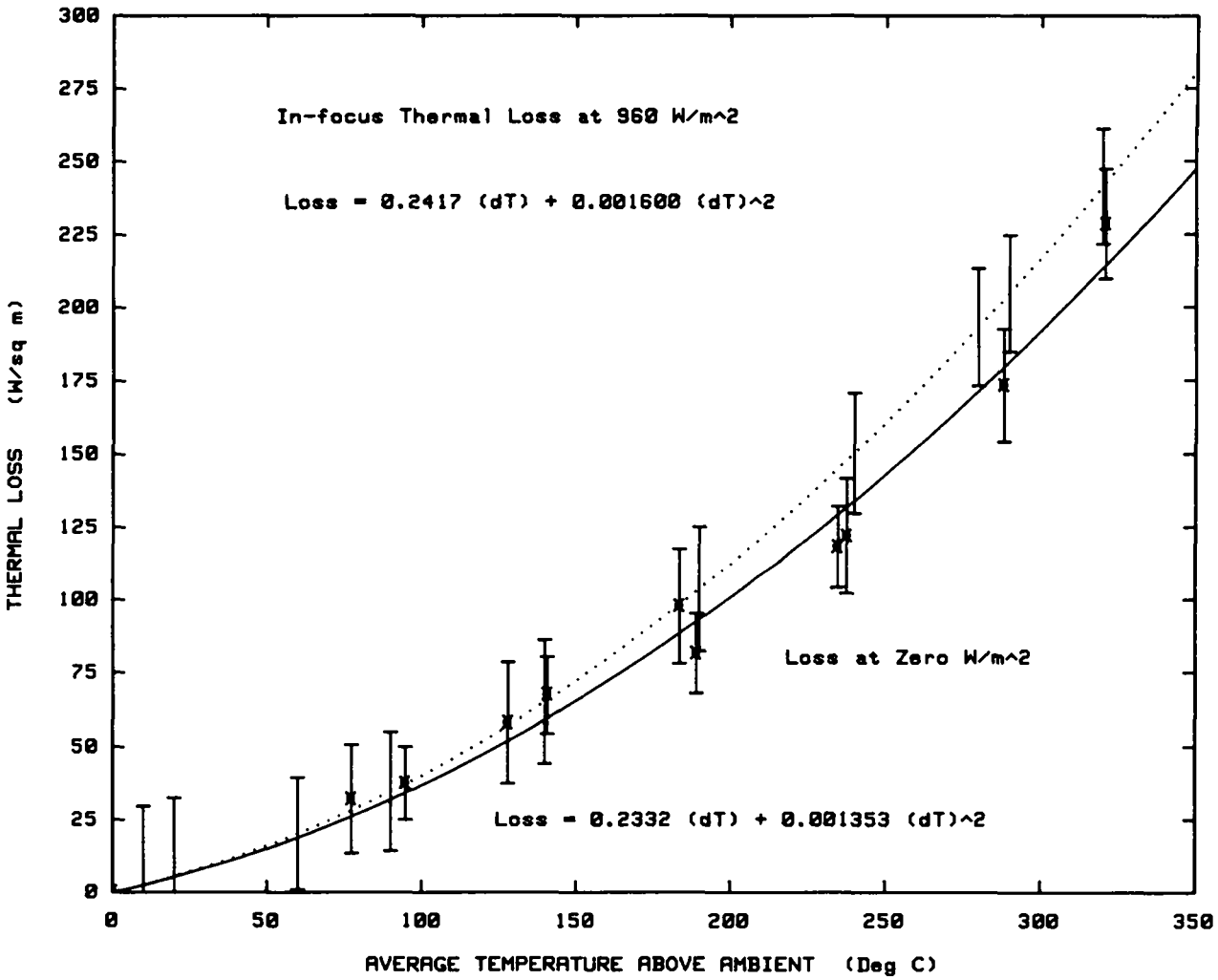

Figure C-2. IST In-Focus Thermal Loss—Black Chrome/Pyrex Receiver

Note that linear scaling between in-focus and out-of-focus loss curves has been confirmed only for collector designs that are not sensitive to changes in solar spectrum with insolation. This appears to be approximately true for aluminum and silver reflectors, Pyrex glass receiver envelopes, and black receivers; such as the IST collector design. Changes of in-focus thermal loss may scale differently for other collectors, such as a Fresnel lens concentrator.

Table C-1

Changes in Efficiency With Insolation

Direct Normal Insolation W/m^2	Optical Efficiency %	Optical Heat Gain W/m^2	Measured Heat Loss @ 300 °C W/m^2	In-focus loss @ 300 °C W/m^2	Calculated Heat Gain W/m^2	Calculated Efficiency %
960	70.17	673.6		216.5	457.1	47.6
960	70.17	673.6	191.7		481.9	50.2
480	70.17	336.8		204.1	132.7	27.6
480	70.17	336.8	191.7		145.1	30.2
300	70.17	210.5		199.45	11.1	3.7
300	70.17	210.5	191.7		18.8	6.3

To derive a performance equation for a tested collector, calculations similar to the above table were made to generate a large matrix of insolation, operating temperature, and heat gain. A multiple linear regression of the data table then produces a heat gain equation of the following form:

$$Q = A(I) - B(I)(\Delta T) - C(\Delta T) - D(\Delta T^2) \quad (5)$$

Where:

Q = Operating heat gain (W/m^2) at zero incident angle
ΔT = Average fluid temperature (°C) above ambient air temperature
I = Direct normal insolation (W/m^2)

For the IST collector tests, equation (5) should be valid for operating temperatures from ambient to about 350 °C, and for direct insolation values from zero to about 1100 W/m^2.

Equation (5) is valid only at zero incident angle. An incident angle modifier term must be added to obtain collector heat gain at any other incident angle. Since the end effect of incident angle is to reduce the value of insolation arriving at the receiver absorber surface, the incident angle modifier, K, can be applied to the insolation in the first two terms of equation (5):

$$Q = K[A(I) - B(I)(\Delta T)] - C(\Delta T) - D(\Delta T^2) \quad (6)$$

When the heat gain from equation (6) is divided by the incident insolation, the result is an efficiency equation for the collector. The equation should be valid over the full expected range of operating temperature, insolation, and incident angles.

$$\eta = K[A - B(\Delta T)] - C(\Delta T / I) - D(\Delta T^2 / I) \quad (7)$$

Equations (5), (6), and (6) are not complete physical models of the collector; rather they are empirical fits to experimental data. Equations like (7) have been used to predict all-day, steady state thermal output from small solar collector fields; the predictions were within about 1% of actual measurements. (See Ref. 2 and 3). Note that the equation is valid only for the collector itself, and only for steady state operation. Other calculations must be made to include the thermal mass and heat capacity of the collector field and other equipment. Including all equipment is necessary if the result is to correctly reflect the collector field during warm-up and the temperature variations of a typical intermittently cloudy day.

Because the test at Sandia included only a single collector module, the added thermal loss from any field interconnecting fluid pipe is also not included in Equation (7).

Figure C-3 shows Equation (7) for the IST collector, with a silver film mirror and black nickel/solgel glass receiver, at a zero incident angle. Collector efficiency decreases along a hyperbolic path as insolation is reduced, and along a quadratic polynomial path with increases in temperature. A small "floor" area is visible, where heat gain is zero or negative. The floor defines combinations of temperature and insolation where positive heat gain is not possible. For another way to show the same equation for a more limited range of insolation, see Figures 6 and 7 in the introduction to this report.

Figure C-4 illustrates the same collector equation, but now for an incident angle of 50 degrees, which would occur in mid-December for a North-South IST collector field.

References

Dudley, V. E., and Workhoven, R. M., 1982. SAND81-0984, *Performance Testing of the Solar Kinetics T-700 Solar Collector.* Albuquerque, N. M.: Sandia National Laboratories.

Cameron, C. P., and Dudley, V. E., 1986. SAND85-2316, *Acurex Solar Corporation Modular Industrial Solar Retrofit Qualification Test Results.* Albuquerque, N. M.: Sandia National Laboratories.

Cameron, C. P., and Dudley, V. E., 1986. SAND85-2320, *Solar Kinetics, Incorporated Modular Industrial Solar Retrofit Qualification Test Results.* Albuquerque, N. M.: Sandia National Laboratories.

Dudley, V. E., Kolb, G. J., Sloan, M., and Kearney, D. 1994. SAND94-1884, *Test Results: SEGS LS-2 Solar Collector.* Albuquerque, N. M.: Sandia National Laboratories.

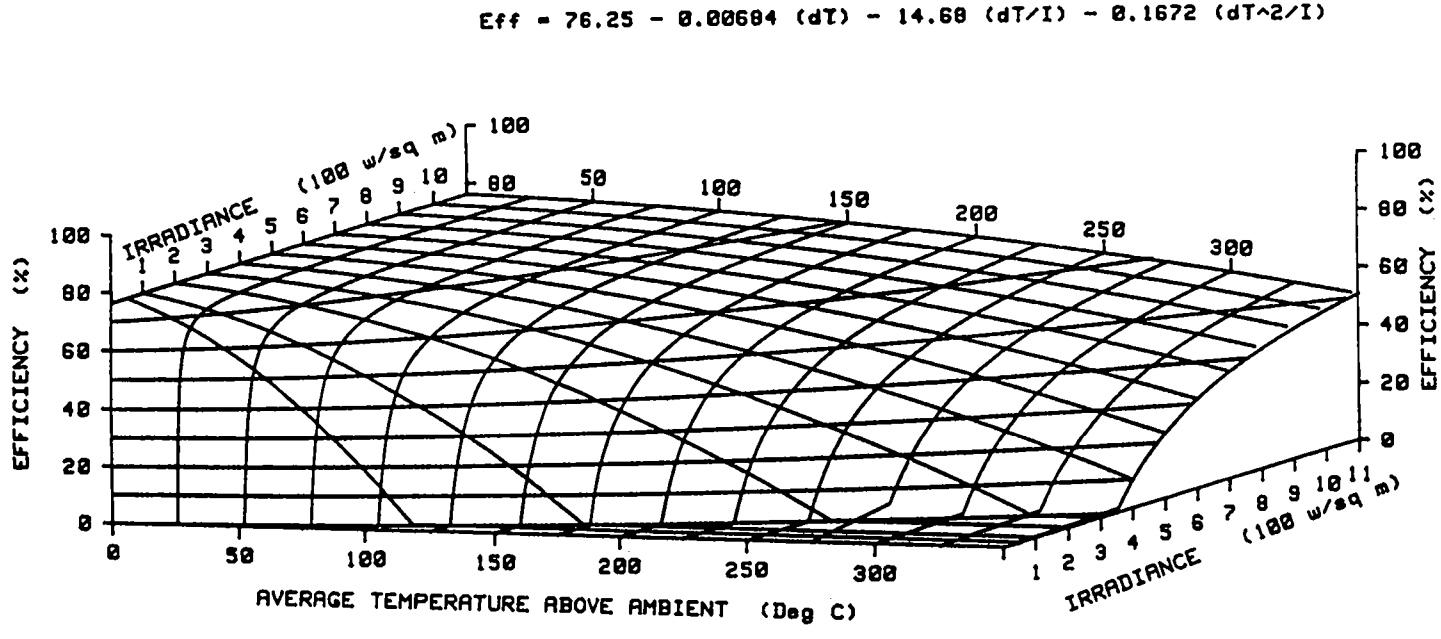

Figure C-3. IST - ECP-305/Black Nickel/Solgel Glass at Zero Incident Angle

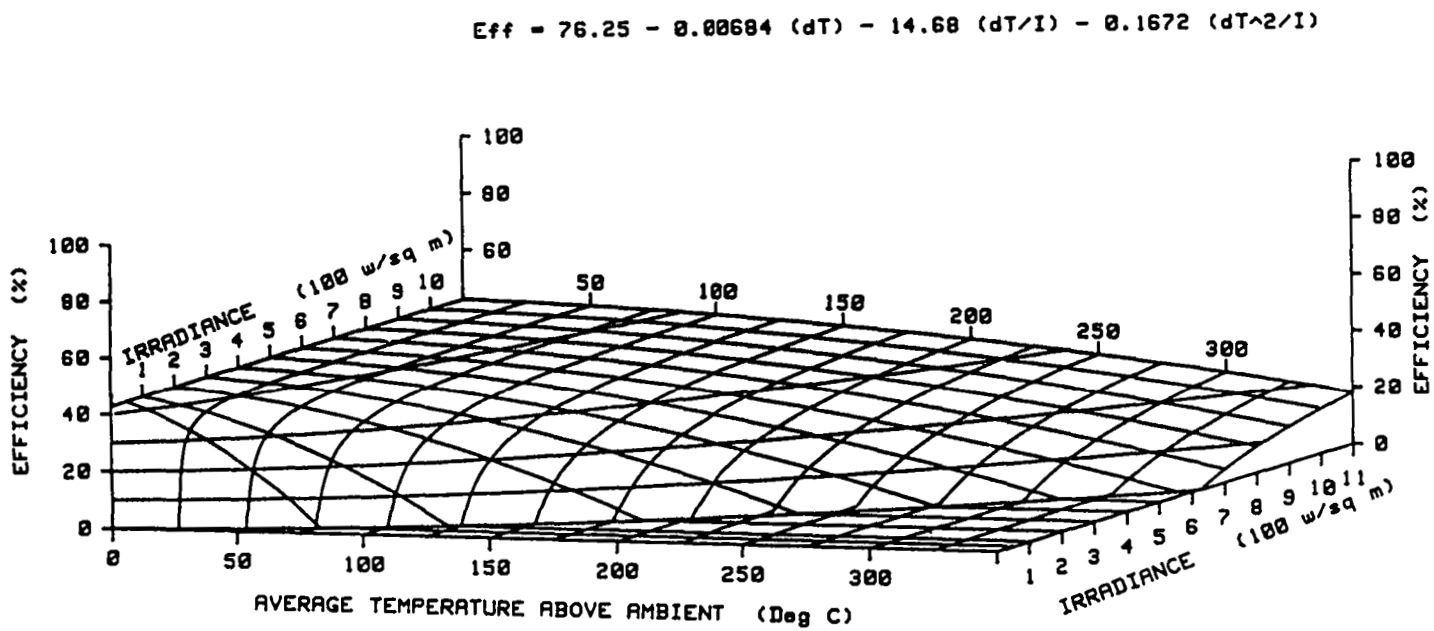

Figure C-4. IST - ECP-305/Black Nickel/Solgel Glass at 50 Deg Incident Angle

Intentionally Left Blank

APPENDIX D

TEST RESULTS

Intentionally Left Blank

TEST RESULTS

Introduction

Initial testing of the IST collector module was done with a 3M SA-85™ aluminized-film reflector. After a few days of initial checkout testing, concentrated light spilling past the receiver made it obvious that the mirror was not focusing well on one end of the receiver tube. When the reflector is viewed in the focal plane from a long distance, the black image of the receiver should appear to fill the entire reflector. In this case, about 10% of the reflector area was not focused on the receiver. The unfocused mirror appears as white areas in a photograph (see Figure D-1); the black area is the magnified image of the black chrome receiver. Inspection of this area of the reflector revealed a buckle running diagonally across the mirror, apparently due to damage by wind loads after installation. The reflector was not field repairable, so it was replaced by another reflector using 3M ECP-305™ silvered acrylic film. Except for Table 1, all the data reported here was obtained using the silver-film reflector assembly.

For field installations, IST uses heat-transfer fluid flow-rates that are much higher than is possible with the fluid system available at the Sandia test site. To promote turbulent flow within the receiver with our maximum 50 liters/minute flow rate, a closed-end, 31.75 mm diameter plug tube was installed within the IST receiver. This plug tube confined the fluid flow to a narrow annulus next to the heated surface. Figure D-2 shows the Reynolds numbers attained with the test setup as a function of the fluid temperature.

The first receiver installed for testing used a black chrome selective surface, and was enclosed in a solgel anti-reflective coated glass envelope. Air at ambient atmospheric pressure filled the space between the glass and the receiver surface. This receiver was used with both the aluminized film reflector and the silver film reflector.

Initial testing was done with cold domestic water as the heat transfer fluid. These tests were made to obtain the approximate optical efficiency of the collector, and to measure the change in performance of the collector as the incident angle was increased from zero to 60 degrees. After completing tests with the solgel anti-reflective glass receiver envelope, testing was repeated using a conventional borosilicate Pyrex® glass receiver envelope to access how much improvement is realized by anti-reflective coating the glass.

After testing was completed with the black chrome receiver tube, it was replaced with another receiver tube with a black nickel selective coating. All the black nickel tests were done with the original solgel glass receiver envelope.

Included with each data point in the data tables below is the estimated error in collector efficiency or thermal loss. The error shown includes estimates of calibration (bias) error and data scatter (statistical) error; these errors are discussed further in Appendix F.

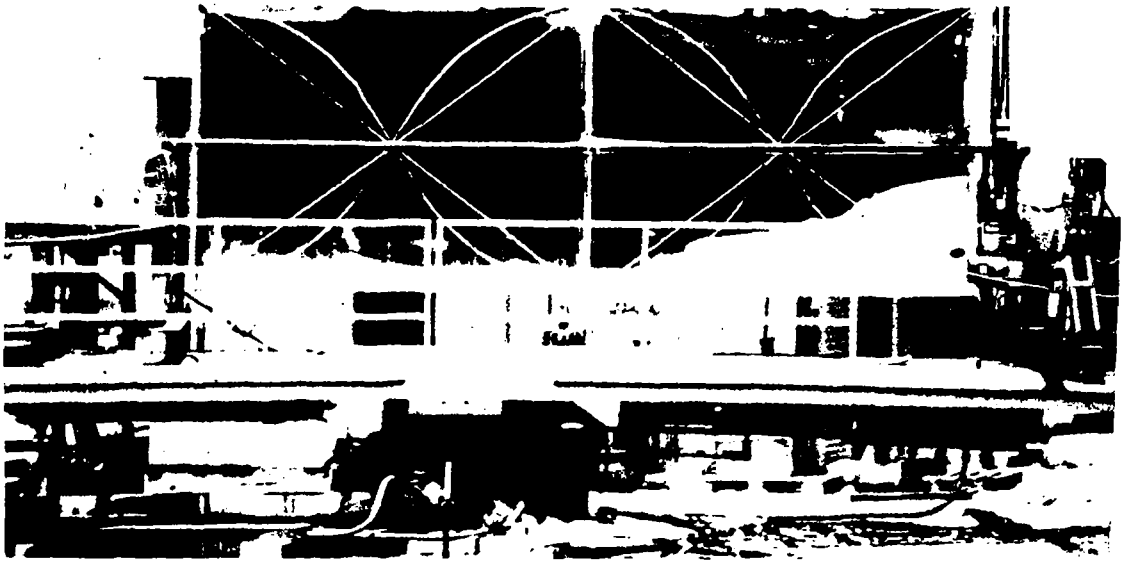

Figure D-1. IST Collector on AZTRAK Rotating Platform

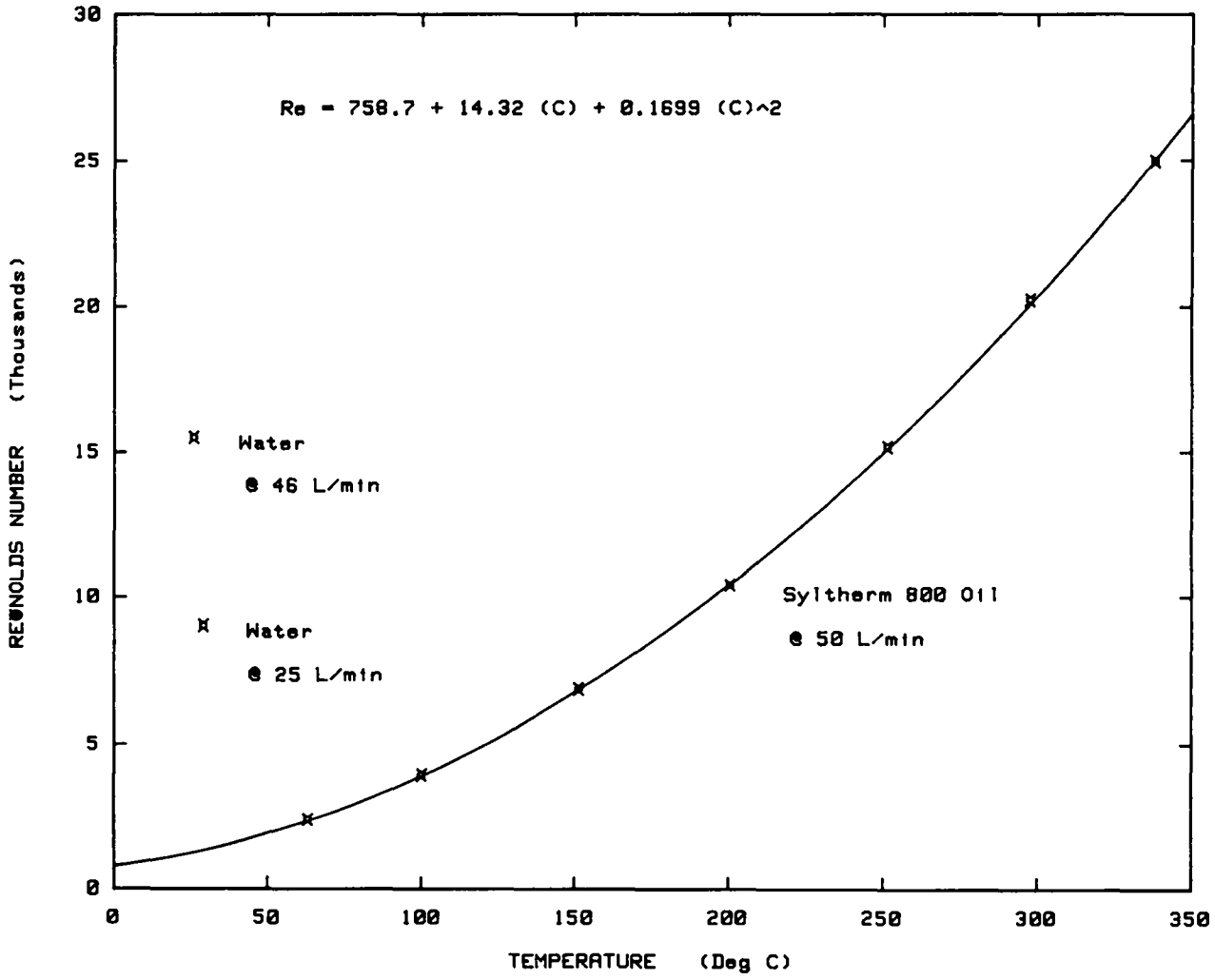

Figure D-2. Reynolds Number vs Temperature

APPENDIX D

Receiver Response Time

Two tests were made to determine the receiver response time, i.e., the time required for the system to stabilize after a step change in heat input. Figure D-3 shows the receiver efficiency and heat gain as the collector was placed into focus. Figure D-4 was obtained as the collector was defocused. In both cases the heat transfer fluid was cold water at near-ambient air temperatures. The tests illustrated in the figures were done with the original aluminum reflector; later tests with the silver mirror produced somewhat higher final efficiencies, but did not appreciably change the time constant. The receiver's response to a large (~930 W/m^2) step change in insolation was substantially complete within two minutes.

For the data included in this report, the system was operated for approximately one hour at each test temperature, until fluid flow and all temperatures were stabilized. To obtain a reportable data point, data collection was then accomplished for a minimum of three time constants, while maintaining stable flow and temperatures. An example of a data run is shown in Appendix F, Table F-1.

Efficiency Tests With Black Chrome Receiver

Testing began with an aluminum-film mirror and cold domestic water as the heat transfer fluid. After only a few days during the setup and checkout period, efficiency was found to have decreased, as mentioned in the introduction to this section. Some data was obtained during initial checkout, and is given in Table D-1 below.

Table D-1

Measured Efficiency Test Data

Black Chrome Selective Coating, Solgel Coated Glass, Aluminum Film Reflector

Test Date 1993	NIP W/m2	Wind speed m/sec	Air Temp °C	Temp In °C	Temp Out °C	Delta Air °C	Flow rate L/min	Meas Effic %	Est Error ±%
14/05	916.2	3.5	21.1	21.7	27.1	3.32	21.3	66.15	3.09

The 66.1% optical efficiency obtained in this test is approximately what would be expected from a mirror of 0.84 reflectivity, so this test point is believed to represent the undamaged mirror. The damaged reflector was not repairable; it was replaced with a silver-film mirror for continued testing.

Testing continued using the silver-film reflector and the original black chrome receiver. Five peak efficiency test points were obtained in four test days; these are shown in Table D-2. The average near-optical efficiency using anti-reflective receiver glass with a black chrome receiver and silver film reflector was 74.06%, measured with the average receiver fluid temperature at 1.2 °C above ambient-air temperature.

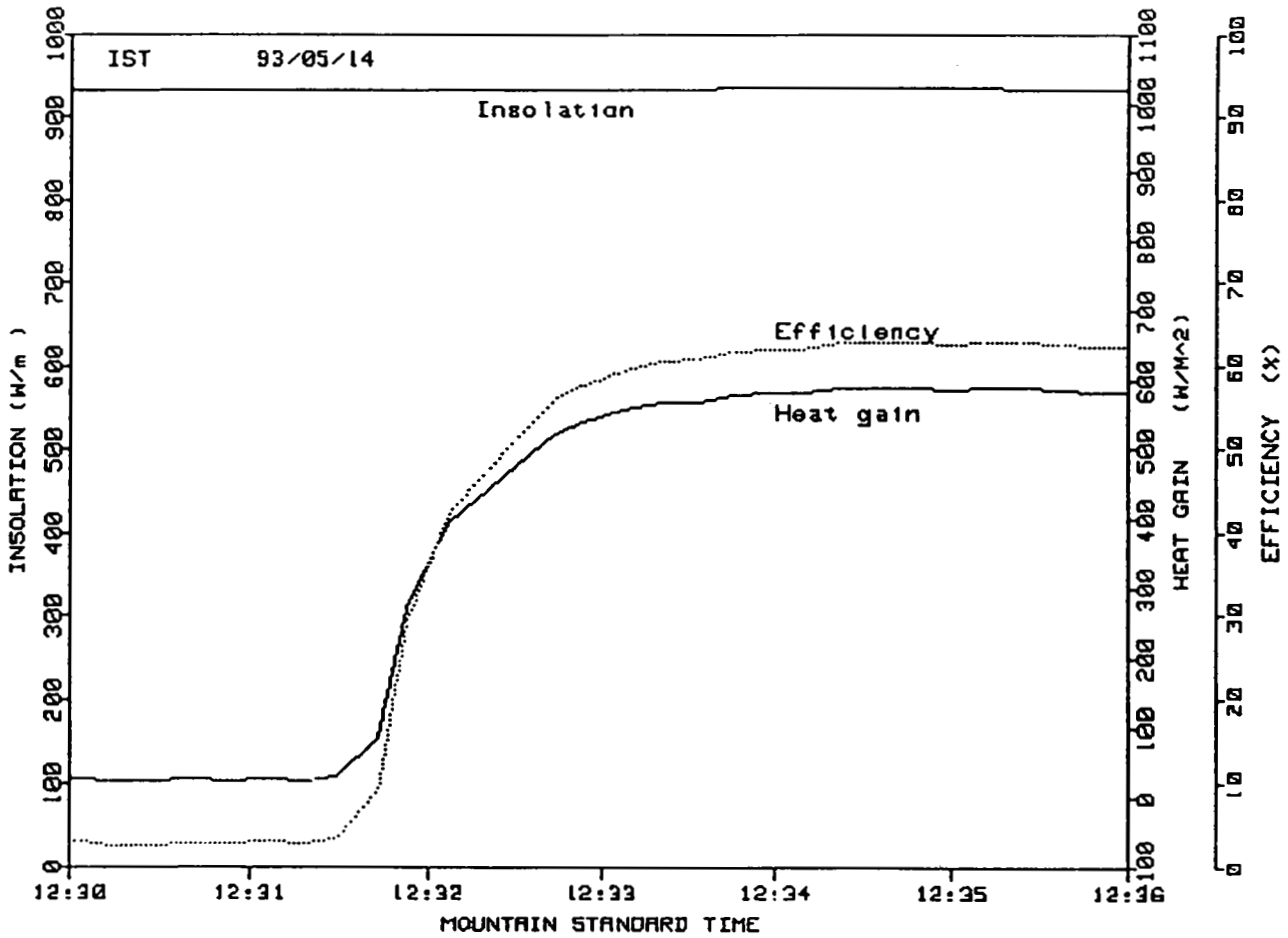

Figure D-3. IST Receiver Time Constant to In-focus

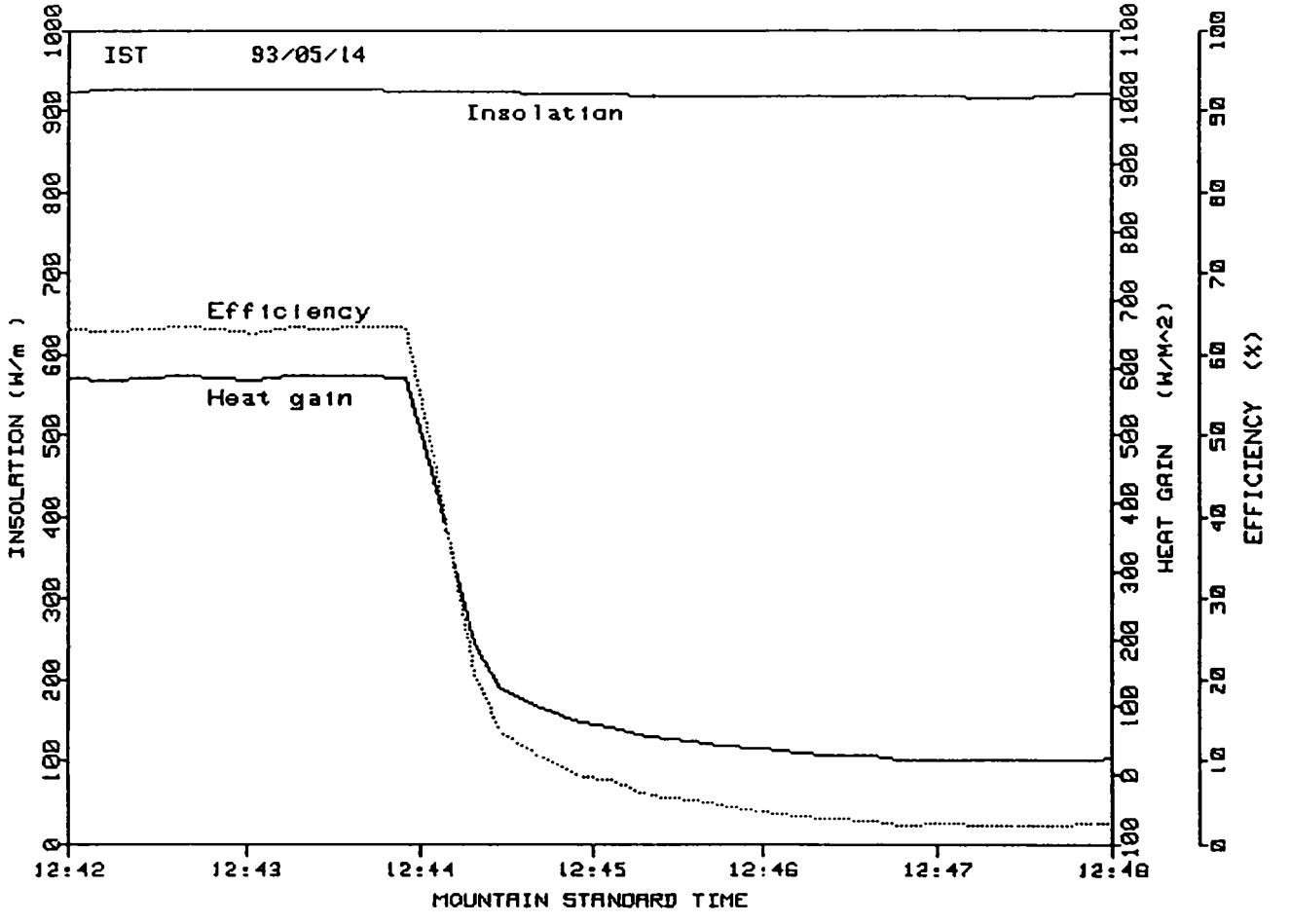

Figure D-4. IST Receiver Time Constant to Out-of-focus

Table D-2

Measured Efficiency Test Data

Black Chrome Selective Coating, Solgel Coated Glass, Silver Film Reflector

Test Date 1993	NIP W/m2	Wind speed m/sec	Air Temp °C	Temp In °C	Temp Out °C	Delta Air °C	Flow rate L/min	Meas. Effic. %	Est. Error ±%
11/08	962.4	3.7	31.9	30.06	35.51	0.91	24.7	73.40	3.28
11/08	941.0	3.1	32.9	30.05	35.35	-0.22	24.9	73.76	3.37
12/08	942.3	2.4	32.9	30.14	35.56	-0.09	24.8	74.81	3.32
23/08	977.7	0.1	28.3	29.05	34.60	3.52	24.8	74.12	3.26
24/08	981.9	1.8	30.3	29.34	34.91	1.82	24.9	74.20	3.26

After completing tests with the anti-reflective glass receiver envelope, tests were repeated using the conventional Pyrex® glass envelope. The black chrome receiver tube and silver film reflector were not changed. Four efficiency points were obtained in two days of cold water testing; these points are shown in Table D-3. Efficiency average with a plain glass receiver envelope was 70.33%, a decrease of 3.7 points, or about 5%. Receiver temperature during these tests averaged 4.4 °C above ambient air temperature.

On 3 Sept. 1993, an attempt was made to compare performance with clean and dirty mirrors. A recent high wind and dust, followed by light rain, had visibly coated the silver film reflector with dirt. The collector optical efficiency was first measured with the dirty reflector. After cleaning the reflector and receiver glass with deionized water, the efficiency was measured again. The efficiency difference was only about 1 percentage point, or about 1.4% degradation due to the dirty reflector.

Incident angle performance data was also obtained with both types of receiver glass on the black chrome receiver tube. The type of receiver glass appeared to make little difference. The measured incident angle modifier data points are shown later in this section, beginning at Table 7.

On 15 Sept., 1993, cold water plumbing was removed, and the system was replumbed to the high-temperature oil fluid loop for elevated temperature testing. Testing was then delayed for more than a month due to failure of the electric fluid-heater controller. After replacing the controller, 12 test points were obtained in five test days, covering the temperature range from approximately 100°C to nearly 330°C. These test data are included in Table D-3 and are shown in graphical form in Figure D-5.

An equation for the efficiency curve is also shown in Figure D-5. The equation was obtained from a second-order-polynomial least-squares regression of the data in Table D-3. The curve and the test data points show the expected decrease in collector efficiency due to increasing thermal losses from the heated receiver. Note that the efficiency equation is valid only at the average insolation present during the tests, as noted in the figure.

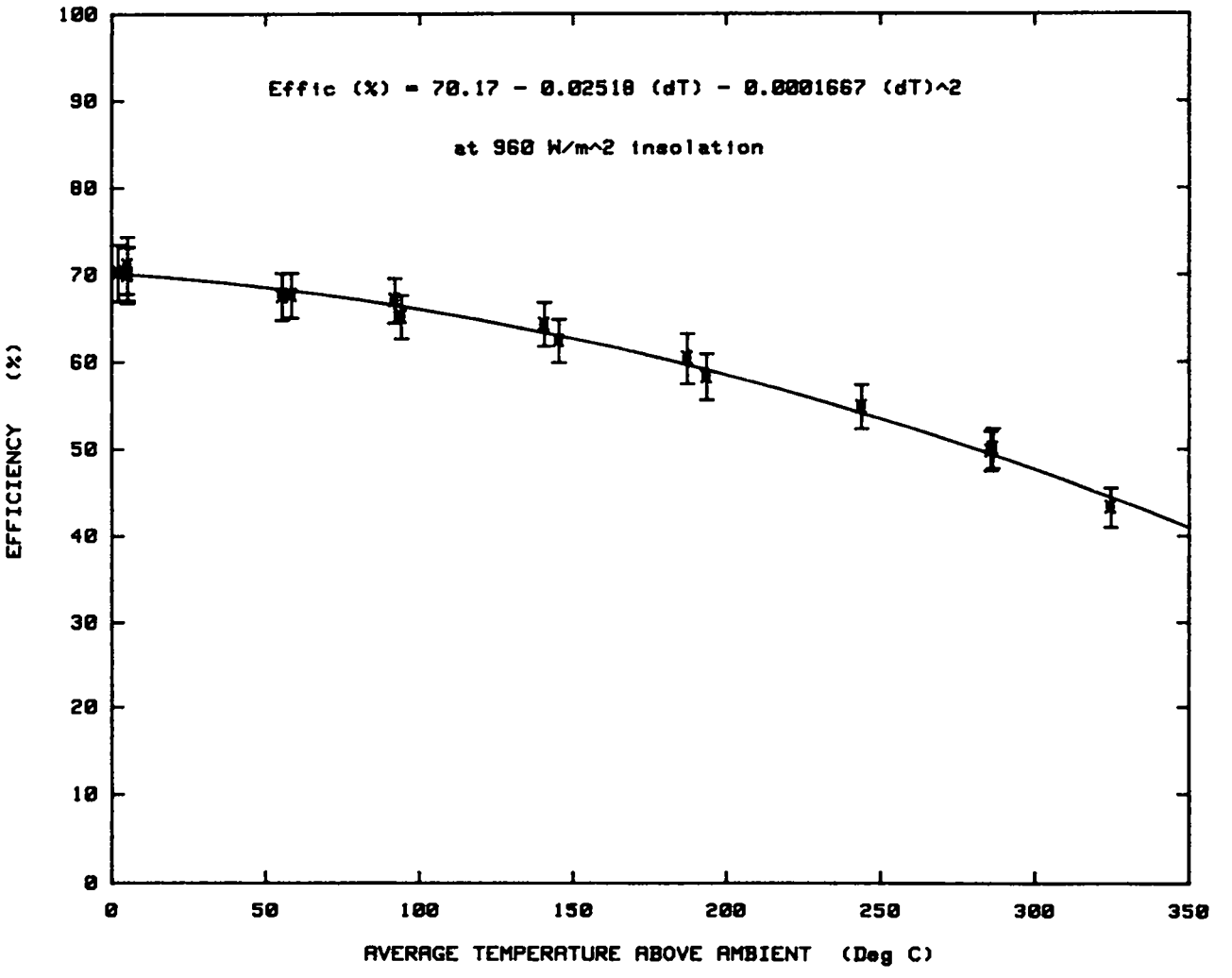

Figure D-5. IST Efficiency—ECP-305/Black Chrome/Pyrex Glass

Table D-3

Measured Efficiency Test Data

Black Chrome Selective Coating, Pyrex™ Glass, Silver Film Reflector

Test Date 1993	NIP W/m2	Wind speed m/sec	Air Temp °C	Temp In °C	Temp Out °C	Delta Air °C	Flow rate L/min	Meas. Effic. %	Est. Error ±%
25/08	940.7	1.8	31.4	29.25	34.40	5.16	24.7	71.07	3.31
25/08	936.0	2.1	29.6	29.18	34.26	2.11	24.6	70.20	3.26
03/09	987.1	0.1	25.4	27.88	33.23	5.14	24.6	69.93	3.22
03/09	991.2	0.3.	25.4	27.93	33.31	5.20	24.6	70.10	3.12
20/10	995.1	2.9	11.8	100.20	107.38	91.94	48.2	67.01	2.54
20/10	1005.7	3.9	14.1	151.38	158.09	140.67	50.4	64.26	2.52
20/10	875.5	1.8	16.1	200.65	206.16	187.28	51.0	60.35	2.91
21/10	927.2	3.7	10.2	251.34	256.69	243.80	51.9	54.82	2.54
21/10	994.9	4.1	14.0	297.75	303.11	286.41	52.5	50.04	2.30
21/10	977.1	4.4	16.0	338.16	342.86	324.55	53.0	43.27	2.30
22/10	920.3	1.2	11.4	63.27	70.35	55.46	45.5	67.46	2.68
27/10	927.9	3.1	7.8	62.76	69.87	58.48	45.9	67.60	2.57
27/10	969.6	2.4	8.8	99.47	106.25	94.04	48.4	65.12	2.47
27/10	972.7	2.5	10.2	152.42	158.73	145.40	50.3	62.37	2.49
27/10	933.0	3.1	11.4	202.14	207.74	193.54	51.7	58.24	2.62
01/11	1001.3	1.5	15.5	298.57	303.95	285.73	52.3	49.73	2.28

Figure D-6 shows a comparison of the black chrome / solgel glass receiver with the black chrome / Pyrex® glass receiver. The curve for Pyrex® is the same one as in Figure D-5. Since only the optical efficiency was measured for the solgel configuration, elevated temperature data is not directly available for the comparison. Thermal loss measurements with the two different glass envelopes were essentially identical; see below. For the elevated temperature solgel efficiency curve in Figure D-6, we assume that the difference in efficiency for the two receiver configurations over this temperature range will remain approximately the same as the difference in optical efficiencies.

Efficiency Tests With Black Nickel Receiver

On completion of efficiency and thermal loss tests with the black chrome receiver, it was removed and replaced with a new receiver that had a black nickel selective coating. At the same time, the solgel anti-reflective coated receiver glass was installed, and the fluid plumbing was changed back to cold water. This collector configuration was of particular interest because it was to be used in a current solar field construction project.

Testing resumed on 19 Nov. 1993; two optical efficiency points are shown in Table D-4. Incident angle modifier data was obtained during the same test days; this data is covered later in this report. The black nickel receiver was visibly a deeper dull black than the black chrome, indicating

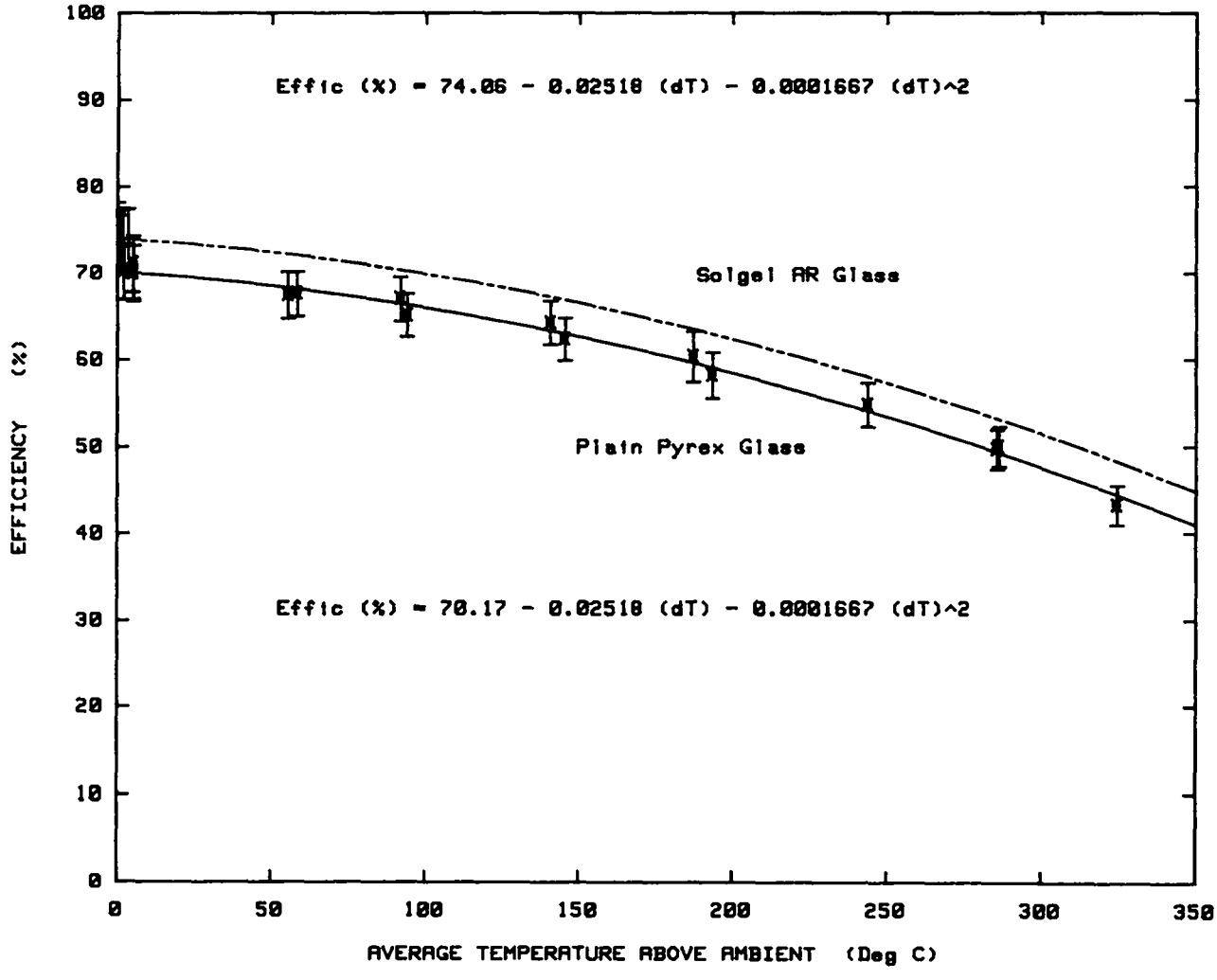

Figure D-6. IST Black Chrome Efficiency Comparison - Solgel Glass/Pyrex Glass

a higher absorptivity. This observation was supported by the average 77.32% measured efficiency, 3.3 percentage points better than the black chrome/solgel receiver, or 4.4% improvement. Only about 2% difference was expected between black nickel and black chrome; however, the black chrome quality is quite sensitive to plating bath parameters, and may not have been an optimum coating. Later absorptivity and emittance measurements confirmed the lower than expected black chrome absorptivity. The black nickel / solgel configuration was also seven percentage points better than the black chrome / Pyrex® receiver, or a 10% improvement.

On 1 Dec. 1993, cold water plumbing was removed from the collector and hot oil plumbing replaced. Eight high temperature test points were obtained in three more test days, as shown below in Table D-4. These data points are also shown in Figure D-7; the plotted curve is from a least-squares polynomial fit to the data. Again note that the equation is valid only for insolation values near the insolation given in the figure.

Also shown in Figure D-7 is a curve for the black nickel / Pyrex glass configuration. Performance of this receiver configuration was measured with cold water, but was not directly measured at high temperature. As for the black chrome receiver, there should be no difference in the thermal loss characteristics of the two receiver glasses. The operating efficiency difference at temperature is assumed to be the same as the optical efficiency difference measured with cold water.

Finally, Figure D-8 summarizes the efficiency data for all four receiver configurations.

Thermal Loss Tests -- Black Chrome

The difference in solar-averaged transmittance between the solgel anti-reflective glass and plain Pyrex glass receiver covers was not expected to change the measured thermal losses. The solgel coating process does not change the infrared transmittance of the glass; therefore, no loss measurements were made with the black chrome / solgel configuration. Concurrently with the black chrome / Pyrex efficiency testing at elevated temperatures, heat losses from the receiver assembly were also measured. Ten test points were obtained in five test days. The complete set of measured thermal loss data is shown in Table D-5, and a graph is shown in Figure D-9. A least-squares regression of the data in Table D-5 produced the equation shown in Figure D-9. For each black chrome efficiency data point in Table D-5, we can calculate the thermal loss required to lower the measured efficiency from the optical efficiency (first points in Table D-5) to the observed value at elevated temperature. These calculated "in-focus loss" points are also plotted in Figure D-9. Because the receiver surface temperatures are higher when concentrated sunlight is focused on the receiver, the in-focus losses are higher than the measured out-of-focus losses with no light on the receiver. Note that the in-focus losses are valid only at the value of insolation present during the efficiency tests, because the receiver surface temperatures change with changes in insolation. See Appendix C of this report for a discussion of in-focus losses and their use in deriving a general performance equation for the collector.

Table D-4

Measured Efficiency Test Data

Black Nickel Selective Coating, Solgel Glass, Silver Film Reflector

Test Date 1993	NIP W/m2	Wind speed m/sec	Air Temp °C	Temp In °C	Temp Out °C	Delta Air °C	Flow rate L/min	Meas. Effic. %	Est. Error ±%
19/11	856.4	0.5	4.3	16.47	22.06	14.94	22.4	77.52	3.81
19/11	924.3	5.7	9.4	18.60	25.73	12.81	19.1	77.13	3.12
01/12	907.5	2.0	5.5	61.36	69.33	59.83	44.3	73.44	2.73
01/12	957.9	2.3	6.7	98.82	106.45	95.89	48.0	70.95	2.65
01/12	966.7	5.6	9.7	150.82	157.91	144.65	50.2	67.43	2.93
01/12	939.8	5.8	10.2	200.93	207.44	193.96	51.7	63.97	2.71
01/12	902.5	5.1	10.8	249.00	254.95	241.13	52.3	59.29	2.84
02/12	904.4	2.6	10.1	298.15	303.80	290.84	52.8	54.40	2.64
07/12	995.3	2.2	9.9	150.56	164.01	147.37	27.0	69.45	1.95
07/12	990.0	2.3	10.3	150.83	158.30	144.30	49.6	70.82	2.60

Table D-5

Measured Thermal Loss Data

Black Chrome Selective Coating, Pyrex™ Glass

Test Date 1993	Wind speed m/sec	Air Temp °C	Temp In °C	Temp Out °C	Delta Air °C	Flow rate L/min	Meas. Loss W/m2	Est. Error W/m2
14/10	3.7	21.3	98.81	98.46	77.37	48.2	32.07	18.60
14/10	4.9	24.5	152.83	152.23	128.07	50.4	58.07	20.54
15/10	3.0	16.4	200.56	199.54	183.62	51.3	97.76	19.69
18/10	3.1	13.5	251.68	250.40	237.57	51.8	121.84	19.76
18/10	2.9	10.9	299.99	298.12	288.13	52.5	173.31	19.25
21/10	3.7	16.9	339.12	336.59	320.92	53.2	228.33	18.83
28/10	0.9	4.4	99.48	98.86	94.78	31.4	37.50	12.54
28/10	4.5	10.7	152.05	150.98	140.79	33.5	67.42	12.95
28/10	2.3	13.6	203.30	202.05	189.04	35.1	81.51	13.73
28/10	2.3	15.8	251.43	249.64	234.71	36.0	118.13	13.97

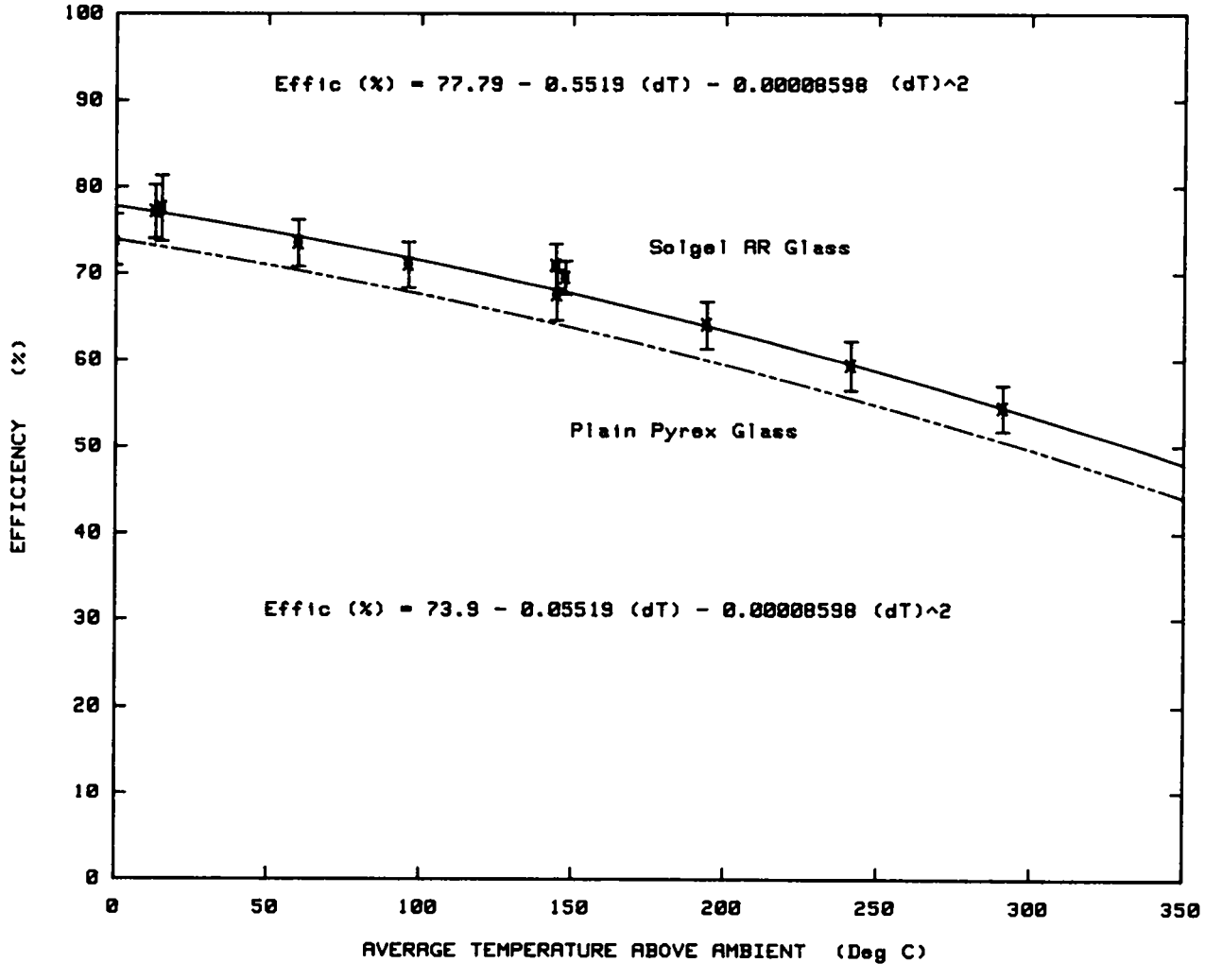

Figure D-7. IST Black Nickel Efficiency Comparison - Solgel Glass/Pyrex Glass

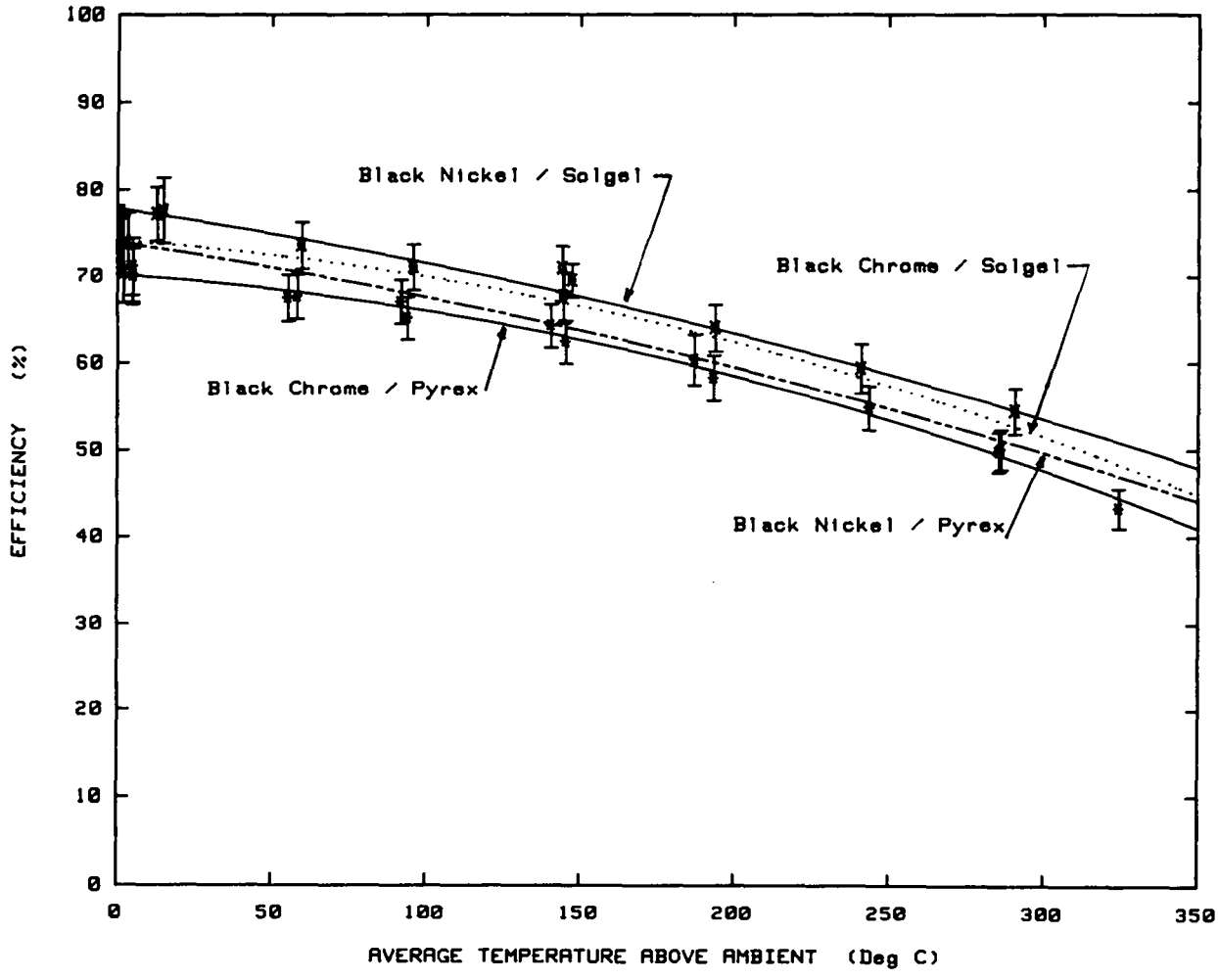

Figure D-8. IST Efficiency Comparison - All Receiver Combinations

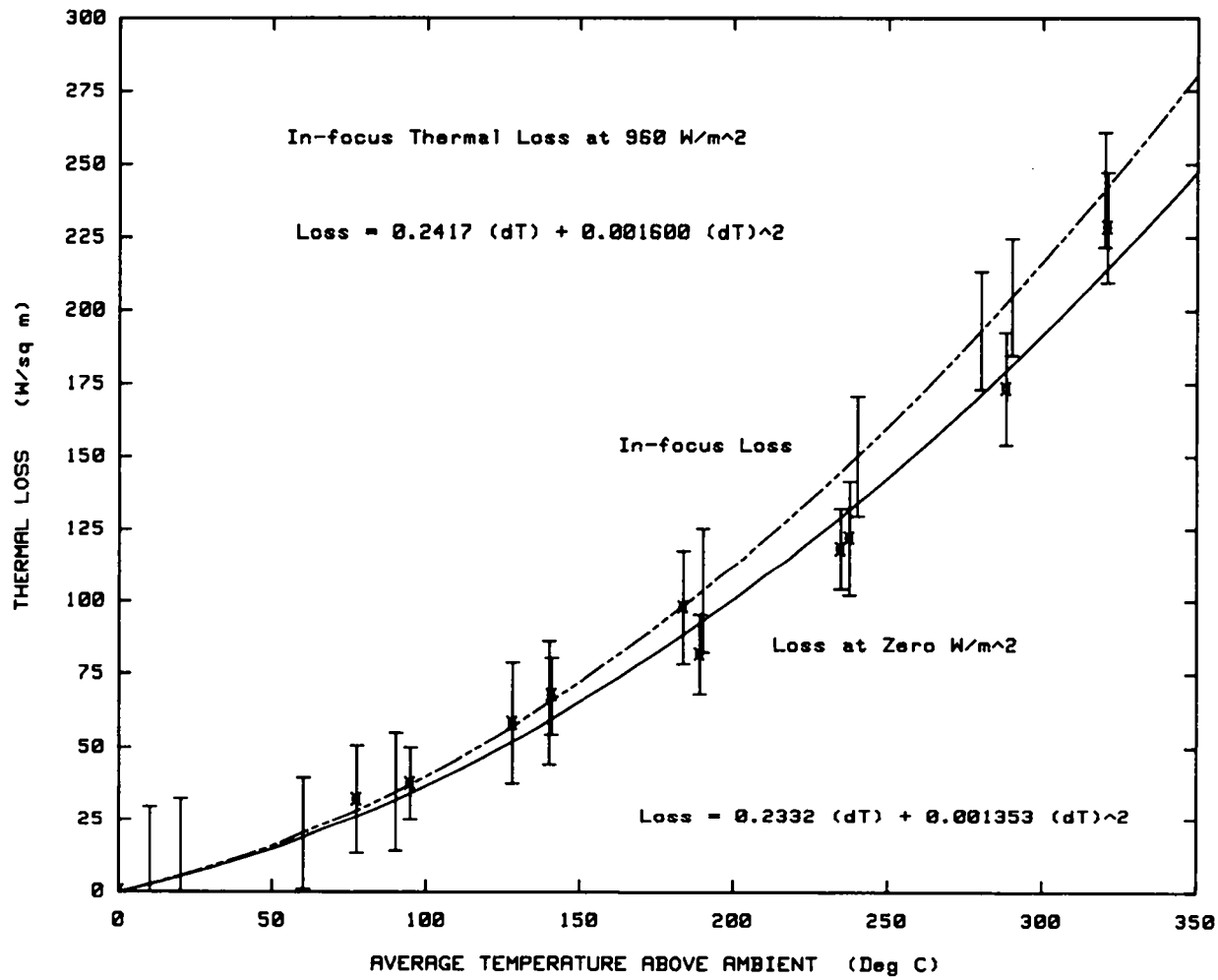

Figure D-9. IST Thermal Loss—Black Chrome/Pyrex Glass Receiver

APPENDIX D

Thermal Loss Tests -- Black Nickel

Eighteen thermal loss test points were obtained in five test days, covering the temperature range from 60°C to nearly 300°C. These data are shown below in Table D-6, and are plotted in Figure D-10. Also shown in Figure D-10 are the "in-focus" loss points and equations for both curves. A least-squares curve fit to the data points was used to derive the equations.

Table D-6

Measured Thermal Loss Data

Black Nickel Selective Coating, Solgel Glass

Test Date 1993	Wind speed m/sec	Air Temp °C	Temp In °C	Temp Out °C	Delta Air °C	Flow rate L/min	Meas. Loss W/m2	Est. Error W/m2
01/12	3.5	11.2	250.02	248.98	238.31	52.3	134.91	20.05
01/12	4.4	10.3	249.30	247.03	237.84	27.4	132.34	10.31
02/12	0.7	0.3	61.28	61.07	60.86	23.0	16.74	8.88
02/12	2.1	3.7	96.48	96.01	92.55	25.0	33.46	9.74
02/12	2.7	1.3	151.73	150.80	149.93	26.4	61.69	10.41
02/12	2.6	6.2	152.17	151.77	145.72	49.8	64.71	19.17
02/12	2.4	9.1	199.90	198.08	190.06	26.9	91.40	10.29
02/12	1.9	8.4	200.57	199.96	191.90	51.2	91.86	19.48
02/12	2.5	10.1	298.29	296.75	287.41	52.9	178.51	19.45
02/12	2.2	8.7	297.52	294.48	287.27	28.9	174.29	10.63
07/12	2.5	-2.2	63.24	63.06	65.37	36.1	12.59	13.97
07/12	0.1	5.4	95.94	95.50	90.33	25.5	21.27	9.94
07/12	3.3	8.5	150.07	149.07	141.04	27.0	51.34	10.44
10/12	1.7	6.5	98.30	98.07	91.65	46.9	20.39	18.25
10/12	1.3	8.7	98.71	98.37	89.79	33.4	22.23	12.95
10/12	2.1	12.1	149.42	148.14	136.67	20.4	49.28	8.18
10/12	1.7	12.6	150.09	149.59	137.23	49.6	46.94	19.45
13/12	6.2	2.8	199.98	198.98	196.69	51.4	95.62	20.43

Figure D-11 compares the measured thermal loss curves for both black nickel and black chrome. There is little difference between the two, as would be expected from the similar values of emittance measured for the two receivers. The two sets of thermal loss data were also obtained with different receiver glass envelopes: solgel anti-reflective glass on the black nickel receiver and plain Pyrex® glass on the black chrome receiver. The two glass types were not expected to make any difference in measured thermal loss, and little was seen.

Incident Angle Tests

Incident angle modifier is defined as the ratio of collector performance (efficiency) at any given incident angle to the performance at a zero incident angle. Domestic cold water was used as the

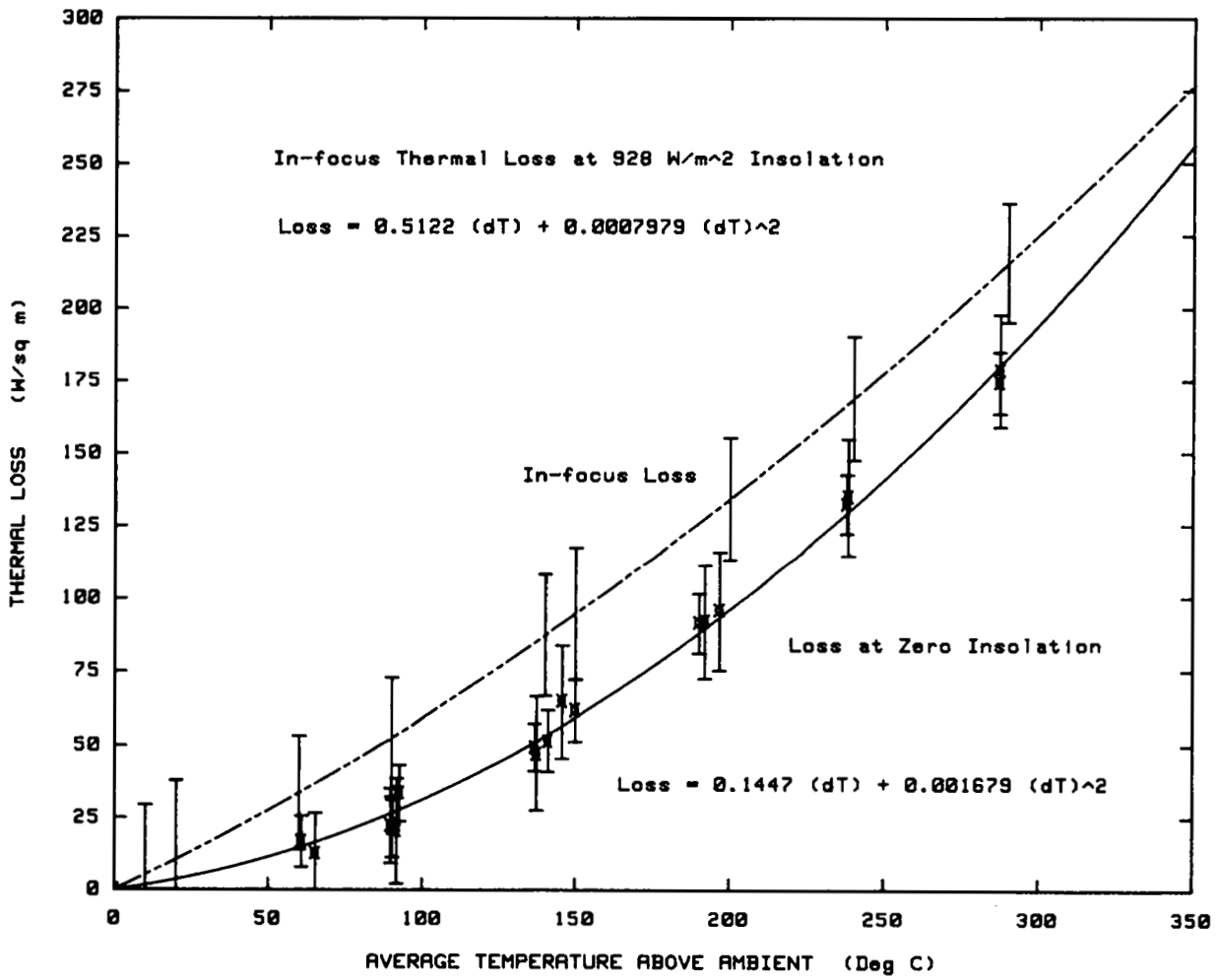

Figure D-10. IST Thermal Loss—Black Nickel/Solgel Glass Receiver

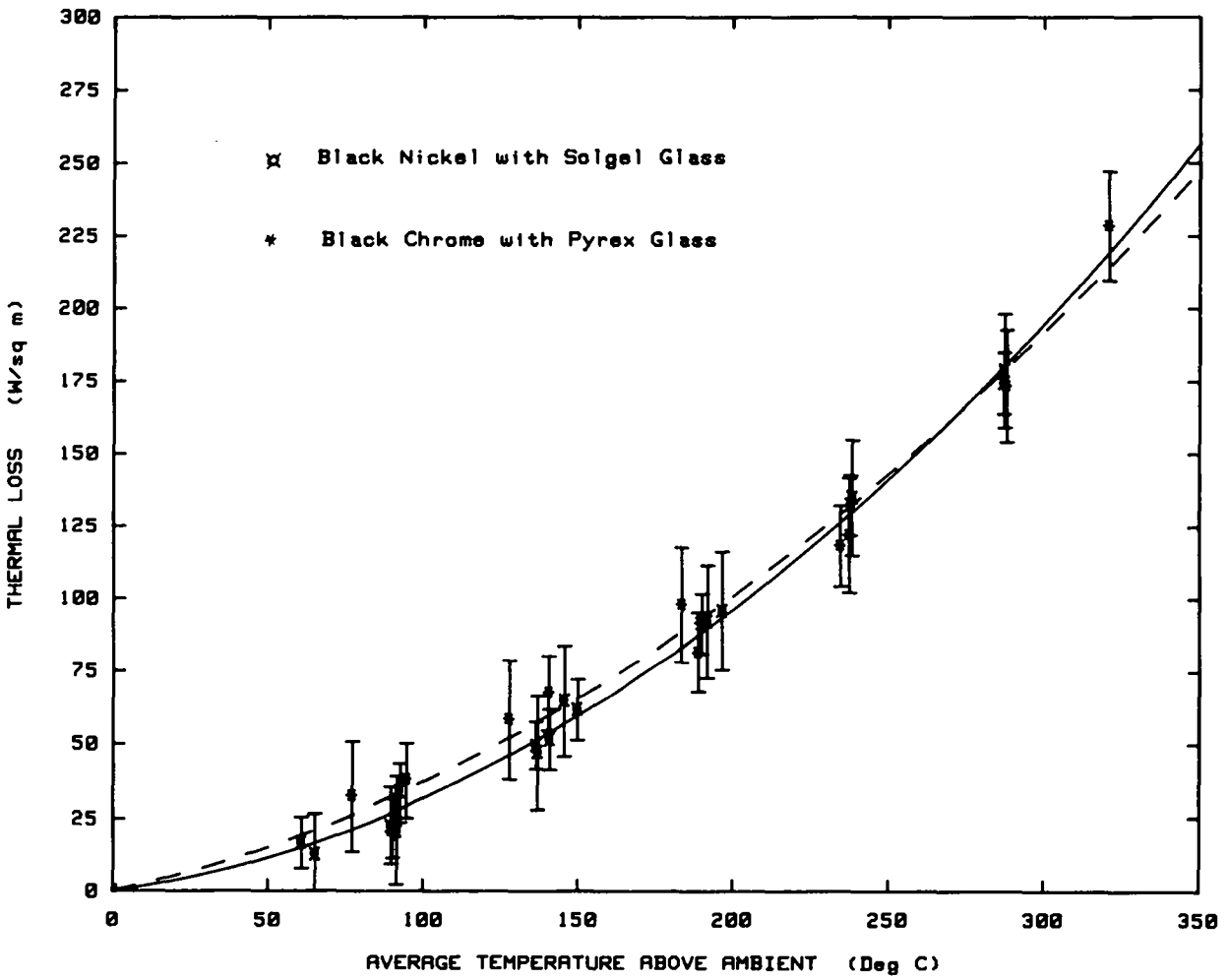

Figure D-11. IST Thermal Loss Comparison - Black Nickel / Black Chrome

heat-transfer fluid for all incident angle tests. These tests were made to obtain the approximate optical efficiency of the collector, and the change in performance of the collector as the incident angle was increased from zero to more than 60 degrees. Test points were obtained every five degrees to identify any difference in positive or negative incident angles. Also of interest was any difference that might be caused by the two different receiver glasses and receiver absorptive surface coatings. Some tests several years ago with a different type of anti-reflective glass coating had seemed to show a larger improvement at high incident angles than at zero angle. No such difference was noted during the current tests.

The IST collector uses a large diameter drive-wheel and cables to rotate the collector to point at the sun. This arrangement allows several rows of collectors to be tracked by a single drive motor. The drive-wheel is normally located in the center of a collector row, with several mirror modules on each side. As installed for tests at Sandia, only a single mirror module was used, with the drive wheel located at the East end. Initially we thought that the drive wheel would cause a shadow on the mirror when the sun was off the East end of the collector. No wheel shadow would be present when the sun was toward the West. The drive wheel shadow could cause the measured incident angle performance to be non-symmetrical. However, the drive-wheel shadow was not extensive or dense, and no discernible performance difference was noted between positive and negative incident angles.

Figures D-12 through D-17 show the positive and negative incident angle data obtained for three of the receiver configurations. Figure D-18 combines all the incident angle data; any differences in the receivers are within the measurement errors. The complete set of incident angle modifier data are shown in Table D-8 and Table D-9. All calculated efficiencies in these tables are corrected for the short test-collector end-loss as outlined in Appendix C. The incident angle modifier K is thus intended for use with a long collector row.

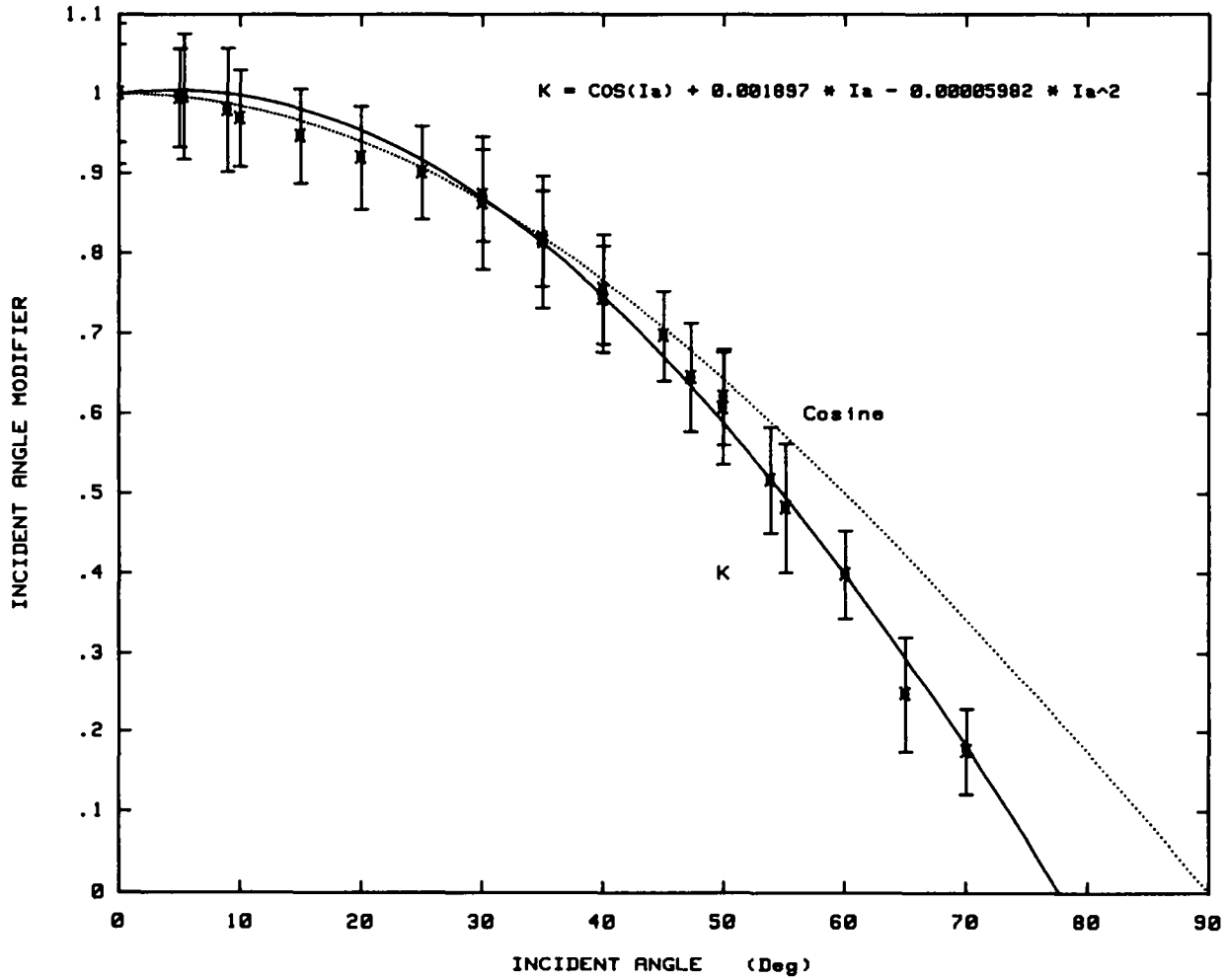

Figure D-12. IST Incident Angle Modifier (+) Black Chrome/Solgel Glass

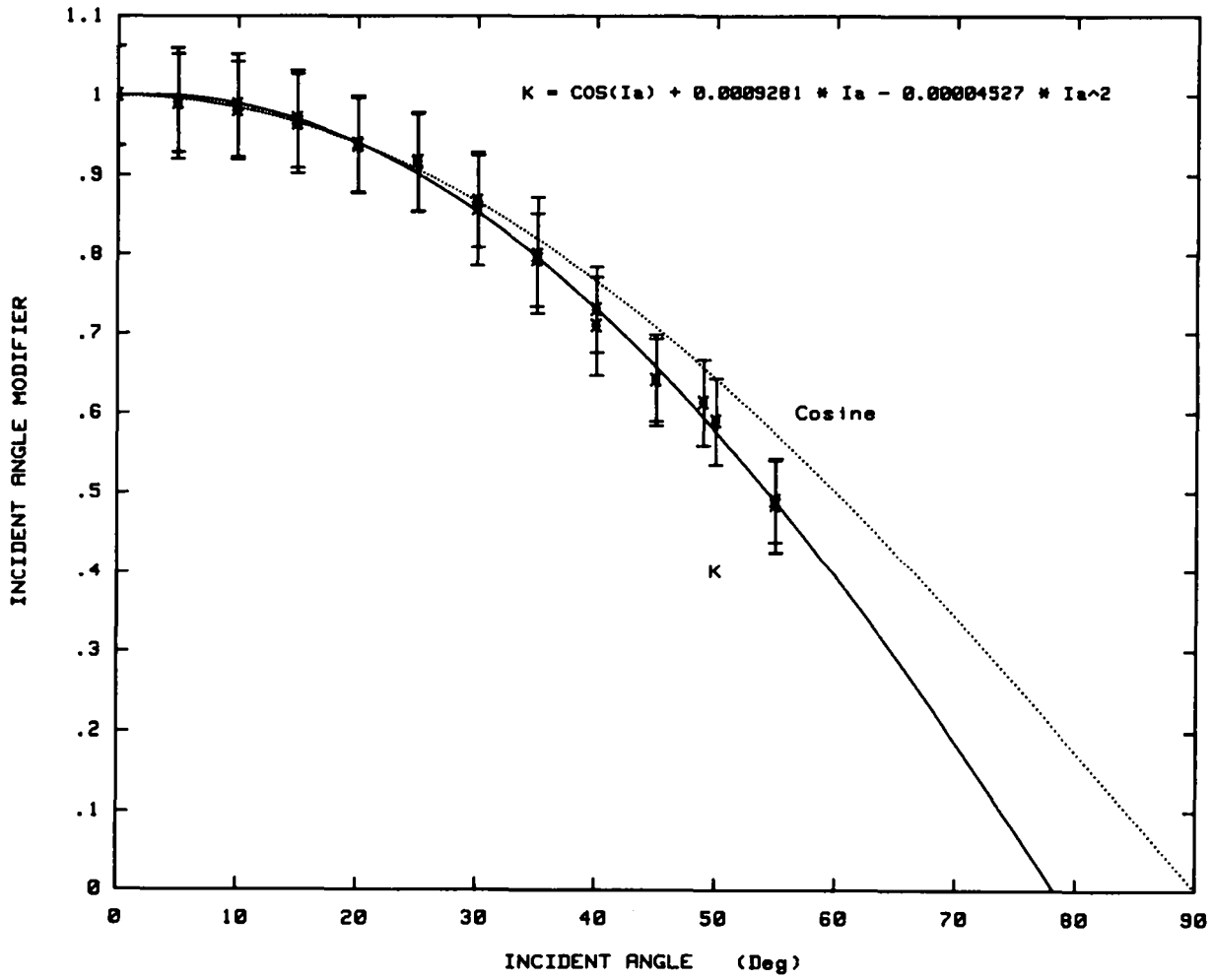

Figure D-13. IST Incident Angle Modifier (-) Black Chrome/Solgel Glass

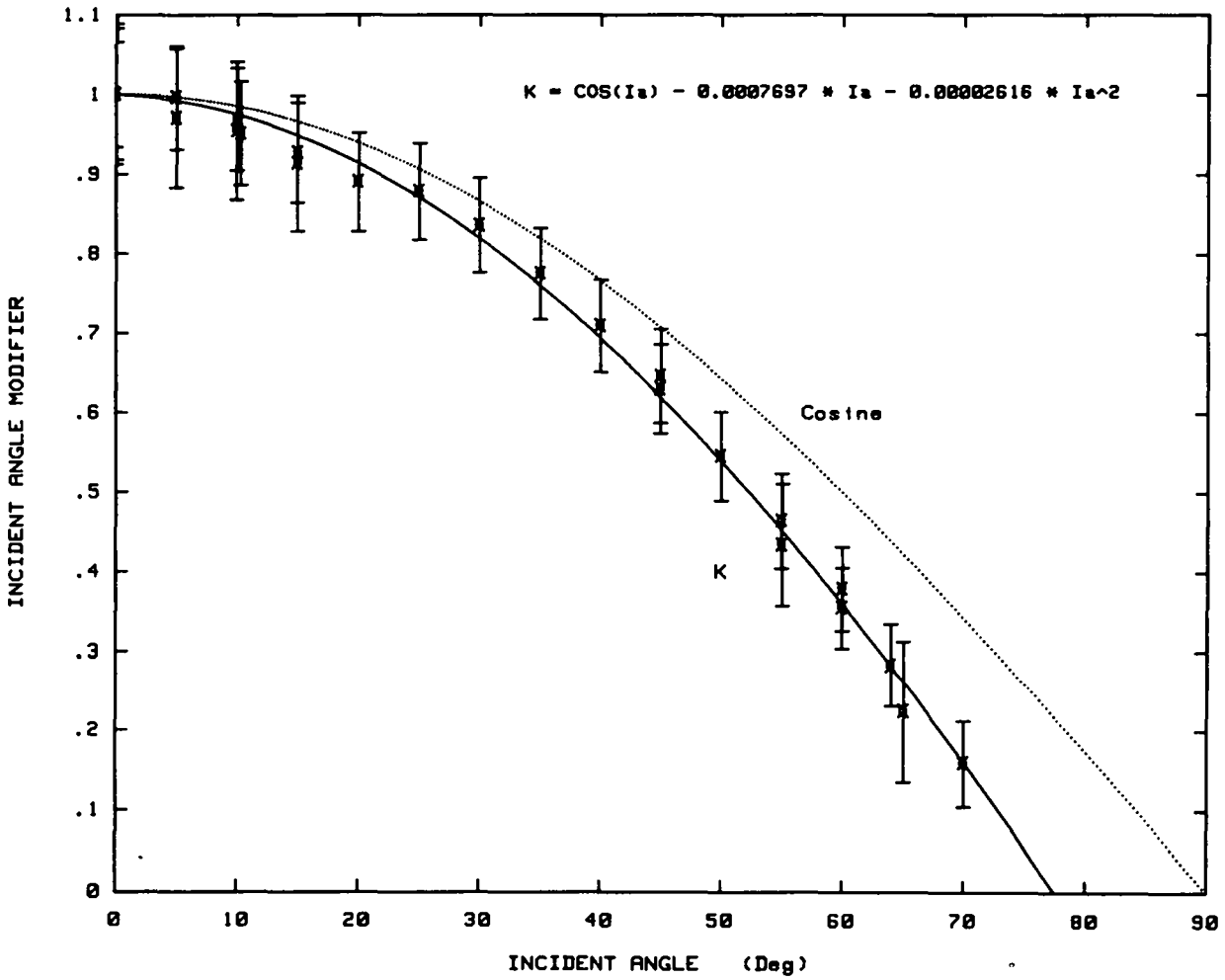

Figure D-14. IST Incident Angle Modifier (+) Black Chrome/Pyrex Glass

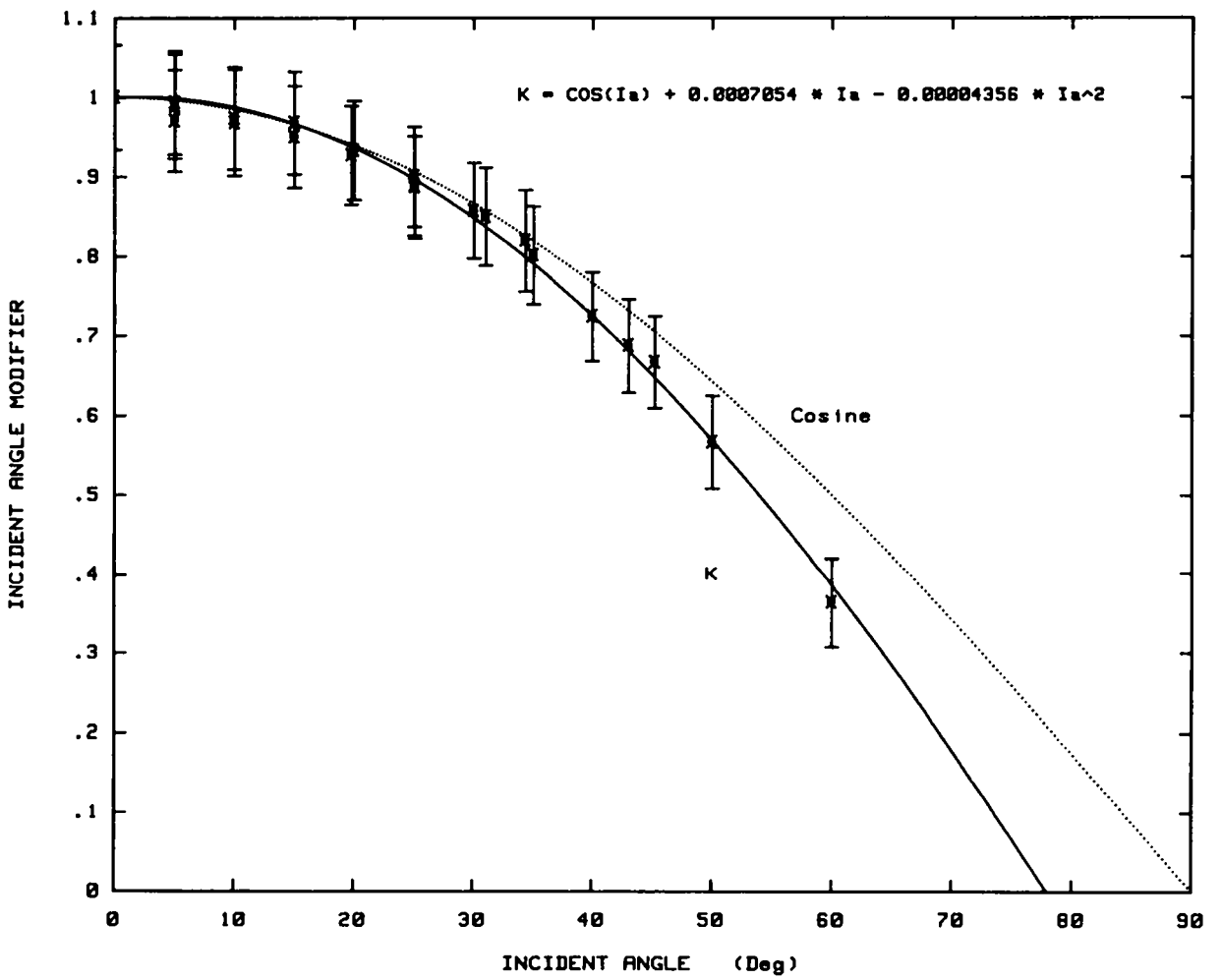

Figure D-15. IST Incident Angle Modifier (-) Black Chrome/Pyrex Glass

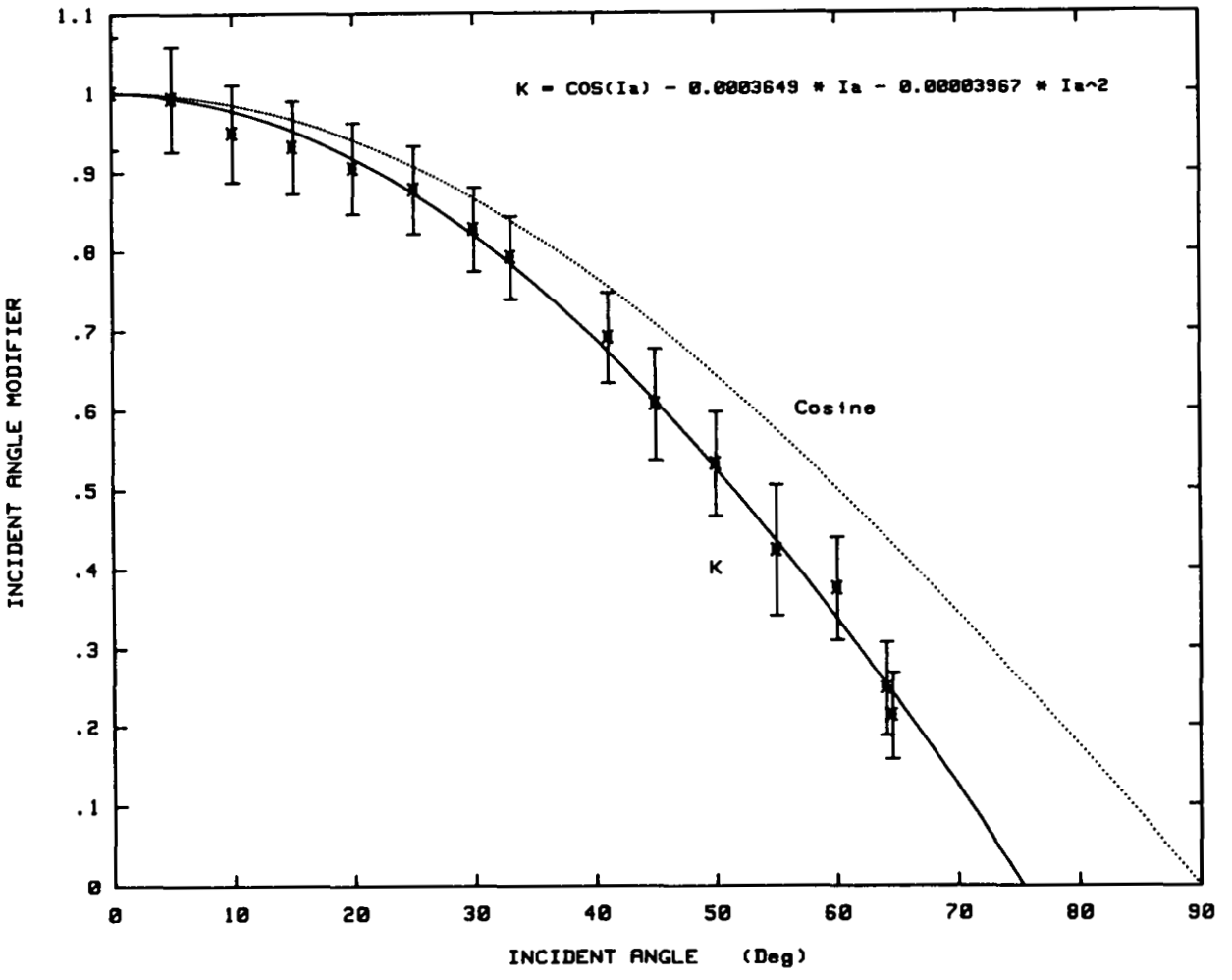

Figure D-16. IST Incident Angle Modifier (+) Black Nickel/Solgel Glass

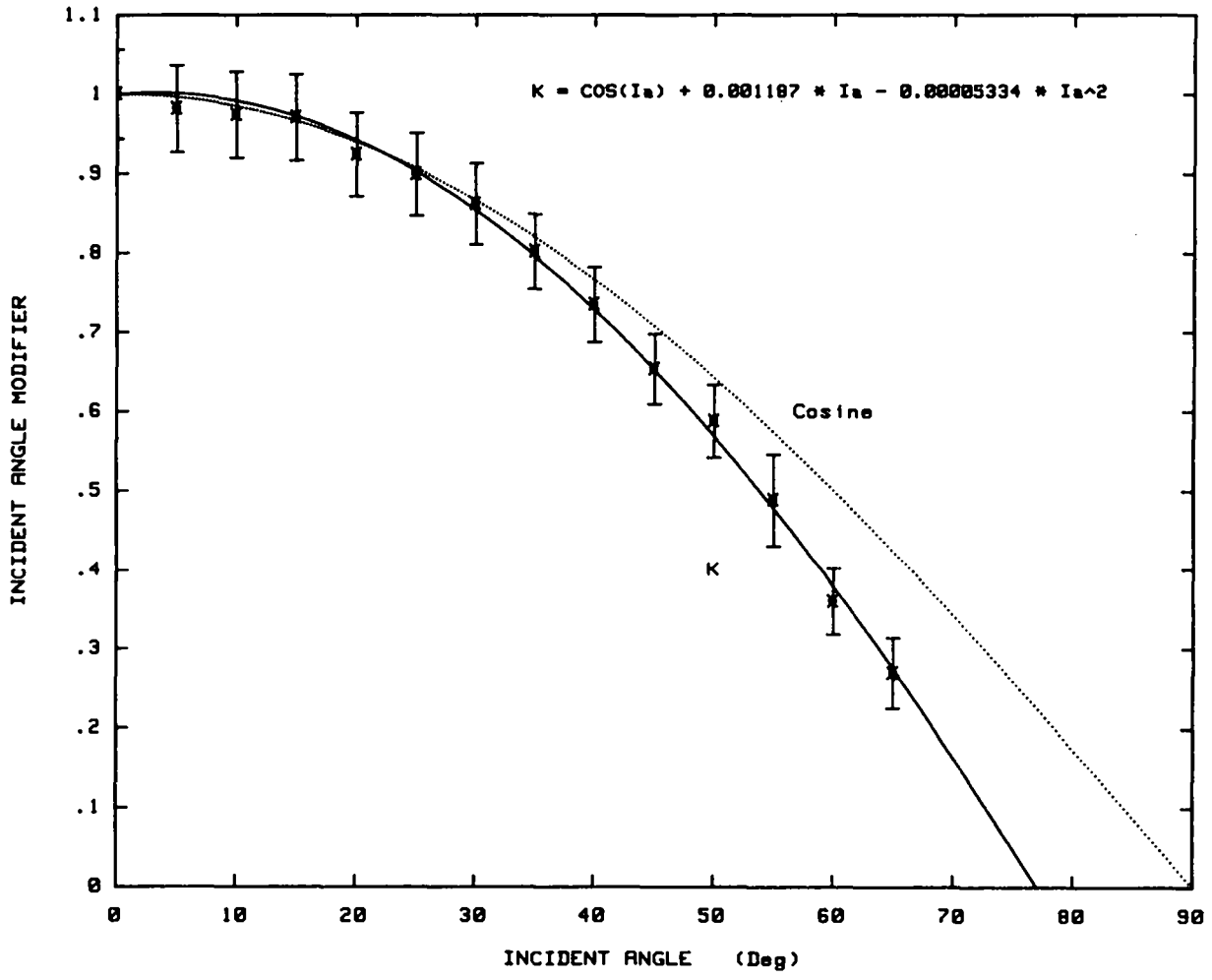

Figure D-17. IST Incident Angle Modifier (-) Black Nickel/Solgel Glass

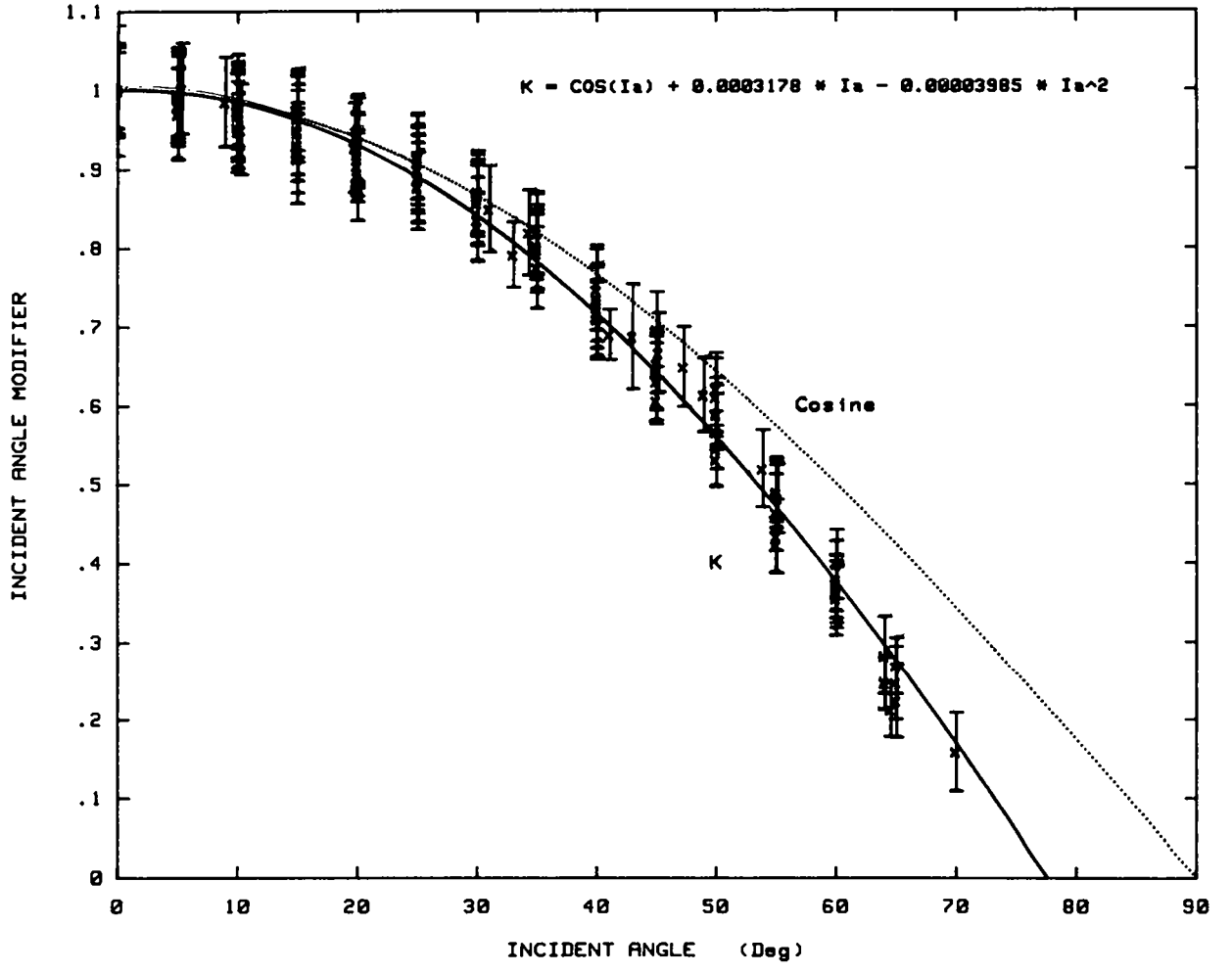

Figure D-18. IST Incident Angle Modifier for All Receivers

Table D-7

Incident Angle Performance Test Data

Black Chrome / Solgel Glass Receiver, Silver Film Reflector

Test Date 1993	NIP W/m2	Amb Temp °C	Temp In °C	Temp Out °C	Delta Air °C	Flow rate L/m	Incid. Angle °	Calc. Effic %	Effic. Ratio	Ratio Error
13/08	981.9	30.31	29.34	34.91	1.82	24.9	0.00	74.6	1.0000	0.0889
13/08	904.2	32.61	29.94	35.05	-0.15	24.8	5.36	74.41	0.9965	0.0794
13/08	907.8	32.21	29.93	34.91	0.20	24.8	8.99	73.13	0.9794	0.0777
13/08	898.9	30.7	29.7	34.0	1.1	24.8	21.42	66.01	0.9164	0.0769
13/08	885.0	29.9	29.52	33.57	1.64	24.8	30.03	64.42	0.8627	0.0831
13/08	871.3	29.0	29.38	33.07	2.21	24.8	35.03	60.75	0.8136	0.0823
13/08	864.1	27.4	29.21	32.47	3.39	24.9	39.99	55.44	0.7426	0.0662
13/08	828.6	26.7	28.93	31.56	3.51	24.8	47.30	48.17	0.6451	0.0678
13/08	827.8	25.9	28.75	31.17	4.05	24.9	49.97	45.29	0.6066	0.0705
13/08	806.5	24.8	28.57	30.52	4.71	24.9	53.94	38.57	0.5166	0.0664
23/08	977.7	28.3	29.05	34.60	3.52	24.9	0.00	74.12	1.0000	0.0620
23/08	844.9	20.4	27.91	32.59	9.89	24.9	-4.99	73.38	0.990	0.0649
23/08	894.5	21.6	28.47	33.36	9.28	24.9	-9.99	73.18	0.9872	0.0649
23/08	931.0	23.6	28.79	33.73	7.63	24.8	-15.0	71.49	0.9664	0.0629
23/08	958.5	24.9	29.00	33.87	6.51	24.8	-20.0	69.58	0.9386	0.0603
23/08	949.9	29.7	28.91	33.52	1.53	25.0	-25.01	67.93	0.9164	0.0621
23/08	940.2	29.7	29.00	33.20	1.35	25.0	-30.01	63.52	0.8569	0.0712
23/08	934.2	29.4	28.91	32.74	1.42	24.9	-35.03	59.17	0.7983	0.0734
23/08	928.7	29.9	28.92	32.33	0.68	24.9	-40.04	54.09	0.7297	0.0543
23/08	915.1	30.9	28.92	31.80	-0.59	24.9	-45.00	47.52	0.6410	0.0520
23/08	895.3	30.9	28.89	31.52	-0.64	24.9	-48.97	45.43	0.6128	0.0539
23/08	872.6	30.9	28.83	30.77	-1.09	25.0	-55.02	35.85	0.4836	0.0590
24/08	981.9	30.3	29.34	34.91	1.82	24.9	0.00	74.20	1.0000	0.0619
24/08	990.3	29.9	29.31	34.83	2.19	24.9	5.01	73.79	0.9946	0.0620
24/08	990.7	28.8	29.26	34.58	3.09	24.9	10.01	71.87	0.9687	0.0607
24/08	988.0	28.6	29.23	34.32	3.19	25.0	15.02	70.22	0.9465	0.0592
24/08	982.3	28.3	29.18	34.04	3.28	25.0	20.00	68.21	0.9193	0.0649
24/08	977.7	28.0	28.94	33.61	3.26	25.0	25.01	66.82	0.9006	0.0584
24/08	967.8	27.3	28.86	33.25	3.71	25.0	30.05	64.70	0.8721	0.0576
24/08	958.9	27.0	28.82	32.84	3.86	25.0	35.00	60.71	0.8182	0.0597
24/08	949.1	25.6	28.69	32.33	4.92	24.8	40.03	56.00	0.7548	0.0685
24/08	935.2	24.6	28.53	31.76	5.52	24.7	45.06	51.70	0.6968	0.0560
24/08	918.9	23.9	28.36	31.09	5.82	24.8	50.02	46.04	0.6205	0.0596
24/08	900.0	22.4	28.21	30.21	6.77	24.8	55.15	35.76	0.4820	0.0811
24/08	869.6	21.3	28.07	29.59	7.57	24.8	60.04	29.57	0.3985	0.0550
24/08	831.3	20.7	27.95	28.78	7.70	24.9	64.99	18.34	0.2473	0.0730
24/08	767.6	20.5	27.99	28.47	7.69	24.9	70.02	12.98	0.1750	0.0537
24/08	979.3	30.6	29.39	34.82	1.52	24.9	-5.04	73.50	0.9906	0.0620
24/08	979.9	31.1	29.40	34.73	0.91	24.9	-9.99	72.77	0.9808	0.0615
24/08	980.4	32.2	29.46	34.67	-0.13	24.9	-14.99	71.96	0.9699	0.0614
24/08	963.3	31.5	29.42	34.30	0.37	24.9	-20.02	69.50	0.9367	0.0598

Table D-7 (continued)

Incident Angle Performance Test Data

Black Chrome / Solgel Glass Receiver, Silver Film Reflector

Test Date 1993	NIP W/m2	Amb Temp °C	Temp In °C	Temp Out °C	Delta Air °C	Flow rate L/m	Incid. Angle °	Calc. Effic %	Effic. Ratio	Ratio Error
24/08	959.4	32.5	29.38	34.06	-0.77	24.8	-24.96	67.88	0.9149	0.0616
24/08	959.5	33.1	29.38	33.74	-1.56	24.9	-30.02	64.30	0.8667	0.0582
24/08	957.7	32.7	29.35	33.27	-1.37	24.8	-35.01	58.82	0.7927	0.0589
24/08	952.1	33.3	29.40	32.80	-2.21	24.9	-40.03	52.60	0.7090	0.0619
24/08	936.5	32.4	29.33	32.29	-1.61	24.9	-44.99	47.55	0.6408	0.0575
24/08	917.7	31.9	29.28	31.87	-1.37	24.9	-50.00	43.70	0.5890	0.0542
24/08	889.3	32.6	29.21	31.21	-2.43	24.9	-55.00	36.27	0.4888	0.0517

Table D-8

Incident Angle Performance Test Data

Black Chrome / Pyrex® Glass Receiver, Silver Film Reflector

Test Date 1993	NIP W/m2	Amb Temp °C	Temp In °C	Temp Out °C	Delta Air °C	Flow rate L/m	Incid. Angle °	Calc. Effic. %	Effic. Ratio	Ratio Error
25/08	940.7	31.4	29.25	34.41	0.38	24.7	0.00	71.07	1.0000	0.0659
25/08	942.4	32.3	29.30	34.35	-0.49	24.8	-5.01	70.59	0.9932	0.0652
25/08	939.2	32.7	29.38	34.27	-0.85	24.7	-10.01	69.18	0.9734	0.0647
25/08	929.8	33.0	29.36	34.11	-1.28	24.7	-15.03	68.76	0.9675	0.0649
25/08	933.6	33.3	29.42	33.96	-1.64	24.7	-20.00	66.30	0.9329	0.0624
25/08	924.3	33.4	29.46	33.73	-1.82	24.7	-25.02	63.95	0.8998	0.0630
25/08	915.1	33.7	29.45	33.37	-2.28	24.7	-31.02	60.37	0.8494	0.0617
25/08	912.6	34.4	29.48	33.10	-3.11	24.7	-35.02	56.92	0.8009	0.0620
25/08	900.1	34.0	29.41	32.59	-3.02	24.7	-39.99	51.44	0.7238	0.0557
25/08	872.2	34.3	29.39	32.27	-3.46	24.7	-43.02	48.84	0.6872	0.0587
26/08	936.2	29.7	28.99	34.01	1.77	24.7	-5.03	70.27	0.9887	0.0657
01/09	961.1	24.5	28.81	33.62	6.76	24.8	-15.03	67.52	0.9500	0.0641
01/09	939.0	24.9	28.44	32.70	5.63	24.8	-25.07	63.02	0.8868	0.0645
02/09	971.3	26.9	28.14	33.25	3.76	24.6	-5.02	68.97	0.9705	0.0643
02/09	945.3	27.6	28.26	33.18	3.12	24.6	-10.03	68.79	0.9680	0.0672
02/09	941.1	27.6	28.26	32.84	2.99	24.5	-19.78	65.88	0.9270	0.0622
02/09	934.1	28.9	28.35	32.64	1.58	24.6	-25.03	63.16	0.8888	0.0626
02/09	925.6	30.4	28.53	32.56	0.14	24.6	-30.02	60.90	0.8570	0.0603
02/09	916.9	30.4	28.59	32.33	0.10	24.7	-34.35	58.23	0.8193	0.0639
02/09	900.4	28.7	28.14	30.99	0.84	24.7	-45.21	47.37	0.6665	0.0576
02/09	897.7	29.5	28.25	30.60	-0.07	24.6	-50.03	40.25	0.5663	0.0585
02/09	846.5	29.5	28.05	29.36	-0.75	24.6	-60.01	25.82	0.3633	0.0565

Table D-8 (continued)

Incident Angle Performance Test Data

Black Chrome / Pyrex® Glass Receiver, Silver Film Reflector

Test Date 1993	NIP W/m2	Amb Temp °C	Temp In °C	Temp Out °C	Delta Air °C	Flow rate L/m	Incid. Angle °	Calc. Effic. %	Effic. Ratio	Ratio Error
25/08	940.7	31.4	29.25	34.41	0.38	24.7	0.00	71.07	1.0000	0.0659
25/08	936.0	29.6	29.18	34.26	2.11	24.6	0.00	70.24	1.0000	0.0651
25/08	946.0	31.5	29.23	34.33	0.30	24.7	4.99	70.77	0.9957	0.0649
25/08	942.6	30.8	29.24	34.12	0.84	24.7	10.02	68.83	0.9685	0.0643
25/08	940.5	30.8	29.31	33.91	0.79	24.7	15.01	65.87	0.9268	0.0629
26/08	808.9	21.5	28.61	29.90	7.77	24.8	60.01	26.93	0.3789	0.0527
26/08	774.8	20.4	28.81	29.68	8.85	24.8	64.01	20.09	0.2827	0.0521
30/08	956.4	20.9	28.63	33.43	10.09	24.9	10.32	67.57	0.9508	0.0650
30/08	946.3	20.4	28.57	32.91	10.33	24.9	20.01	63.28	0.8903	0.0620
30/08	906.3	19.2	28.18	31.33	10.52	25.1	41.20	51.73	0.7279	0.0627
30/08	892.6	19.0	28.10	30.81	10.40	25.0	45.01	45.92	0.6461	0.0592
30/08	844.9	17.7	27.90	29.62	11.04	25.1	54.99	32.96	0.4638	0.0598
03/09	983.2	25.3	26.14	29.04	2.24	45.8	0.00	70.98	1.0000	0.0885
03/09	991.0	25.5	27.92	33.30	5.14	24.6	0.00	70.31	1.0000	0.0883
03/09	961.0	22.0	27.54	32.59	8.10	24.7	5.01	68.94	0.9700	0.0878
03/09	943.2	21.0	27.32	32.13	8.69	24.7	9.99	67.78	0.9538	0.0868
03/09	928.3	20.3	27.28	31.74	9.16	24.8	15.01	64.90	0.9132	0.0849
03/09	913.0	19.6	27.39	31.44	9.78	24.8	20.00	60.76	0.8550	0.0823
02/09	960.1	24.1	27.89	32.20	6.00	24.9	25.02	62.42	0.8782	0.0606
02/09	952.9	23.9	27.84	31.85	5.95	24.8	30.01	59.39	0.8356	0.0596
02/09	945.1	23.6	27.81	31.43	5.99	24.8	35.03	55.07	0.7749	0.0578
02/09	930.7	23.2	27.73	30.93	6.13	24.8	40.01	50.40	0.7091	0.0580
02/09	915.5	22.4	27.65	30.37	6.63	24.8	45.01	44.78	0.6300	0.0565
02/09	896.9	21.7	27.55	29.80	6.97	24.8	49.99	38.75	0.5452	0.0560
02/09	869.4	20.9	27.40	29.07	7.34	24.8	55.05	30.83	0.4337	0.0767
02/09	839.4	20.1	27.28	28.52	7.83	24.9	59.99	25.22	0.3548	0.0507
02/09	802.2	19.3	27.30	28.00	8.34	24.9	65.03	15.93	0.2242	0.0890
02/09	747.0	18.7	27.46	27.87	9.00	24.9	69.99	11.29	0.1589	0.0540

Table D-9

Incident Angle Performance Test Data

Black Nickel / Solgel Glass Receiver, Silver Film Reflector

Test Date 1993	NIP W/m2	Amb Temp °C	Temp In °C	Temp Out °C	Delta Air °C	Flow rate L/m	Incid. Angle °	Calc. Effic. %	Effic. Ratio	Ratio Error
19/11	856.4	4.3	16.47	22.07	14.94	22.4	0.00	77.53	1.00	0.0712
19/11	894.0	9.6	18.48	25.14	12.19	19.4	4.99	76.95	0.9927	0.0661
19/11	966.0	9.3	18.69	25.79	12.98	18.5	10.01	73.53	0.9485	0.0613
19/11	977.5	9.0	18.77	25.75	13.31	18.5	15.01	72.18	0.9311	0.0587
19/11	965.6	8.7	18.85	25.42	13.47	18.6	20.01	70.08	0.9040	0.0573
19/11	973.8	8.5	18.94	25.34	13.63	18.4	25.02	67.96	0.8767	0.0555
19/11	97909	8.2	19.09	25.02	13.85	18.5	30.02	64.07	0.8265	0.0531
19/11	994.3	7.9	19.36	24.99	14.23	18.8	33.04	61.34	0.7912	0.0527
19/11	989.3	7.3	19.01	27.46	15.94	10.5	41.07	53.48	0.6898	0.0568
19/11	987.7	7.1	18.44	24.83	14.51	12.1	45.01	46.95	0.6057	0.0598
19/11	971.2	6.6	17.89	21.23	13.00	19.2	49.99	41.15	0.5308	0.0656
19/11	955.01	6.1	17.68	19.93	12.69	21.4	55.02	32.71	0.4220	0.0827
19/11	946.4	5.8	17.46	19.30	12.62	21.8	60.01	28.95	0.3735	0.0646
19/11	921.1	5.3	17.16	18.26	12.40	22.2	64.03	19.11	0.2464	0.0599
29/11	993.8	5.9	16.34	22.88	13.72	22.3	0.00	77.62	1.0	0.0561
29/11	969.9	4.8	16.44	22.63	14.71	22.0	4.99	75.15	0.9682	0.0674
29/11	1013.6	6.5	16.47	22.95	13.21	22.3	-5.00	76.18	0.9814	0.0549
29/11	1021.0	7.5	16.54	22.93	12.22	22.3	-9.98	75.59	0.9739	00543
29/11	1021.5	8.5	16.51	22.81	11.20	22.3	-14.99	75.32	0.9704	0.0543
29/11	1022.6	9.5	16.64	22.56	10.11	22.3	-20.01	71.72	0.9240	0.0525
29/11	1024.5	10.0	16.71	22.41	9.57	22.3	-25.01	69.77	0.8988	0.0521
29/11	1023.0	10.7	16.70	22.07	8.66	22.3	-30.00	66.87	0.8615	0.0512
29/11	1028.7	11.0	16.74	21.68	8.25	22.3	-34.96	62.20	0.8014	0.0476
29/11	1018.2	11.5	16.80	21.18	7.53	22.3	-40.00	57.05	0.7350	0.0474
29/11	1006.7	11.8	16.82	20.58	6.87	22.3	-45.03	50.72	0.6534	0.0445
29/11	993.9	12.1	16.85	20.09	6.40	22.3	-50.02	45.61	0.5876	0.0461
29/11	956.7	12.3	16.89	19.39	5.88	22.3	-55.01	37.87	0.4879	0.0580
29/11	922.3	12.6	16.83	18.52	5.03	22.3	-60.02	27.89	0.3593	0.0418
29/11	878.6	13.0	16.81	17.93	4.35	22.3	-64.98	20.87	0.2689	0.0446

Performance of the Sun Tracking System

The IST sun-tracking system uses two photocells; one mounted on each side of the receiver glass near the center of the collector module. These cells sense concentrated light focused onto the receiver. For adequate tracking sensitivity, one cell would ideally be located such that the cell would be half illuminated by light from the very top edge of the mirror. The other cell would be half illuminated by light from the bottom edge of the mirror. If the cells are moved such that they see light reflected from some mirror location inward from the edges, there is not enough difference in the received light, unless the mirror moves a relatively large distance away from the true sun position. Since a typical parabolic trough must point at the sun within about 0.2 degrees

for optimum performance, the sun-tracking system must be capable of very small corrections to the apparent motion of the sun.

Figure D-19 shows data taken during one of the low-temperature water tests. The sun elevation position was increasing smoothly; the collector must follow this motion with minimum error. From the figure, collector elevation can be seen to move in small steps of about 0.1 degree. The tracking error line in the plot is the difference between sun elevation and collector elevation. The tracking accuracy shown here is quite good, and should keep the collector properly focused.

Because the tracking system used light reflected from the edges of the mirror, the reflected light may not be balanced at the sensing photocells if there are any imperfections in the mirror surface at either edge. As the incident angle of the incoming solar beam changes, the reflection point moves along the length of the mirror edge. Over the range of incident angles from -70 deg to + 70 deg, the reflection point on the IST test collector moved almost the entire length of the mirror edge. There were slight imperfections along the mirror edge at several places; in general these were small enough that no significant mistracking occurred. There were a few problem areas that are discussed below.

Figures D-20 and D-21 show incident angle, cosine of the incident angle and incident angle modifier on two different test days. The incident angle modifier curve should be a smooth curve approximately paralleling, but slightly less than the cosine curve (for example, see Figure D-14). The variations in the curve are caused by slight changes in the system that are causing the heat gain to change. The small constant variations in the curve are a result of noise and slight fluctuations in the measured flow and temperatures, and are not significant. Two larger variations were seen on all test days; these are at about 60-70 deg incident angle in the morning, and at about 10 deg incident angle in the morning.

At about 60-70 deg angles, the shadows from the drive wheel and other structure at the end of the trough were being reflected to the tracking sensors, resulting in some mistracking. The event at about 10 degrees, most visible in Figure D-21, is the result of shadows from structural bars crossing the front of the mirror. These bars can be seen in the collector photo, Figure D-1. A detail plot of the tracking error from Figure D-20 is shown in Figure D-22.

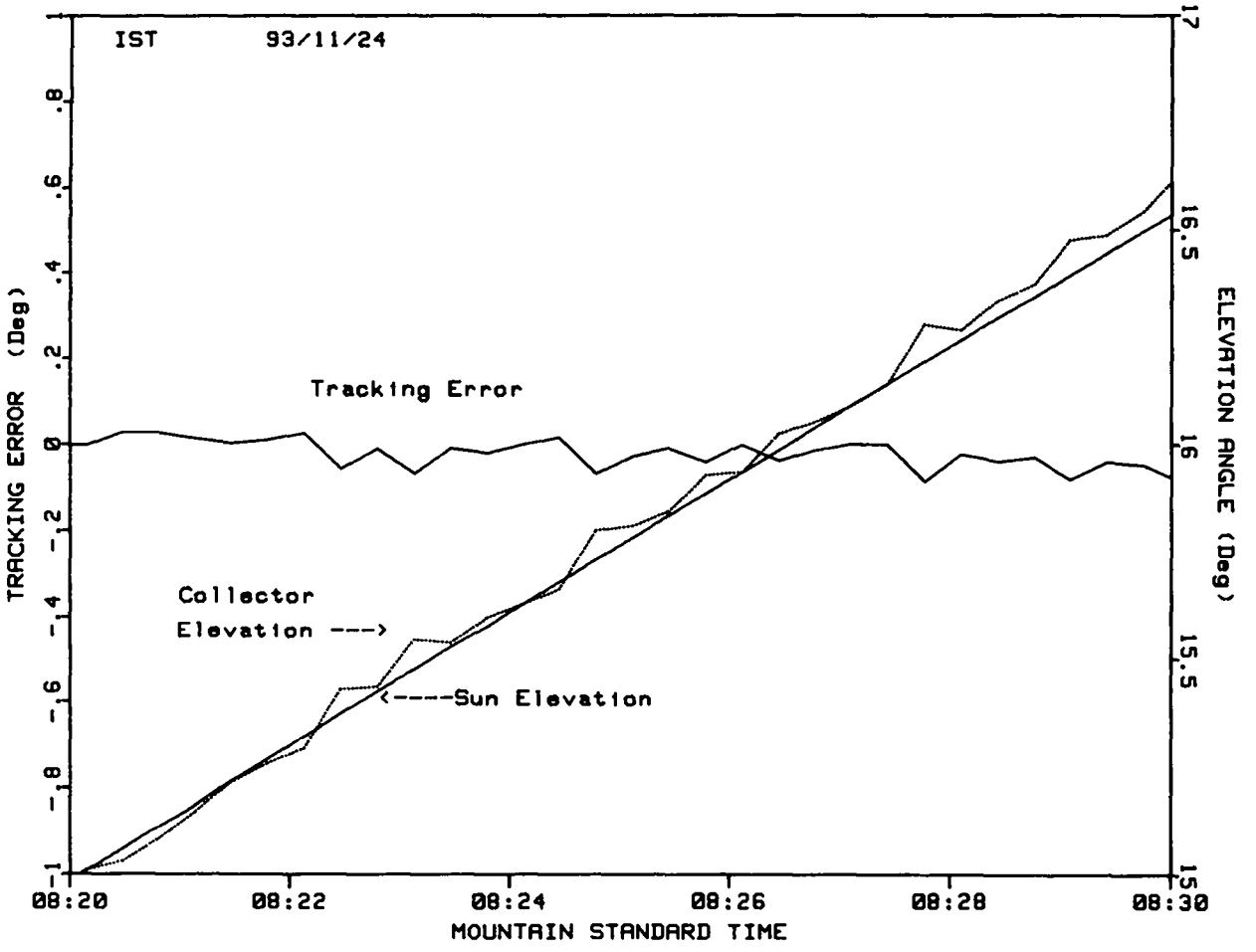

Figure D-19. Tracking Angle and Tracking Error

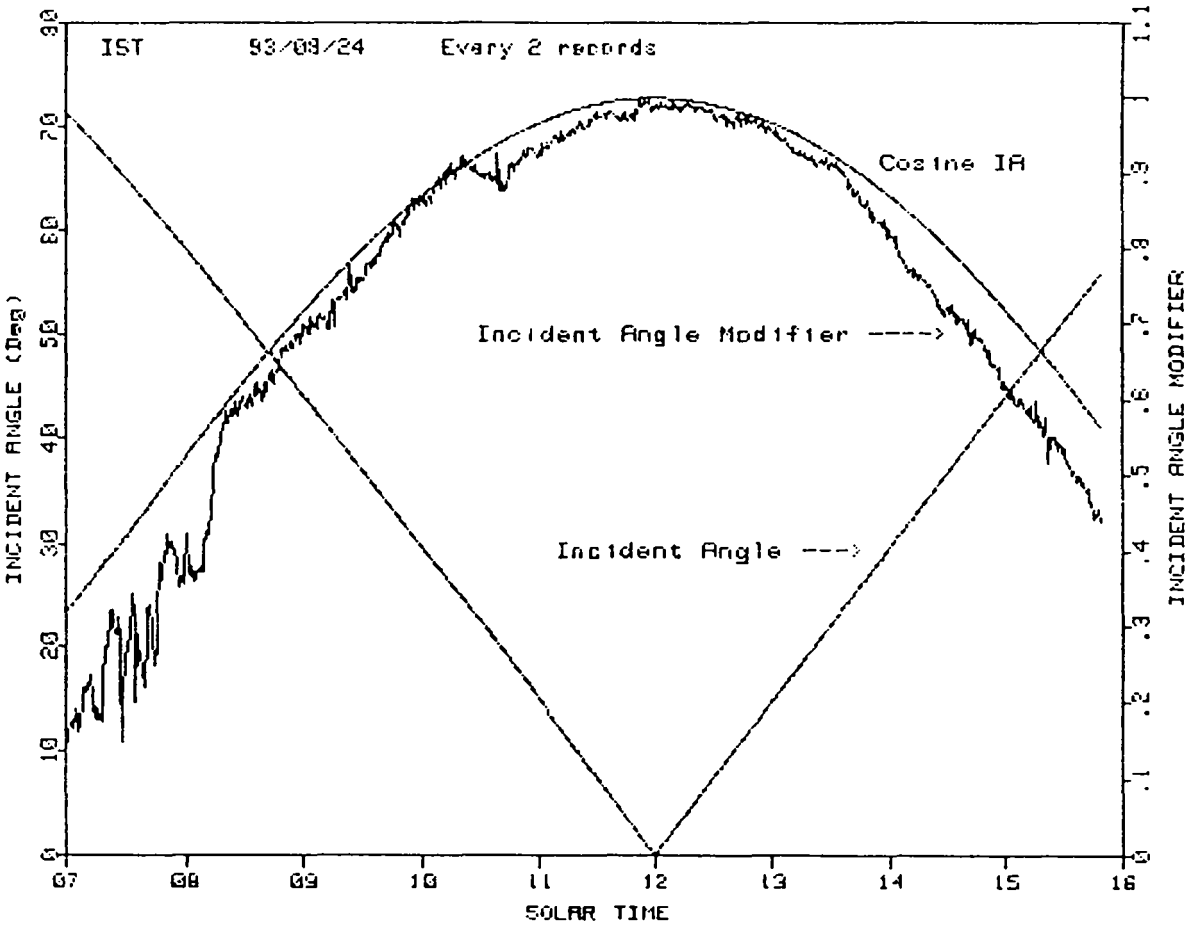

Figure D-20. Incident Angle, Cosine, and Incident Angle Modifier

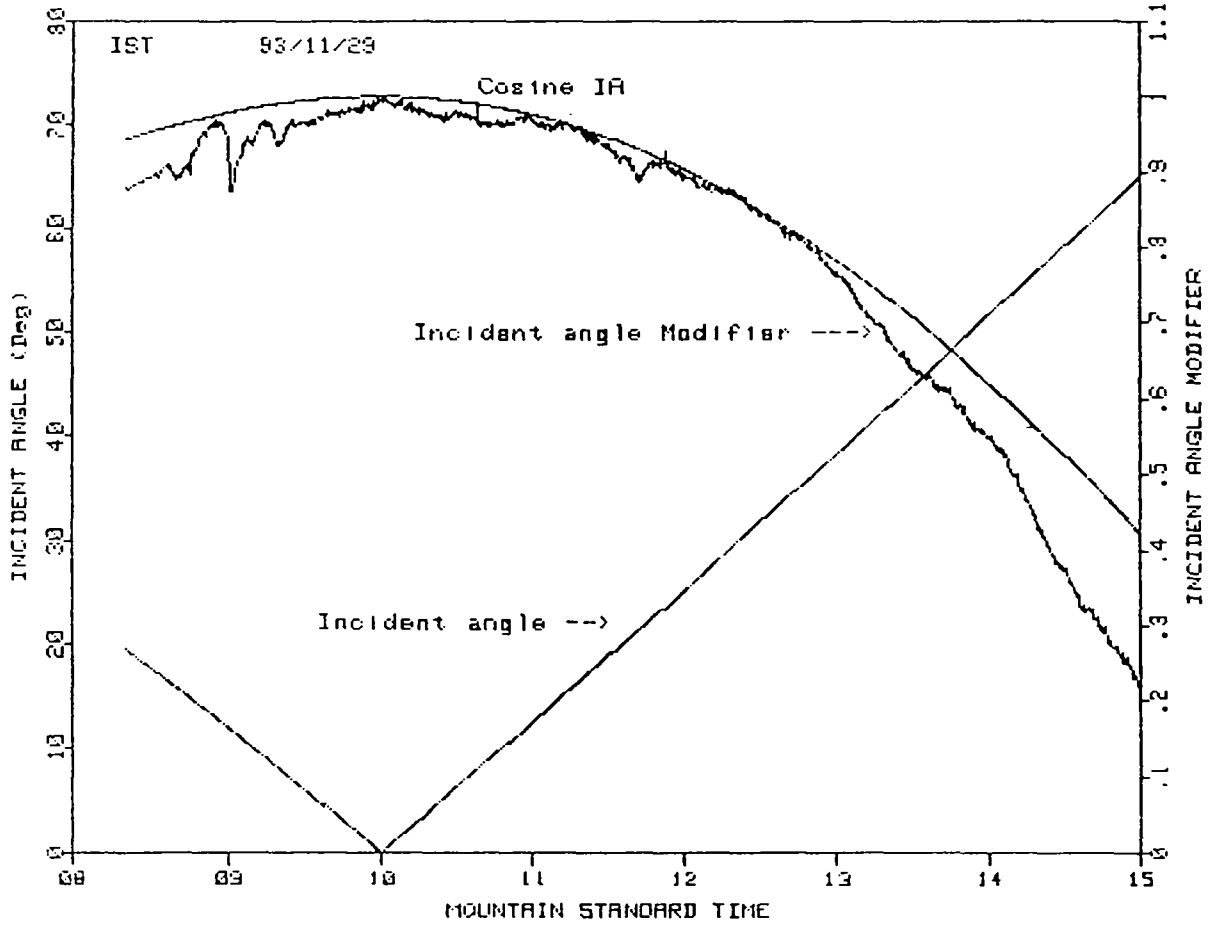

Figure D-21. Incident Angle, Cosine, and Incident Angle Modifier

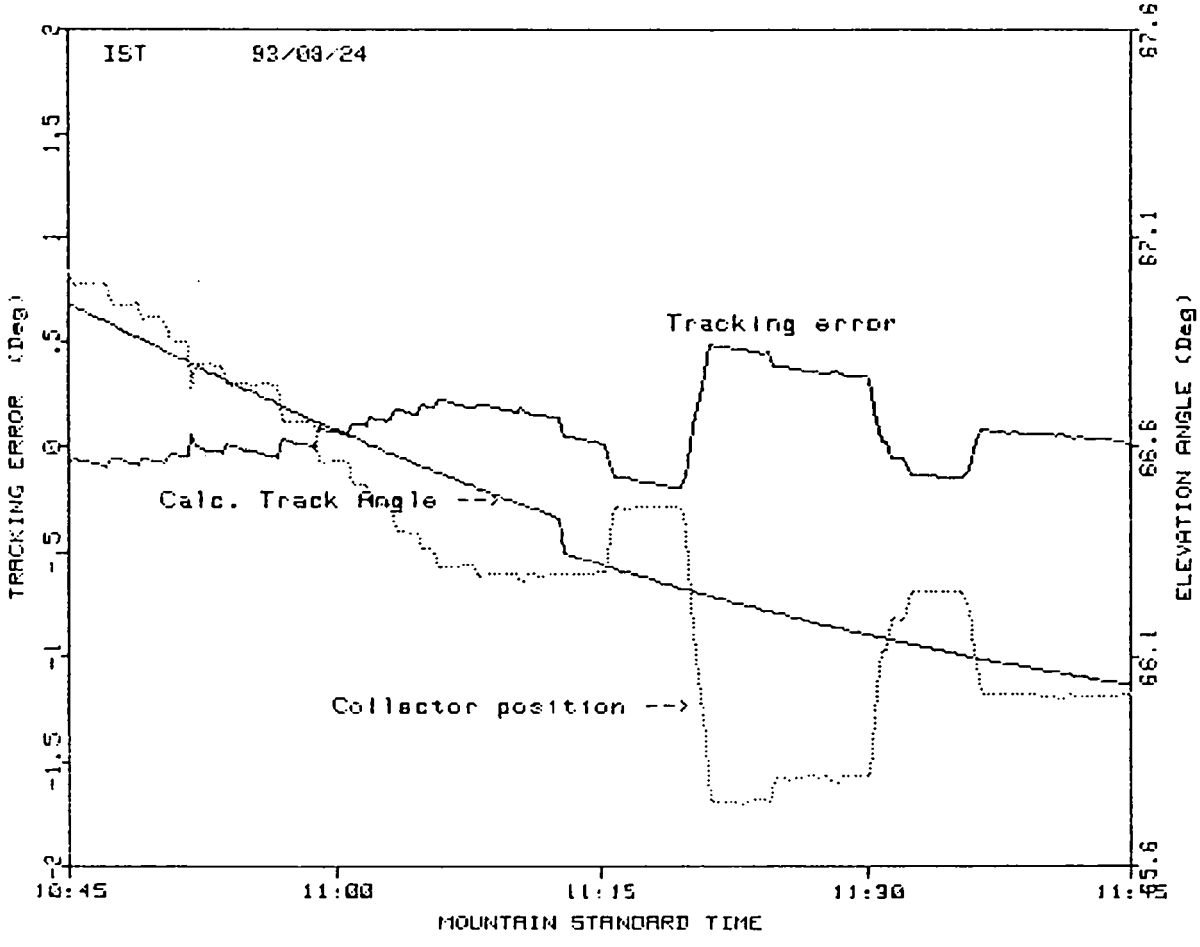

Figure D-22. Tracking Angle and Tracking Error

There is little that can be done to correct these problems with a reflected light tracking system. The errors can be made to move to other times of the day by moving the sensors to a different location along the length of the receiver tube. However, the errors will still be there, just occurring at a different time. Fortunately, the worst errors occur at very high incident angles, where there is little impact on total energy output, since there is little energy that can be collected in any case. The other tracking errors at incident angles less than 50 degrees are much smaller, last for shorter times, and can cause only a small loss of collected energy.

Figure D-23 shows a different way of plotting the tracking corrections a collector makes to follow the sun. The figure is from test data of a different type of optical tracking system, from a different collector manufacturer (See Ref. 1, pp.74). The plot shows time, direction of tracking correction, and magnitude of the correction. Ideally, each tracking update would be evenly spaced in time, and have the same magnitude. Since sun elevation is increasing from sunrise to noon, morning corrections should all be in the same direction. For an East-West collector axis, afternoon corrections would be in the opposite direction. The tracking shown in Figure D-23 was not perfect, but still very good.

Figure D-24 shows a similar tracking plot for the IST reflected light system. The large corrections in early morning correspond to the tracking errors shown at the same time in Figure D-20. Figure D-25 shows an hour of Figure D-24, with an expanded time scale. Tracking error sensitivity may have been set slightly too small, as many of the corrections shown in Figure D-24 are 0.05 degree or less. More important are the track corrections that are too large, which causes the system to have to back up with an opposite correction. Some of these can also be caused by very small irregularities in the edge of the reflecting mirror surface.

Data Analysis

The efficiency and thermal loss equations directly derived from the measured data in this Appendix are of limited use by themselves, because they are limited to narrow ranges of incident solar irradiance. For application to a collector field under constantly changing values of incident sunshine, an extension of the performance equations is needed.

By linear scaling of thermal losses between the in-focus loss (high value of insolation on receiver) and the measured thermal loss (zero insolation) we can derive the collector heat gain and efficiency for any desired incident solar irradiance. This scaling procedure (see Appendix C) was performed for a matrix of insolation and temperatures. A multiple regression of the data matrix then produced a performance equation for the collector. This equation should predict performance over the temperature range from ambient to 350 °C, and for insolation from zero to about 1100 W/m2. Repeated for each of the receiver configurations tested, four equations resulted, and are shown in Table D-11.

A performance equation for the aluminized-film reflector is not shown because of the limited test data obtained. Since the thermal losses would have been the same as the silver-film / black chrome / solgel glass receiver, a close approximation for an aluminized film collector would be the equation for the silver film configuration, with an optical efficiency (first equation term) of about 66-67%.

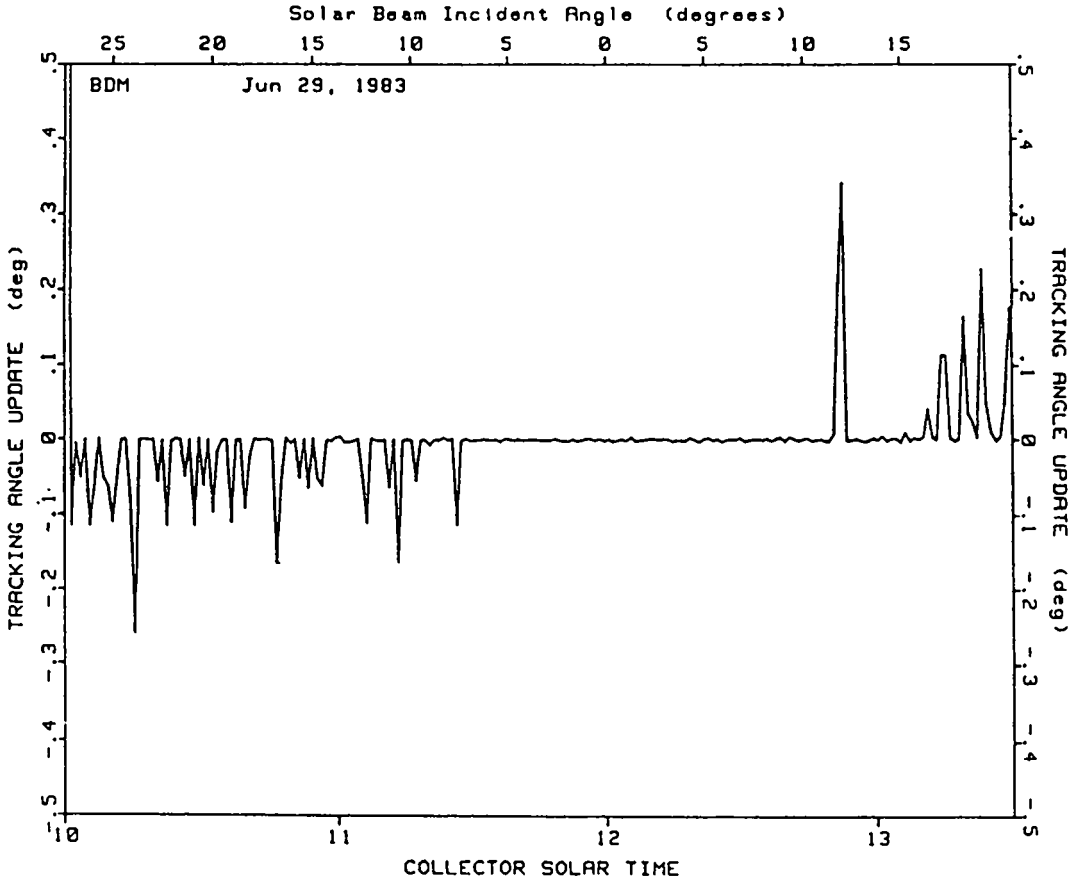

Figure D-23. Example Tracking Angle Updates

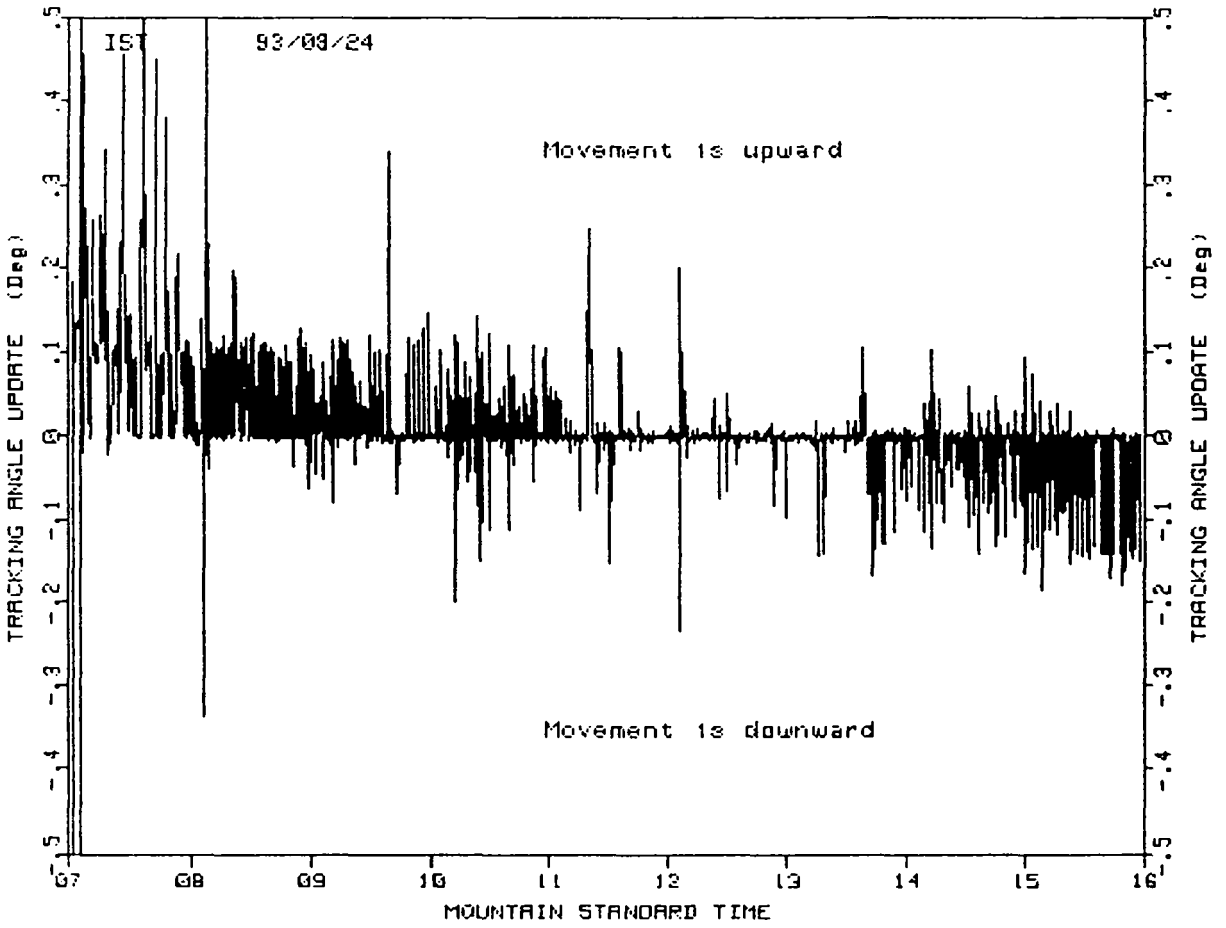

Figure D-24. IST Tracking Angle Updates for 24 August

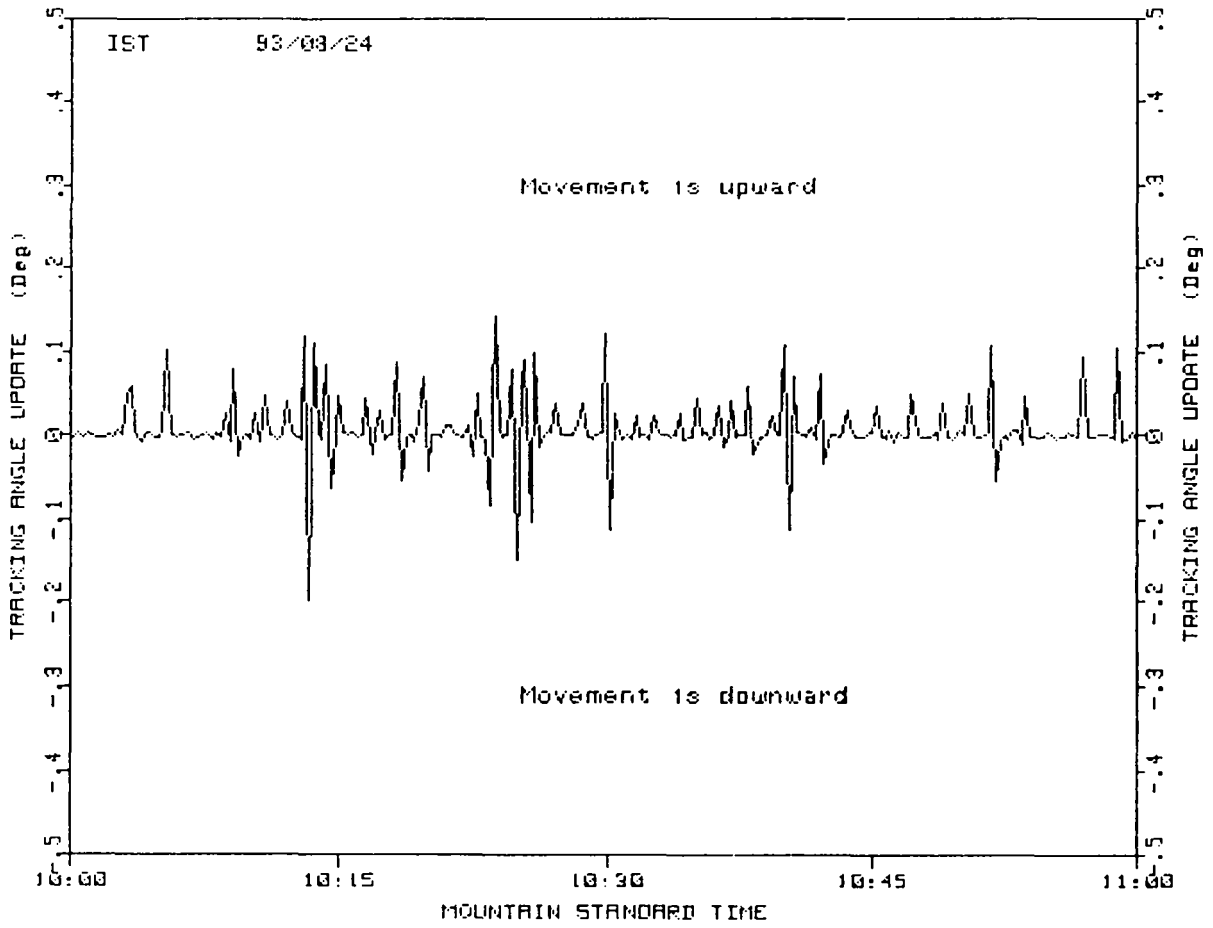

Figure D-25. Tracking Angle Updates -- Expanded Scale

Table D-10

IST Collector Performance Equations For Silver Film Reflector

Black Nickel selective absorber, Solgel receiver glass

$$\eta = K\,[76.25 - 0.006836\,(\Delta T)] - 14.68\,(\Delta T/I) - 0.1672\,(\Delta T^2/I) \quad (1)$$

Black Nickel selective absorber, Pyrex receiver glass

$$\eta = K\,[72.36 - .006836\,(\Delta T)] - 14.68\,(\Delta T/I) - 0.1672\,(\Delta T^2/I) \quad (2)$$

Black chrome selective absorber, Solgel receiver glass

$$\eta = K\,[74.52 - 0.009764\,(\Delta T)] - 23.26\,(\Delta T/I) - 0.1355\,(\Delta T^2/I) \quad (3)$$

Black chrome selective absorber, Pyrex receiver glass

$$\eta = K\,[70.75 - 0.01028\,(\Delta T)] - 23.27\,(\Delta T/I) - 0.1355\,(\Delta T^2/I) \quad (4)$$

Incident Angle Modifier, K

$$K = \cos(Ia) + 0.0003178\,(Ia) - 0.00003985\,(Ia)^2 \quad (5)$$

In Table 10 performance equations (1) through (5):

η	=	Collector efficiency, in percent
K	=	Incident angle modifier
I	=	Incident direct normal solar irradiance, W/m^2
ΔT	=	Avg. receiver fluid temperature above ambient air temperature, °C
Ia	=	Solar beam incident angle, in degrees

Figure D-26 is a plot of the complete performance equation for the silver mirror / black nickel / solgel receiver, for several values of insolation, at zero incident angle. Efficiency is significantly reduced with increases in the sunlight incident angle. Figure D-27 is for the same collector configuration as D-26, but now for a 50 degree incident angle.

Figure D-28 shows the silver mirror / black nickel / solgel collector efficiency for the complete range of temperature and insolation. Performance equation plots for the other three receiver configurations are not shown here; they look very similar to Figure D-28, but are reduced somewhat in heat collection efficiency.

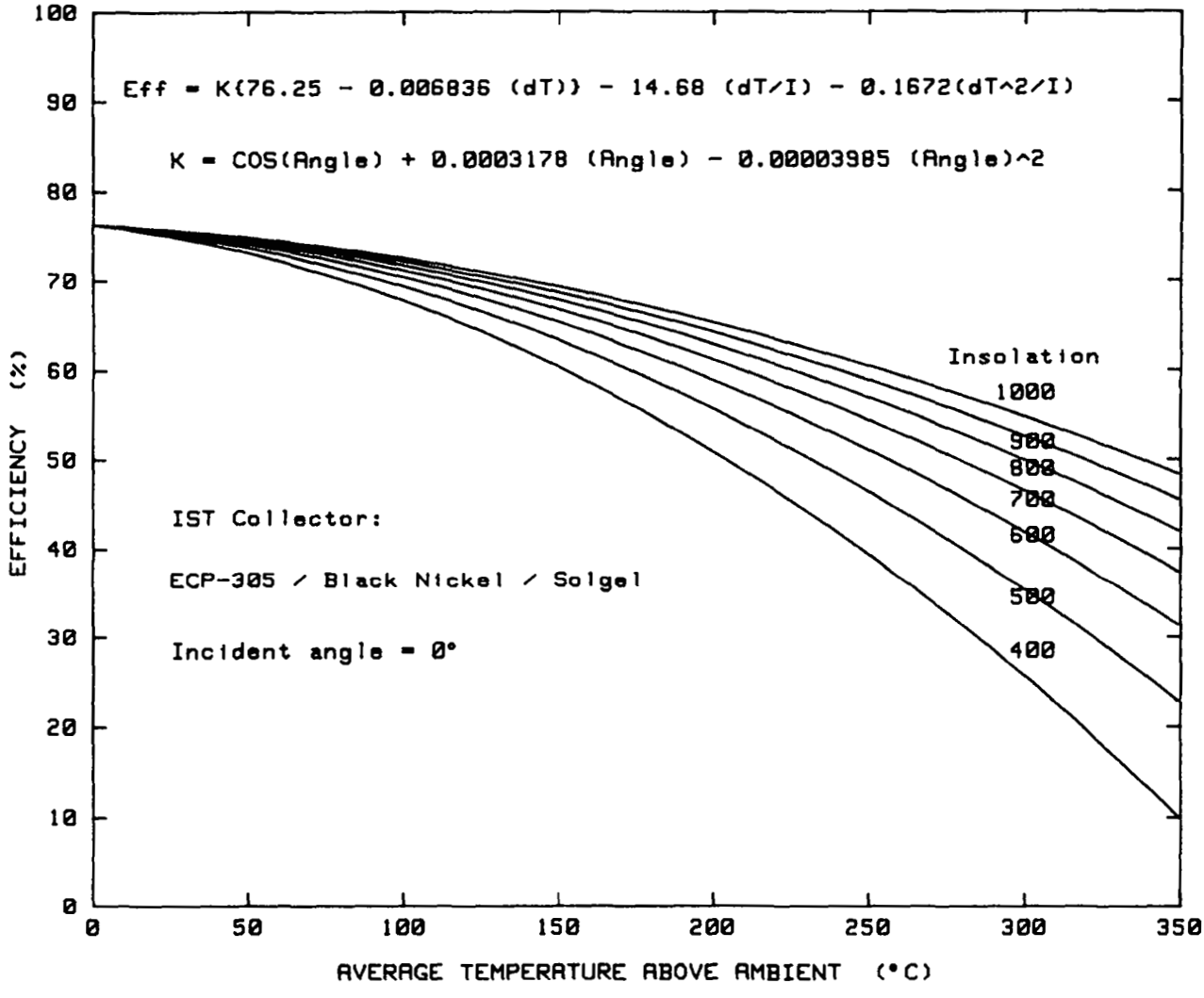

Figure D-26. IST Collector vs Temp & Insolation at Zero Incident Angle

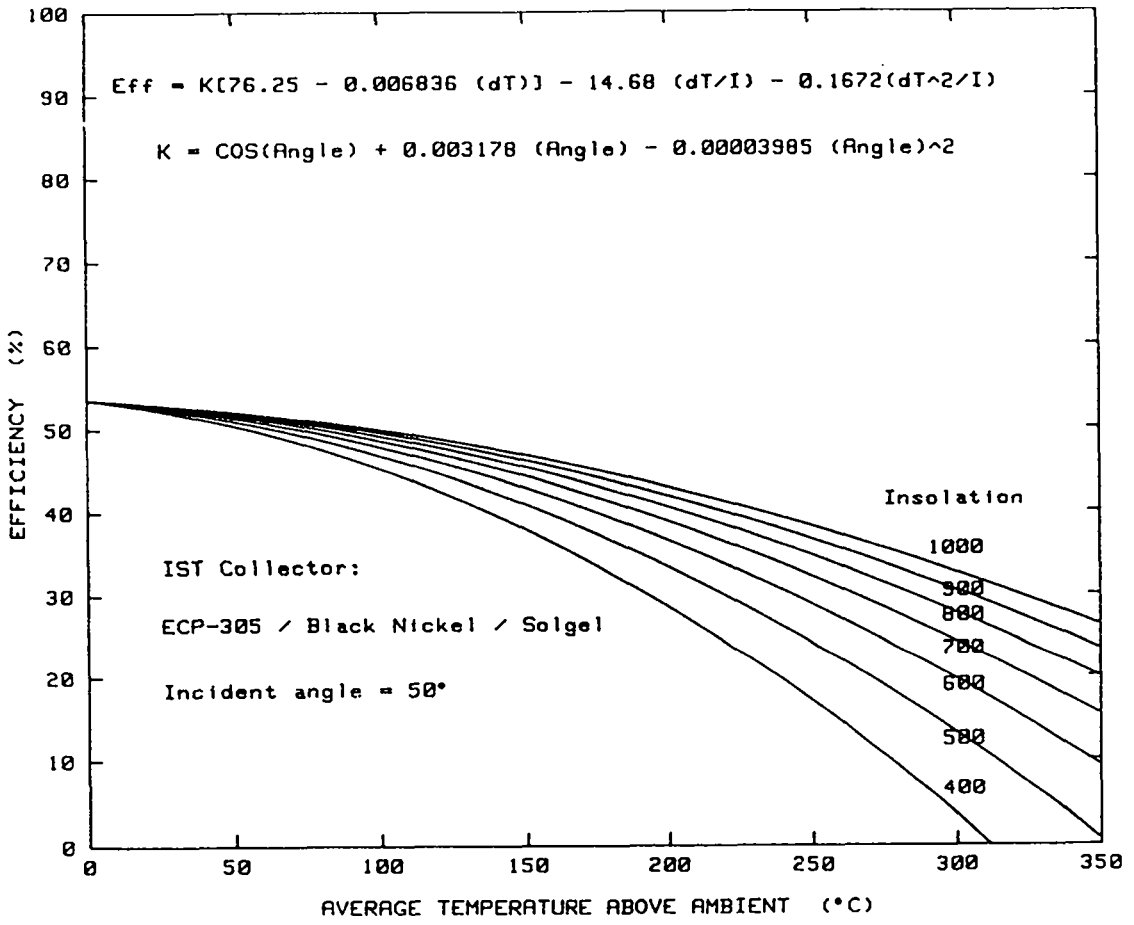

Figure D-27. IST Collector vs Temp & Insolation at 50 Deg Incident Angle

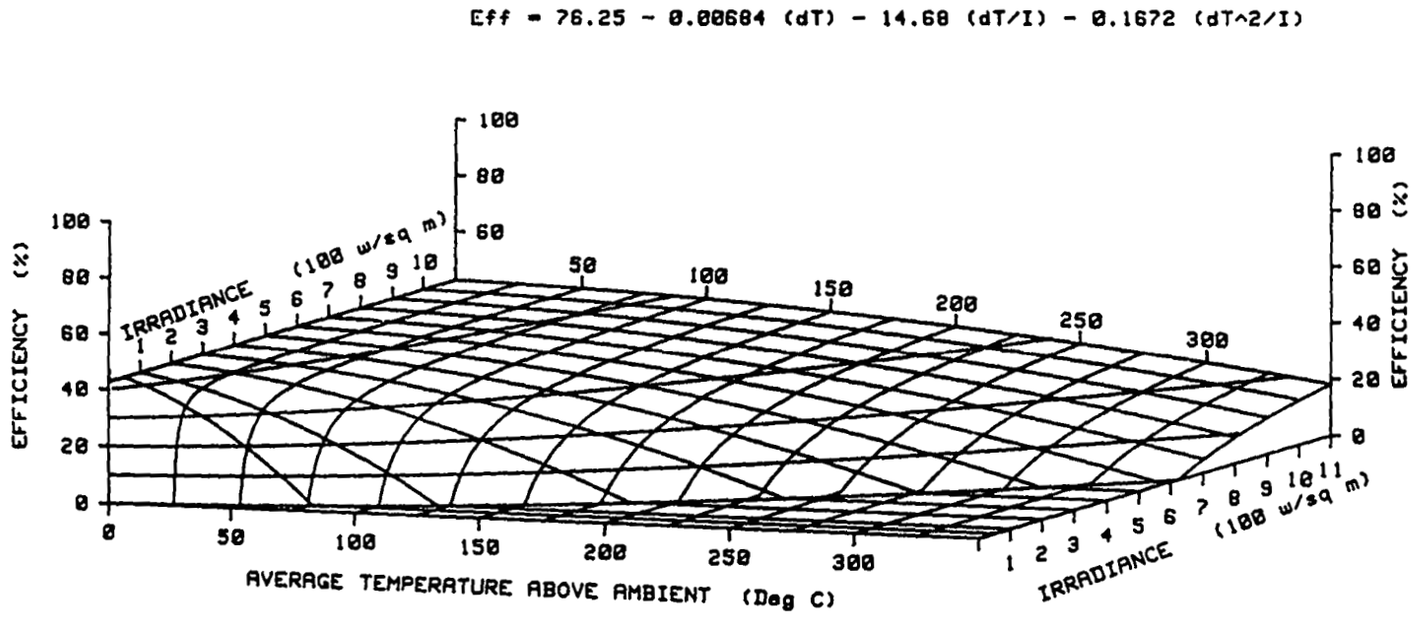

Figure D-28. IST - ECP-305/Black Nickel/Solgel Glass at 50 Deg Incident Angle

APPENDIX D

References

Cameron, C. P., and Dudley, V. E., 1986. SAND85-2317, *BDM Corporation Modular Industrial Solar Retrofit Qualification Test Results.* Albuquerque, N. M.: Sandia National Laboratories.

APPENDIX E

THEORETICAL MODEL

Intentionally Left Blank

Theoretical Model

Introduction

Test data from the IST trough performance tests were compared to results of a heat transfer code used for modeling trough collectors. This code (ref. 1) was originally developed for analyzing the thermal performance of KJC Operating Company's parabolic trough collectors at Boron, California. The model is based on thermal analysis provided by Sandia National Laboratory's Solar Thermal Department. One dimensional, steady-state heat losses and heat gain of the heat transfer fluid are calculated per unit length of a trough receiver. Calculations are a function of fluid flow rate, bulk fluid temperature, and solar conditions (direct normal insolation, date and time). The model was developed by Sloan Solar Engineering, Austin, Texas. It has been validated by comparing Sandia's performance test results of KJC's trough collectors with the model's predicted performance results.

A summary of the model and direct comparisons of IST performance test results to the predicted performance of IST collectors are presented below.

Model Definition

The heat available at the receiver surface is determined directly from specified solar conditions and the trough's optical properties. Under steady state conditions, some portion of this energy will result in sensible heating of the fluid. The remainder of the heat flow will be given up to the environment through conduction, convection and radiation losses. The following outlines the methodology used in this model:

Given:

- Direct normal insolation, site location, date, time, ambient conditions
- Geometric configuration and material optical property data
- Fluid flow rate and bulk inlet temperature

Calculation Method:

- Assume an envelope temperature and an receiver surface temperature
- Iterate for envelope temperature until the net heat flow in the envelope annulus region matches the external heat loss to the environment
- Using the available insolation, calculate the heat loss at the receiver and the heat gain of the fluid
- Compare heat losses from the above two steps and re-iterate on these steps as necessary until the two heat loss calculations are equal.

A flow chart of the model structure is shown in Figure E-1.

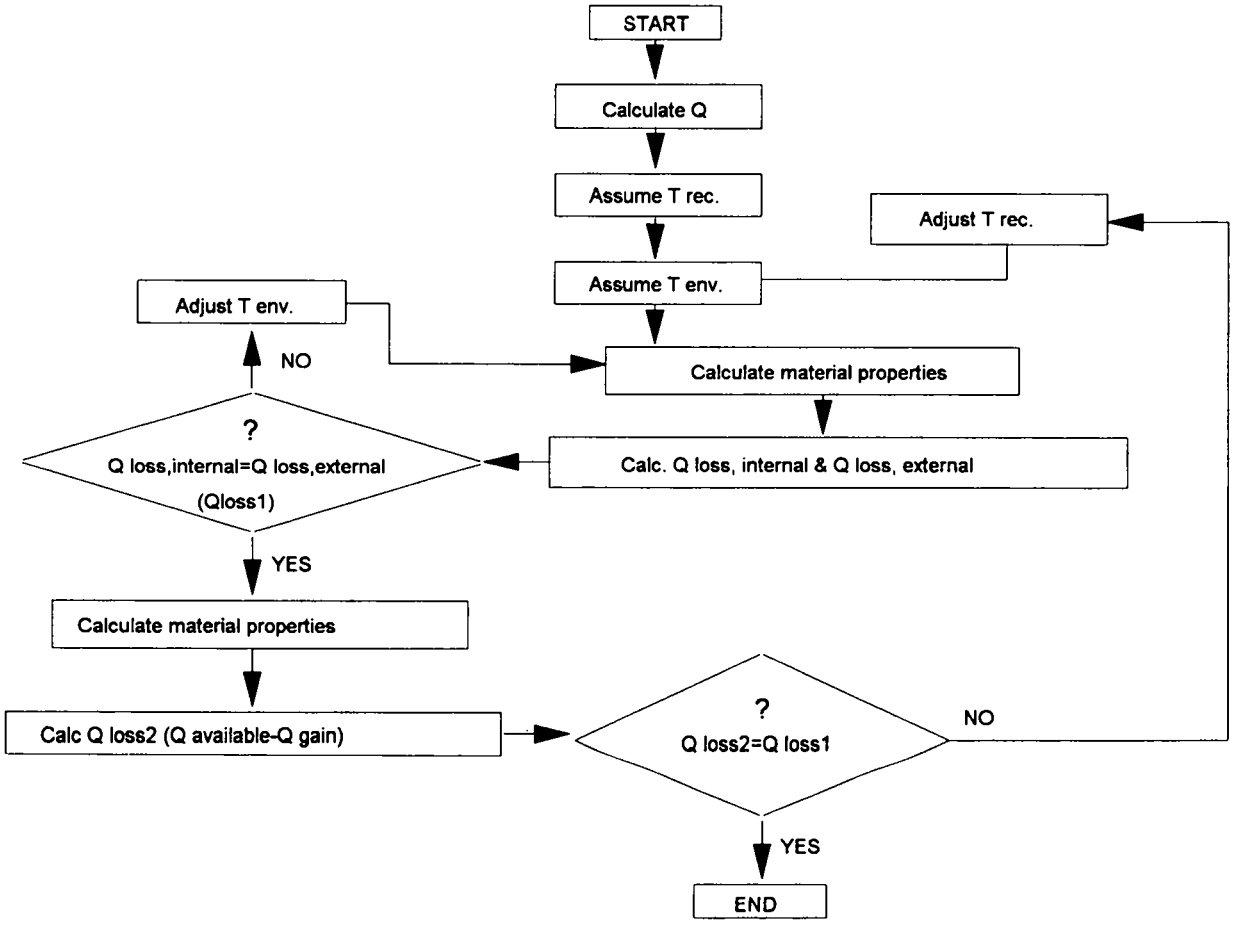

Figure E-1. Model Flow Chart

For the purpose of comparing the model results with empirical data, the optical efficiency test results for the IST collectors were used as the optical efficiency inputs to the model. Comparisons are for an IST collector using ECP-305 silver reflective film, with the following receiver configuration:

- 5.08 cm OD, 4.76 cm ID black chrome receiver with either Pyrex® glass envelope or Pyrex® glass envelope coated with a solgel anti-reflective film (AR)
- 5.08 cm OD, 4.76 cm ID black nickel receiver with AR coated Pyrex® glass envelope
- 3.18 cm flow restriction plug centered inside the receiver tube
- flow rate of 49 L/min of Syltherm® 800 heat transfer oil

The following material optical properties, based on Sandia's test measurements, were used for modeling the IST collector:

- black chrome solar averaged absorbtivity of 0.92
- black nickel solar averaged absorptivity of 0.96
- ECP-305 solar averaged reflectivity of 0.93
- Pyrex® glass solar averaged transmissivity of 0.91
- Pyrex® AR glass solar averaged transmissivity of 0.94

Syltherm® 800 fluid properties were based on manufacturer's specifications.

Emissivity values for the different receiver tubes were based on measured emittance of black chrome and black nickel receiver tube samples. A two-point linear fit of the measured emissivity data was used in the model. Black chrome emissivity used was 0.1 at 100°C and 0.25 at 300°C. Black nickel emissivity used was 0.14 at 100°C and 0.35 at 300°C.

There are several conditions specific to Sandia's test procedure that differ from the normal operating conditions of the IST collector; these are summarized below:

- Sandia's tests incorporate a horizontal axis tracking platform that effectively converts a single axis tracking trough into a two-axis tracking collector.
- The performance tests at Sandia used Syltherm® 800 as the fluid; however, IST plans to use Caloria as a heat transfer fluid. These two types of oil have different fluid properties, thus the thermal characterization will be somewhat different. The overall trough performance should be similar with either type oil.
- Performance tests were conducted at a nominal flow rate of 22.7 L/min of water flow for characterizing optical efficiency and incident angle modifier. A nominal oil flow of 49 L/min, which is about 43% of normal flow conditions for an IST

system, was used to characterize trough performance at elevated temperatures. To accommodate the reduced volumetric flow rates, a 3.18 cm diameter flow restriction was centered in the 4.76 cm inside diameter receiver tube. This restriction helped increase the fluid velocity, thus increasing the Reynolds number. All of the performance tests were operated with Reynolds numbers in either the transition or turbulent regions.

Due to the differences in fluid properties and the reduced Reynolds numbers, the thermal performance tests might over predict thermal losses, and thus report lower thermal efficiencies. To investigate this point, an IST collector without a flow restriction plug was analyzed at 113.6 L/min Syltherm® flow. Results of this analysis are discussed later in this section. The results presented below are direct comparisons between measured and modeled data. The figures are plots of either trough receiver efficiency or thermal loss versus fluid temperature above ambient air temperature. All model runs presented are based on the following assumptions:

- ambient air temperature of 22°C (72°F),
- ambient air pressure of 1 atm,
- direct normal irradiance of 950 W/m^2 for on-sun conditions,
- L/min flow rate, no winds,
- Albuquerque as the site location.

Model Results

Figures E-2, E-3 and E-4 are plots showing on-sun trough efficiency comparisons for either black chrome or black nickel receivers. Within the uncertainty bounds of the test data, a good agreement is shown between the predicted performance and the measured data. The significant factor for the on-sun case is the proper modeling of the fluid internal convection. For the off-sun condition, (Fig. E-5 and E-6) fluid temperatures are generally only a few degrees greater than receiver surface temperatures. Because of small delta-T's when off-sun, the influence of fluid internal convection on the overall heat loss solution is small.

For the on-sun case, the model predicted the receiver surface temperatures to be 8°C to 23°C greater than the bulk fluid temperatures. Since the model is based upon one-dimensional heat flow methods and not two-dimensional heat flow, the actual receiver surface temperature could be much greater than what the model predicts. Clearly, the magnitude of both the measured and predicted heat loss values are dependent upon the actual or assumed receiver surface temperature.

Note that the predicted efficiencies for the black nickel receiver shown in figure E-4 is just outside the uncertainty bounds of the test results. This is not significant enough to be of major concern, since several factors may contribute to this. No wind conditions were assumed for the model, whereas wind was present during some of the tests. Wind during a test would slightly increase the heat losses from the receiver, thus a lower efficiency would be reported. Another factor is the receiver emittance. Emittance values used for the receiver tubes were based on the measurements of small tube sections and not the actual receiver tube used in the test. In addition, the model predicts somewhat higher efficiency values within the temperature range 75-250 C above ambient. If the assumed emittance values within this range were too low, then the model would predict

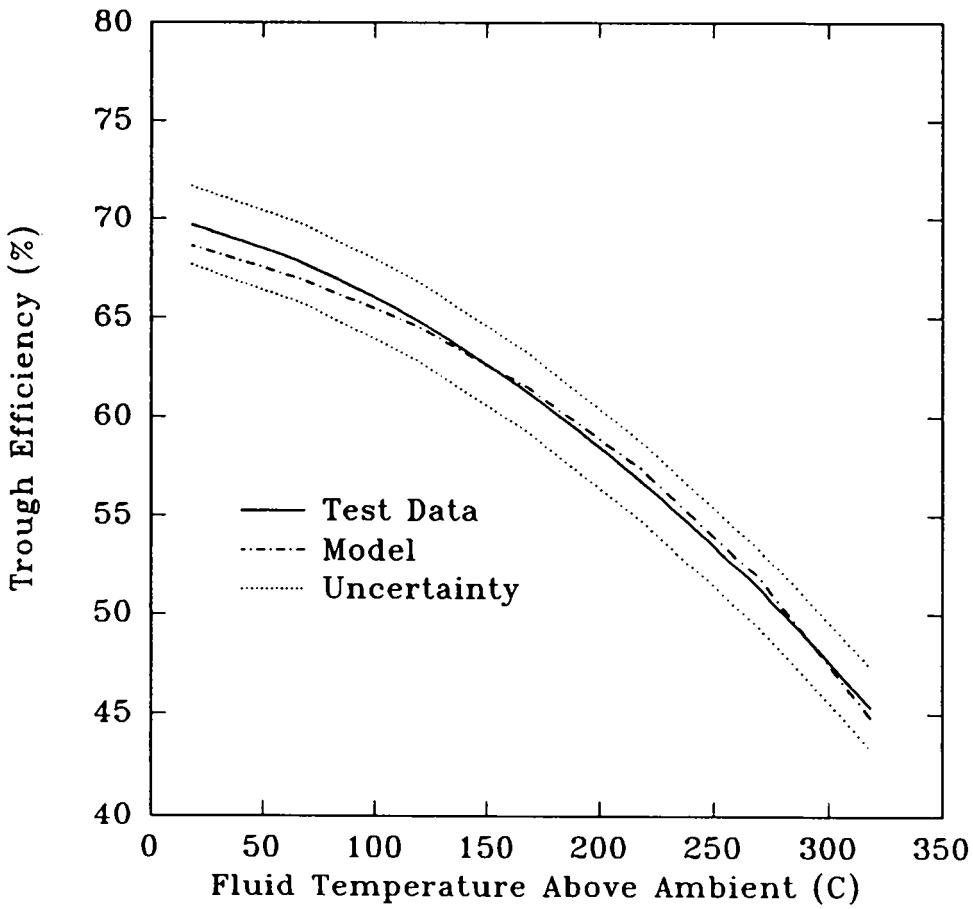

Figure E-2. Comparison of predicted trough efficiency to test data for the IST trough with a black chrome receiver and a Pyrex glass envelope.

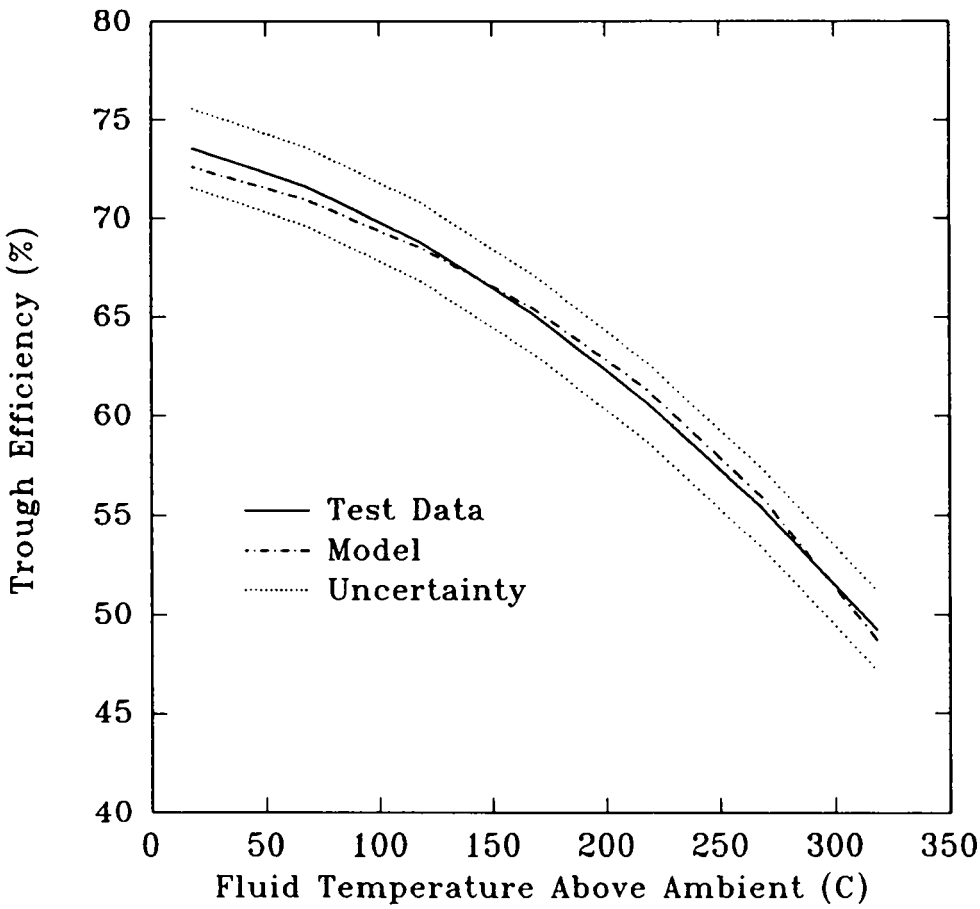

Figure E-3. Comparison of Predicted Trough Efficiency to Test Data for the IST Trough with a Black Chrome Receiver and a Pyrex Glass Envelope Coated with Sol Gel

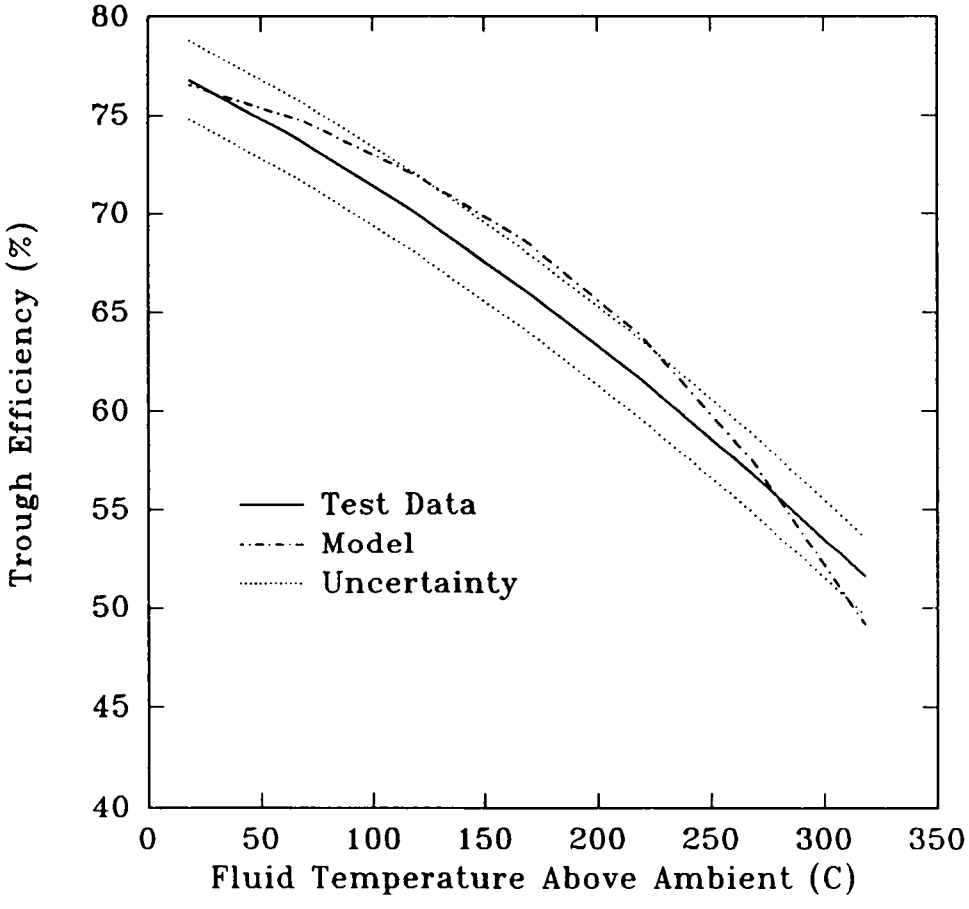

Figure E-4. Comparison of Predicted Trough Efficiency to Test Data for the IST Trough with a Black Nickel Receiver and a Pyrex Glass Envelope Coated with Sol Gel

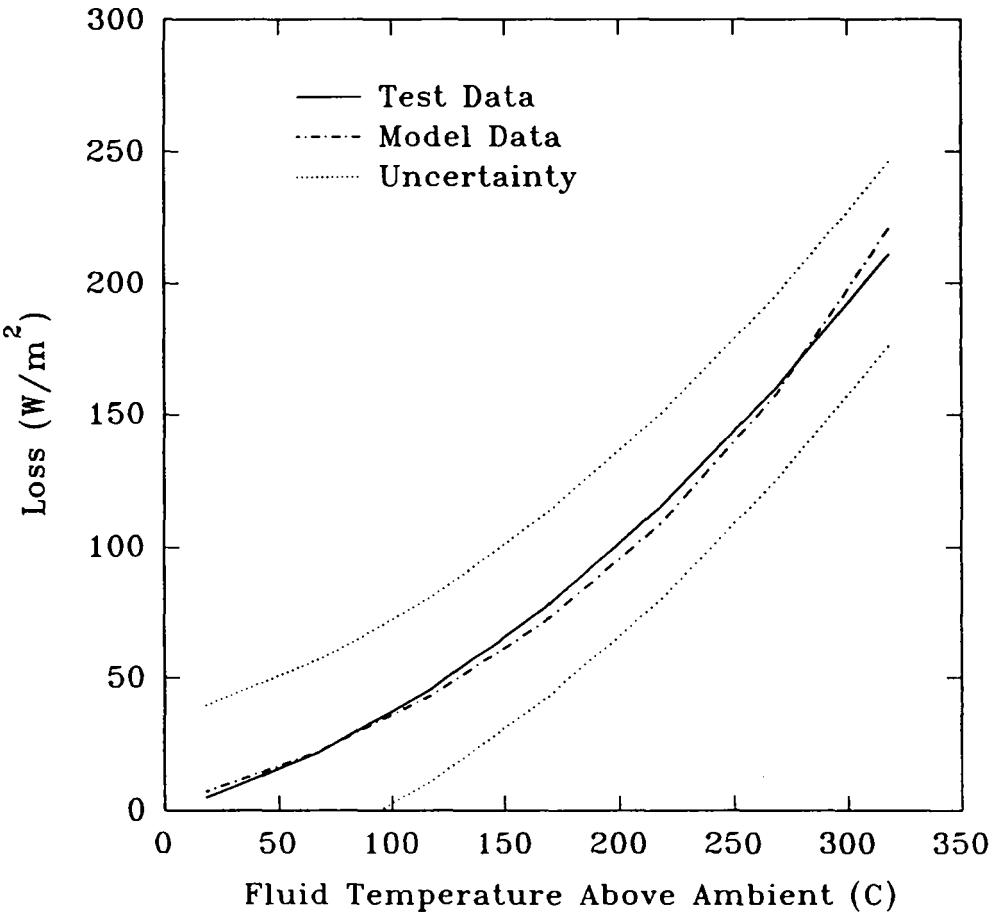

Figure E-5. Comparison of the Out-of-Focus Thermal Loss for the IST Trough with a Black Chrome Receiver

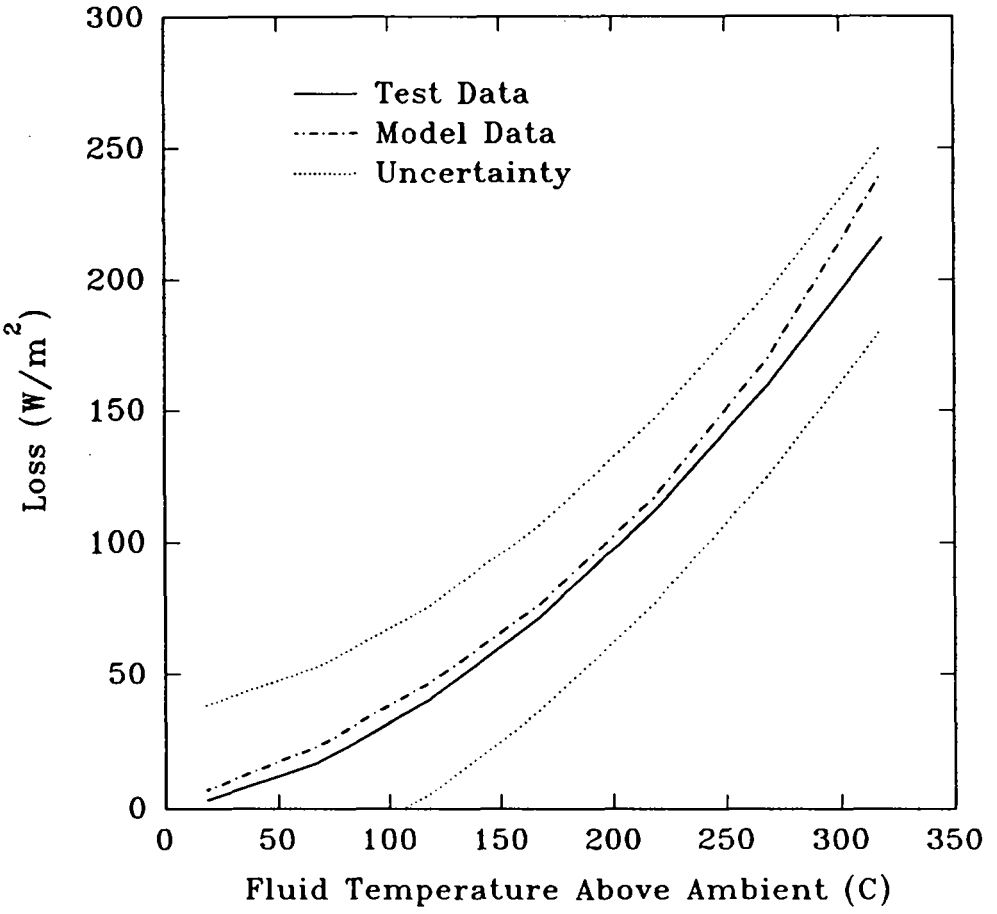

Figure E-6. Comparison of the Out-of-Focus Thermal Loss for the IST Trough with a Black Nickel Receiver

higher than measured efficiency values. Assuming a linear dependence of emittance with temperature over this temperature range probably under estimated the emittance -- thus the over prediction of the thermal performance.

A comparison of the thermal losses, no-sun condition, is presented in figure E-5. Again a good agreement is shown between the predicted losses and the test data. External heat losses are relatively small due to small delta T's between the receiver surface and the fluid temperatures. Since both the fluid and ambient temperatures were measured during a test, the only significant uncertainty is the emittance of the receiver. Predicted radiation losses are directly proportional to the emittance values. Therefore, more detailed characterization of emittance of the actual receiver tube could significantly impact the predicted performance of a trough collector, as previously discussed.

The model was also used to investigate the effect of the flow restriction used in the performance tests. The model was setup to analyze the efficiency of a non-restricted black-nickel receiver with a flow rate of 49 L/min of Syltherm® 800. The results obtained from this test case were essentially the same as the test runs made with the flow restriction placed inside the receiver tube. It would seem that using the flow restriction plug in the trough performance tests did not significantly change the test result. For both the restricted flow and full flow conditions, the predicted receiver surface temperatures ranged from 8-23°C higher than the receiver fluid temperatures.

Overall agreement between the predicted trough performance and the test data is very good. However, reproducing the absolute value of trough performance test data is not the main detail to be gained. The objective in trough performance tests is to achieve stable and reproducible results so that the steady-state boundary of trough performance can be characterized. The use of a one-dimensional model for comparing predicted and measured trough performance can give some indication of how well the test data characterizes trough performance. The comparisons presented in this section indicate that the test results provide a good indication of the level of performance for IST's trough collector.

APPENDIX F

ERROR ANALYSIS

Intentionally Left Blank

Error Analysis

Introduction

An error analysis was carried out for measurements of collector efficiency, thermal loss, and incident angle modifier. All these measurements include a combination of fluid mass flow, specific heat and temperature. Insolation was also included for efficiency and incident angle modifier measurements. Both measuring instrument error and statistical data variability were considered in this analysis. There is some uncertainty in the equations for Syltherm® heat-transfer fluid properties (Dow-Corning, 1982); the magnitude of these is unknown, and was not considered in this analysis. The effect of temperature measurement error on fluid properties was included.

The error analysis applies to a single measurement set, i.e., a computer data scan. These measurement sets were repeated at 15-20 second intervals during each test. In the analysis of the data to obtain a value such as efficiency, the measured data were averaged over a period of several minutes. To determine the length of the averaging period for each data point, receiver time constants were measured at the beginning of the test series; see Figures D-3 and D-4. The IST receiver time constant was found to be about two minutes; data averaging time was then set at a minimum of three time constants, or about 6 minutes. Except for incident angle data, most data point averaging was longer than the minimum, usually about 10 minutes, as in the data samples shown below.

Even though the system was operated at each temperature for a long time (usually an hour or more) to obtain maximum system stability of flow and temperature prior to an averaging period, there is always some scatter in the data during the averaging period due to measuring instrument electrical noise and remaining instabilities in flow, temperature or insolation. In estimating the errors of the averaged data points, the errors associated with each point in the average are assumed to be correlated, since instrument calibration errors are not expected to vary over such short periods of time.

A sample of data from a cold water optical efficiency test with the silver film mirror/black chrome receiver/solgel receiver glass is shown in Table F-1; the mean data values are reported as an efficiency point in Table D-1, line 1. A sample of data from an elevated temperature efficiency test is shown in Table F-2; the mean data values are reported as an efficiency point in Table D-3, line 14. A sample of data taken during a thermal loss test is shown here in Table F-3; the mean data from Table F-3 is shown as a thermal loss data point in Table D-6, line 7. All the data points in Appendix D data tables were obtained from calculated mean values similar to those shown in Tables F-1, F-2, and F-3. Again note that the system was operated at a constant temperature and flow rate for about an hour before the time periods shown in the sample data tables.

For each averaging period, such as those shown in the sample data tables, the population standard deviation of each measurement was calculated as a check on the stability of the system under test. Also, the data range from minimum value to maximum value during the averaging period had to be within the stability criteria outlined in the Test Plan, Appendix C. For example, in Table F-3, the input and output temperature range of about 0.1°C (± 0.05°) is our usual requirement for a

APPENDIX F

Table F-I. Black Chrome/Solgel Efficiency Test Data for Cold Water at 30°C

IST Test	93/08/11	Increment of 1 record			METRIC UNITS		
#403 Clock Standard Time HH:MM:SS	#406 NIP Solar Flux W/m^2	#411 FT100 Collector Flow #1 L/min	#436 Calc. Rec Temp above amb Deg C	#426 TC002 Temp Inlet #2 Deg C	#433 TC009 Temp Out #2 Deg C	#466 Calc. Sub. dT #2 Deg C	#470 Calc. Efficiency Sub 2,Flo2 %
13:19:56	963.66	24.68	1.15	30.07	35.51	5.44	73.17
13:20:16	964.24	24.70	1.17	30.08	35.50	5.42	72.92
13:20:36	964.12	24.70	1.20	30.07	35.53	5.45	73.35
13:20:56	964.12	24.71	1.21	30.08	35.49	5.42	72.89
13:21:16	964.01	24.68	1.23	30.07	35.50	5.43	73.01
13:21:36	963.54	24.69	1.23	30.10	35.52	5.42	72.91
13:21:55	964.01	24.68	1.22	30.11	35.53	5.43	72.96
13:22:15	963.77	24.71	1.21	30.10	35.52	5.42	73.01
13:22:35	964.01	24.68	1.20	30.07	35.54	5.46	73.46
13:22:55	963.54	24.68	1.15	30.06	35.52	5.46	73.51
13:23:15	964.12	24.65	1.13	30.06	35.54	5.48	73.58
13:23:35	964.24	24.70	1.09	30.06	35.49	5.43	73.01
13:23:55	962.85	24.69	1.06	30.05	35.49	5.44	73.31
13:24:14	962.38	24.67	1.06	30.04	35.50	5.47	73.61
13:24:34	961.46	24.66	0.99	30.04	35.49	5.45	73.45
13:24:54	962.27	24.69	1.01	30.06	35.49	5.44	73.28
13:25:14	963.31	24.72	0.96	30.07	35.52	5.45	73.47
13:25:34	963.31	24.68	0.91	30.06	35.49	5.43	73.08
13:25:54	962.27	24.70	0.89	30.07	35.53	5.46	73.64
13:26:14	961.23	24.70	0.83	30.06	35.50	5.44	73.36
13:26:34	960.42	24.70	0.82	30.07	35.54	5.46	73.77
13:26:53	960.88	24.70	0.77	30.06	35.52	5.46	73.74
13:27:13	961.57	24.70	0.69	30.06	35.48	5.42	73.15
13:27:33	961.92	24.70	0.67	30.07	35.50	5.43	73.19
13:27:53	959.95	24.71	0.61	30.06	35.50	5.44	73.51
13:28:13	960.76	24.72	0.59	30.08	35.52	5.44	73.54
13:28:33	960.42	24.73	0.51	30.03	35.51	5.48	74.14
13:28:53	960.65	24.70	0.47	30.04	35.49	5.45	73.60
13:29:13	960.76	24.68	0.43	30.04	35.50	5.46	73.67
13:29:32	960.53	24.73	0.41	30.05	35.51	5.47	73.91
13:29:52	959.03	24.71	0.33	30.02	35.49	5.47	74.09
Statistics for 31 data values.							
Largest data value	964.236	24.734	1.226	30.108	35.538	5.481	74.139
Smallest data value	959.028	24.654	0.331	30.016	35.483	5.416	72.893
Range of data	5.208	0.080	0.896	0.092	0.055	0.065	1.247
Arithmetic mean	962.366	24.696	0.909	30.063	35.509	5.446	73.397
Population Standard Deviation (Sigma)	1.569	0.018	0.288	0.020	0.016	0.019	0.341
3-Sigma	4.708	0.055	0.863	0.061	0.049	0.058	1.024
Population Variance	2.463	0.000	0.083	0.000	0.000	0.000	0.116

Table F-2. Black Chrome/Pyrex Efficiency Test Data at 150°C

IST Test	93/10/27	Increment of 1 records			METRIC UNITS		
#40 3 Clock Standard Time HH:MM:SS	#406 NIP Solar Flux W/m^2	#411 FT100 Collector Flow #1 L/min	#436 Calc. Rec Temp above amb Deg C	#426 TC002 Temp Inlet #2 Deg C	#433 TC009 Temp Out #2 Deg C	#466 Calc. Sub dT #2 Deg C	#470 Calc. Efficiency Sub 2,Flo2 %
12:21:34	972.57	50.33	145.56	152.42	158.67	6.25	61.82
12:21:54	972.45	58.32	145.52	152.42	158.71	6.28	62.10
12:22:13	973.03	58.35	145.51	152.39	158.70	6.31	62.38
12:22:33	972.45	58.37	145.47	152.41	158.70	6.29	62.28
12:22:53	972.34	50.37	145.53	152.43	158.70	6.27	62.05
12:23:13	973.03	58.35	145.58	152.48	158.70	6.30	62.27
12:23:33	972.92	58.34	145.47	152.48	158.70	6.30	62.29
12:23:53	973.38	58.33	145.47	152.42	158.71	6.29	62.16
12:24:13	972.92	58.34	145.46	152.43	158.71	6.29	62.15
12:24:32	973.38	58.34	145.47	152.42	153.72	6.30	62.28
12:24:52	973.26	58.34	145.43	152.48	158.72	6.32	62.48
12:25:12	972.92	58.33	145.43	152.39	158.72	6.33	62.59
12:25:32	972.11	58.28	145.42	152.40	158.72	6.32	62.42
12:25:52	972.80	58.31	145.42	152.48	158.73	6.33	62.57
12:26:12	972.11	58.34	145.40	152.41	158.76	6.35	62.84
12:26:32	972.34	50.33	145.38	152.43	158.77	6.34	62.68
12:26:51	971.76	58.34	145.33	152.39	158.72	6.33	62.67
12:27:11	971.53	58.34	145.33	152.42	158.72	6.30	62.41
12:27:31	971.99	58.29	145.34	152.42	158.74	6.32	62.52
12:27:51	971.99	50.33	145.34	152.45	158.75	6.30	62.36
12:2S:11	972.69	50.33	145.35	152.46	158.76	6.30	62.30
12:28:31	971.76	50.28	145.36	152.46	158.76	6.30	62.28
12:28:51	972.92	58.36	145.34	152.46	158.76	6.29	62.23
12:29:11	972.11	50.25	145.35	152.47	158.79	6.32	62.39
12:29:30	971.99	58.40	145.38	152.47	158.79	6.32	62.65
12:29:50	973.96	58.35	145.33	152.44	158.75	6.30	62.24
12:30:10	973.03	58.37	145.34	152.45	158.78	6.32	62.54
12:30:30	973.26	58.33	145.34	152.41	158.74	6.33	62.52
12:30:50	972.92	58.30	145.31	152.41	158.70	6.29	62.12
12:31:10	974.19	58.33	145.31	152.41	158.70	6.29	62.08
12:31:30	973.73	58.34	145.28	152.37	158.72	6.34	62.66
Statistics for 31 data values.							
Largest data value	974.190	50.397	145.556	152.469	158.788	6.351	62.843
Smallest data value	971.528	50.246	145.275	152.374	158.672	6.252	61.823
Range of data	2.662	0.151	0.281	0.095	0.116	0.099	1.020
Arithmetic mean	972.704	58.333	145.402	152.422	158.729	6.307	62.366
Population Standard Deviation (Sigma>	0.661	0.030	0.076	0.026	0.030	0.022	0.227
3-Sigma	1.983	0.089	0.228	0.077	0.089	0.066	0.681
Population Variance	0.427	0.001	0.006	0.001	0.001	0.000	0.052

APPENDIX F

Table F-3. Black Nickel/Solgel Thermal Loss Test Data at 200°C

IST Test	93/12/02	Increment of 1 records			METRIC UNITS		
#403 Clock Standard Time HH:MM:SS	#425 TC001 Temp Inlet #1 Deg C	#434 TC010 Temp Out #1 Deg C	#407 Tcamb Ambient Temp Deg C	#436 Calc. Rec Temp above amb Deg C	#408 WS100 Wind Speed m/s	#411 FT100 Collector Flow #1 L/min	#445 Calc. Heat Gain Sub 1,Flo1 W/m^2
12:49:51	199.87	198.04	8.98	190.14	2.67	26.87	-91.56
12:50:10	199.86	198.05	8.98	190.14	2.33	26.94	-91.24
12:50:30	199.89	198.05	8.98	190.17	1.79	26.85	-92.19
12:50:50	199.92	198.08	8.99	190.17	1.68	26.87	-92.59
12:51:10	199.94	198.09	8.99	190.20	2.18	26.85	-93.00
12:51:30	199.93	198.12	8.99	190.20	1.99	26.89	-90.68
12:51:50	199.94	198.12	9.00	190.20	4.18	26.88	-91.34
12:52:10	199.94	198.12	9.01	190.19	3.36	26.86	-91.06
12:52:29	199.91	198.09	9.03	190.14	2.94	26.88	-91.33
12:52:49	199.88	198.08	9.03	190.12	2.22	26.87	-90.34
12:53:09	199.88	198.06	9.03	190.11	2.16	26.86	-91.16
12:53:29	199.91	198.05	9.05	190.11	1.95	26.89	-93.41
12:53:49	199.91	198.05	9.06	190.10	2.05	26.91	-93.30
12:54:09	199.98	198.07	9.07	190.10	1.82	26.89	-91.91
12:54:29	199.91	198.08	9.09	190.07	2.00	26.86	-91.67
12:54:48	199.91	198.07	9.11	190.06	1.80	26.85	-92.45
12:55:08	199.91	198.09	9.11	190.07	1.63	26.86	-91.36
12:55:28	199.98	198.09	9.12	190.06	1.53	26.86	-98.86
12:55:48	199.89	198.10	9.14	190.03	1.57	26.88	-90.03
12:56:08	199.98	198.09	9.16	190.01	1.85	26.86	-90.88
12:56:28	199.S9	198.10	9.16	190.01	1.80	26.88	-89.72
12:56:48	199.89	198.09	9.17	190.00	2.06	26.98	-90.31
12:57:08	199.92	198.11	9.17	190.03	2.04	26.86	-90.91
12:57:27	199.93	198.12	9.18	190.02	2.17	26.85	-91.12
12:57:47	199.91	198.10	9.20	189.99	2.12	26.87	-90.75
12:58:07	199.94	198.12	9.20	190.00	3.14	26.88	-91.12
12:58:27	199.92	198.09	9.22	189.95	3.24	26.89	-91.78
12:58:47	199.91	198.08	9.23	189.94	3.22	26.83	-91.47
12:59:07	199.88	198.07	9.24	189.90	3.62	26.84	-90.76
12:59:27	199.98	198.05	9.24	189.91	4.17	26.86	-92.77
12:59:47	199.S4	198.04	9.28	189.83	3.58	26.86	-90.40
Statistics for 31 data values							
Largest data value	199.940	198.121	9.282	190.203	4.181	26.944	-89.716
Smallest data value	199.841	198.038	8.977	189.827	1.534	26.830	-93.406
Range of data	0.099	0.083	0.305	0.376	2.647	0.113	3.690
Arithmetic mean	199.904	198.082	9.104	190.064	2.412	26.871	-91.402
Population Standard Deviation (Sigma)	0.024	0.825	0.894	0.897	0.772	0.022	0.936
3-Sigma	0.072	0.076	0.283	0.291	2.316	0.067	2.807
Population Variance	0.001	0.001	0.009	0.009	0.596	0.000	0.875

stable data point, and is also about the best the fluid supply system can maintain, and the best we can reasonably measure with current equipment. Operation for less than an hour at a given temperature produces less stable temperatures, operation for a longer time results in little improvement. An important stability requirement for the data averaging period is that there be no trend of temperatures (or flow rates) toward higher or lower values, which would indicate that energy is being stored in (or removed from) the mass of the test system.

Even a stringent ± 0.05°C temperature stability requirement is not as good as would be desirable; as the result is a 4% scatter in the measured thermal losses shown in Table F-3.

Data measurement errors were calculated using the root-sum-square method, defined as: (Ref. 2; Ref. 3):

$$E_{rss} = \sqrt{\left[\Delta\mu_1\left(\frac{\partial F}{\partial\mu_1}\right)\right]^2 + \left[\Delta\mu_2\left(\frac{\partial F}{\partial\mu_2}\right)\right]^2 + \text{☹} + \left[\Delta\mu_n\left(\frac{\partial F}{\partial\mu_n}\right)\right]^2} \qquad (1)$$

Where:

Erss	=	root-sum-square error
u_i	=	measured quantity
Δu_i	=	error in measured quantity
$\partial F/\partial u_i$	=	partial derivative of the calculated function with respect to the measured quantity.

Two error sources were considered: the instrument calibration (bias) errors, and statistical errors due to scatter in repeated measurements of the same quantity. Instrument errors were calculated using equation (1) above. Statistical error was calculated by using the measurement standard deviation multiplied by the Student's T statistic for the measurement degrees of freedom (n measurements -1). The two errors were then combined using the root-sum-square method for a final error estimate.

Heat Gain Errors

The following equation was used in calculating heat gain (or loss):

$$Q = (\text{flow rate}) * (\text{density}) * (\text{specific heat}) * (\text{delta-temperature}) \qquad (2)$$

Density of the heat transfer fluid:

$$\rho = A + B\,(\text{temperature}) + C\,(\text{temperature})^2 + D\,(\text{temperature})^3 \qquad (3)$$

For water, coefficients A, B, C and D were obtained from an equation fitted to data from Keenan and Keys (Ref. 4); for Syltherm®, the coefficients were from Dow Corning (Ref. 1). In each case, the temperature used was the temperature of the fluid at the flow meter. For density, the coefficients are:

	Water	Syltherm® oil
A	0.99971 kg/L	954.0 kg/m^3
B	-1.42399 x 10^{-4}	-0.919
C	-2.69909 x 10^{-6}	4.25 x 10^{-4}
D	0.0	-1.67 x 10^{-6}

For specific heat of the heat transfer fluid, the equation is:

$$Cp = E + F\,(\text{temperature}) + G\,(\text{temperature})^2 \qquad (4)$$

Coefficients for specific heat are from the same sources as for density. The average temperature of the fluid in the collector's receiver tube was used to evaluate the equations. For specific heat, the coefficients are:

	Water	Syltherm® oil
E	4.0803 kJ/kg°C	1575 J/kg°C
F	-6.379 x 10^{-4}	1.708
G	4.487 x 10^{-6}	0.0

Instrument calibration errors were as follows:

Temperature	Et	=	0.5°C	(Calibrated type T thermocouples)
Delta-temperature	Edt	=	0.2°C	(Matched pair, type T thermocouples)
Flow rate	Ef	=	1% of flow	(Liters/minute)
Insolation	Ei	=	2% of DNI	(Watts/m^2)

For heat gain Q, the error equation (1) due to instrumentation bias error becomes:

$$Eq = \sqrt{\left[E\rho\left(\frac{\partial q}{\partial \rho}\right)\right]^2 + \left[Edt\left(\frac{\partial q}{\partial dt}\right)\right]^2 + \left[Ef\left(\frac{\partial q}{\partial f}\right)\right]^2 + \left[Ecp\left(\frac{\partial q}{\partial cp}\right)\right]^2} \qquad (5)$$

Where:

$\partial q/\partial \rho$ = Flow * Cp * dt
$\partial \rho/\partial t$ = B + 2C * Temp + 3D * Temp^2
$\partial cp/\partial t$ = F + 2G * Temp
$\partial q/\partial dt$ = ρ * Flow * Cp
$\partial q/\partial f$ = ρ * Cp * dt
$\partial q/\partial cp$ = ρ * Flow * dt
ρ = fluid density, kg/ m^3
Eρ = Et * $\partial \rho/\partial t$
Ecp = Et * $\partial cp/\partial t$
Flow = fluid flow in m^3/sec

Ef = flow measurement error, m^3/sec
Temp = fluid temperature, °C
Et = temperature measurement error, °C
dt = receiver fluid delta temperature, °C
Edt = delta temperature measurement error, °C
Cp = fluid specific heat, J/kg °C
q = Heat gain (Loss), Watts

Efficiency Errors

Efficiency is derived from heat gain and input insolation:

η = heat gain / heat input = Q / insolation * collector aperture

For an efficiency measurement, the error equation due to instrumentation bias error is:

$$E\eta = \sqrt{Eq\left[\frac{\partial \eta}{\partial q}\right]^2 + Ei\left[\frac{\partial \eta}{\partial i}\right]^2} \quad (6)$$

Where:

Eq = error in heat gain
Ei = error in insolation
$\partial_\eta / \partial q$ = 1/ (insolation * aperture)
$\partial_\eta / \partial_I$ = -q / (insolation^2 * aperture)

Incident Angle Modifier

Incident angle modifier K is the ratio of efficiency performance at some incident angle to the efficiency at zero incident angle:

$$K = \eta_{IA} / \eta_0 \quad (7)$$

The incident angle modifier instrument bias error equation is:

$$Ek = \sqrt{EA\left[\frac{\partial k}{\partial \eta_A}\right]^2 + E_0\left[\frac{\partial k}{\partial \eta_0}\right]^2} \quad (8)$$

Where:

E_k = Error in incident angle modifier K
E_A = Error in efficiency at incident angle A
E_0 = Error in efficiency at incident angle zero
$\partial k / \partial \eta_A$ = $1 / \eta_0$
$\partial k / \partial \eta_A$ = $-\eta_A / \eta_0^2$

APPENDIX F

Sample Efficiency Error Analysis

When the equations above are evaluated at 150 °C inlet temperature (last entry in Table D-4), the values are:

Inlet temp	= 150.83 °C
Outlet temp	= 158.30 °C
Delta-Temp	= 7.43°C
Ambient air	= 10.28 °C
Oil flow rate	= 0.000827217 m^3 /sec
Density	= 819.30 kg/m^3 @ 150.86 °C
Specific heat	= 1839.02 J/kg °C @ 154.57 °C
Insolation	= 990.0 W/m^2
Heat gain Q	= 701.31 W/m^2
Efficiency	= 70.82 %
Et	= 0.6058 °C
Edt	= 0.206 °C
Ei	= 20.14 W / m^2
Ef	= 0.00000839 m^3 /sec
Ecp	= 1.03 J/kg °C
Eρ	= -0.5481 kg/m^3
$\partial q/\partial cp$	= 5.03761
$\partial q/\partial dt$	= 1246.37
$\partial q/\partial f$	= 11199322
$\partial q/\partial \rho$	= 11.3076
$\partial \rho/\partial t$	= -0.90479
$\partial cp/\partial t$	= 1.708
Eq	= 20.74 W / m^2 gain error
∂_η/∂_Q	= 0.0010101
$\partial_\eta/\partial i$	= -0.00071554
E_η	= 2.60 % efficiency error due to instrumentation & data scatter

For the measurement analyzed above, 31 data measurements were made over a period of 10 minutes. The efficiency standard deviation for the data set was 0.367 %, and the 95% confidence T statistic for 31 measurements was 2.042.

The calculations for estimated error outlined above were repeated for each entry in the data tables; the results are listed in the 'Est Error' column of each data table in Appendix D, and are also used to size the error bars shown on the curves.

The critical measurements which have the most effect on error magnitude are fluid flow rate, delta-temperature, and insolation. A large sample size with a small standard deviation is also needed for a small error bound, again reinforcing the requirement for maximum system stability before data measurements begin.

References

Dow Corning; 1985. Properties of Sylltherm 800 Heat Transfer Liquid. Midland, Michigan.

Doebelin, E. O., 1983. Measurement Systems; Application and Design. New York: McGraw-Hill, Inc.

Bevington, P. R., 1969. Data Reduction and Error Analysis for the Physical Sciences. New York: McGraw-Hill, Inc.

Dieck, Ronald H., 1992. Measurement Uncertainty: Methods and Applications. Instrument Society of America

Keenan, J H., Keys, F. G., Hill, J. G., Moore, J. G. 1978. Steam Tables. New York: Wiley-Interscience.

Attn: Tom Tracey
6922 S. Adams Way
Littleton, CO 80122

Attn: Tom Brumleve
1512 Northgate Road
Walnut Creek, CA 94598

Attn: Jamie Chapman
Number 402
15 Sleeper Street
Boston, MA 02210

Attn: Karl Thomas Feldman, Jr.
Mechanical Engineering Consultant
1704 Stanford Drive NE
Albuquerque, NM 87106

Attn: Hilda Frazier
2740 Centerview Drive
Tallahassee, FL 32399-2100

Attn: David Hagen
134 Kitchener Street
Garran, ACT 2605, AUSTRALIA

Attn: J. McGuirk
10202 North 58th Place
Scottsdale, AZ 85253-1104

Attn: Pat Montoya
625 Silver Avenue SW, Suite 130
Albuquerque, NM 87102

Attn: Ricardo Xavier Zuniga
119 East Marcy, Suite 101
Santa Fe, NM 87501

3M - Solar Optics Program
Attn: Paul Jaster
3M Center
Building 225-2N-06
St. Paul, MN 55144-1000

AAA Solar Service and Supply, Inc.
Attn: Chuck Marken
2021 Zearing Avenue, NW
Albuquerque, NM 87104

Acurex Corporation
Attn: Hans Dehne
555 Clyde Avenue
Mountain View, CA 94039

Acurex Corporation
Attn: John Schaeffer
555 Clyde Avenue
Mountain View, CA 94039

Advanced Energy Systems
Attn: Charles Bensinger
P.O. Box 2685
Santa Fe, NM 87504

Advanced Thermal Systems
Attn: Dave Gorman
7600 East Arapahoe Road, Suite 215
Englewood, CO 80112

Alabama Energy Office
Attn: Terri Adams
401 Adams Avenue
P.O. Box 5690
Montgomery, AL 36103-5690

Alabama Power Company
Attn: J.G. Boyles
P.O. Box 2641
Birmingham, AL 35291

Alabama Solar Energy Center
Attn: Leonard Adcock
University of Alabama in Huntsville
Huntsville, AL 35899

Alliance to Save Energy
Attn: Malcolm Verdict
1725 K Street NW, Suite 509
Washington, DC 20006

American Energy Technologies, Inc.
Attn: Greg Peebles
3530 Enterprise Way
Green Cove Springs, FL 32043-1865

American Hydrogen Assoc.
Attn: Roy McCalister
216 S. Clark, MS-103
Tempe, AZ 85281

American Institute of Architects
Attn: Richard C. Depta
Director Energy Information
1735 New York Avenue NW
Washington, DC 20006

American Solar Energy Society
Attn: Larry Sherwood
2400 Central Avenue, Suite G-1
Boulder, CO 80301

American Sun Co.
Attn: Miles Maiden
777 Parker Point Road
Blue Hill, ME 04614

AMTECH
Attn: Jeffrey Keating
7441 NW 8th Street
Bay M
Miami, FL 33126

Argonne National Laboratory
Attn: Robert Baker
9700 S. Cass Avenue
Building 900
Argonne, IL 60439

Arizona Public Service Co.
Attn: Scott McLellan
P.O. Box 53999
MS 1424
Phoenix, AZ 85072-3999

Arizona Solar Energy Office
Attn: Frank P. Mancini, Ph.D.
Department of Commerce
3800 N. Central
Suite 1200
Phoenix, AZ 85012

Arizona State University
Attn: Paul Russell
College of Engineering
Tempe, AZ 85287

Arizona State University
Attn: Byard D. Wood, Ph.D., P.E.
College of Engineering & Applied Sciences
Tempe, AZ 87287-5806

Arkansas Energy Office
Attn: Chris Benson
One State Capitol Mall
Suite 4B-215
Little Rock, AR 72201

Ascension Technology
Attn: Ed Kern
Box 314
Lincoln Center, MA 01773

Austrialian National University
Attn: Stephen Kaneff
Information Technology
0200 Canberra ACT, AUSTRALIA

Bechtel National, Inc.
Attn: Pascal (Pat) DeLaquil III
P. O. Box 193965
San Francisco, CA 94119-3965

Bechtel National, Inc.
Attn: Stuart Fry
50 Beale Street
50/15 D8
P.O. Box 193965
San Francisco, CA 94119-3965

Bechtel National, Inc.
Attn: Bruce Kelly
50 Beale Street
50/15 D25
P.O. Box 193965
San Francisco, CA 94119-3965

Bergquam Energy Systems
Attn: Jim Bergquam
8611 Folsom Boulevard
Sacramento, CA 95826

Brookhaven National Laboratories
Attn: John Andrews
National Center for Analysis of Energy Systems
Upton, NY 11973

California Energy Commission
Attn: Alec Jenkins
Energy Technology Development Div. R&D Office
1516 9th Street
MS-43
Sacramento, CA 95814-5512

California Energy Commission
Attn: Promod Kulkarni
Energy Technology Development Div. R&D Office
1516 9th Street
MS-43
Sacramento, CA 95814-5512

California Energy Commission
Attn: Phil Misemer
Energy Technology Development Div. R&D Office
1516 9th Street
MS-43
Sacramento, CA 95814-5512

California State Polytechnic University
Attn: William B. Stine
Department of Mechanical Engineering
3801 West Temple Avenue
Pomona, CA 91768-4062

Carrizo Solar Corporation
Attn: Mike Elliston
P.O. Box 10239
1011-C Sawmill Road NW
Albuquerque, NM 87184-0239

Carrizo Solar Corporation
Attn: John Kusianovich
P.O. Box 10239
1011-C Sawmill Road NW
Albuquerque, NM 87184-0239

Central and South West Services
Attn: E. L. Gastineau
1616 Woodall Rogers Freeway
MS 7RES
Dallas, TX 75202

CIEMAT - PSA
Attn: Manuel Sanchez-Jimenez
Apartado 22
E-04200 Tabernas (Almeria), SPAIN

City of Albuquerque
Attn: Mike Minturn
Resource Management Division
General Services Department
P.O. Box 1293
Albuquerque, NM 87103-1293

City of Las Cruces
Attn: Jerry Trojan
P.O. Drawer CLC
Las Cruces, NM 88004

Colorado State University
Attn: Allan T. Kirkpatrick
Department of Mechanical Engineering
Ft. Collins, CO 80523

Commonwealth of Virginia
Attn: Susie Thomas
Institutional Conservation Program
Ninth Street Office Blvd., 8th Floor
202 North Ninth Street
Richmond, VA 23219

Condumex
Attn: Enrique B. Hill
So juana ines de la Cruz
34402o. Piso Tiainepantia. Edo. de Mexico
C.P. 54000, MEXICO

County of Hawaii
Attn: Steve Burns
Dept. of Research and Development
25 Aupuni Street
Hilo, HI 96720

Cummins Power Generation Inc.
Attn: Isoroku (Rocky) Kubo
Mail Code 60125
P.O. Box 3005
500 Jackson Street
Columbus, IN 47202-3005

Cummins Power Generation South
Attn: Monte McGlaun
150 Tannehill Drive
Abilene, TX 79602

Daggett Leasing Corporation
Attn: Bill Ludlow
35100 Santa Fe St.
P.O. Box 373
Daggett, CA 92327

Daggett Leasing Corporation
Attn: Wayne Luton
35100 Santa Fe St.
P.O. Box 373
Daggett, CA 92327

Daggett Leasing Corporation
Attn: Eric Wills
35100 Santa Fe St.
P.O. Box 373
Daggett, CA 92327

Delaware Energy Office
Attn: John Posdon
P.O. Box 1401
O'Neill Building
Dover, DE 19903

DEO Enterprises
Attn: Dave Ochenreider
P.O. Box 2110
26443 Corona Drive
Helendale, CA 92342

Department of Natural Resources
Attn: Diane Smith
Energy Division
625 N. 4th Street
P.O. Box 44156
Baton Rouge, LA 70802

Department of Natural Resources
Attn: Cher Stuewe-Portnoff
Divison of Energy
P.O. Box 176
1500 Southridge
Jefferson City, MO 65102

Dept. of Business, Economic Dev. & Tourism
Attn: Maurice H. Kaya
Energy Program Administrator
335 Merchant Street, Room 110
Honolulu, HI 96813

Distributed Utility Associates
Attn: Joseph J. Iannucci
3170 Crow Canyon Place
Suite 140
San Ramon, CA 94583

DLR
Attn: Berthold Oberle
Pfaffenwaldring 38-40
7000 Stuttgart 80, GERMANY

DLR - Koln MD - ET
Attn: Manfred Becker
Linder Hohe
P.O. Box 90 60 58
D-51140 Koln, GERMANY

DLR - Koln MD - ET
Attn: Klaus Hennecke
Linder Hohe
P.O. Box 90 60 58
D-51147 Koln, GERMANY

DLR - Stuttgart EN - TT
Attn: Reiner Buck
Pfaffenwaldring 38-40
D-70569 Stuttgart, GERMANY

Electric Ideas Clearinghouse
Attn: Douglas Kilpatrick
809 Legion Way SE FA-11
Olympia, WA 98504

Electric Power Research Institute
Attn: Ed DeMeo
P.O. Box 10412
3412 Hillview Avenue
Palo Alto, CA 94303

Electric Power Research Institute
Attn: Dick Holl
1938A Avenida Del Oro
Oceanside, CA 92056

Electric Power Research Institute
Attn: Doug Morris
P.O. Box 10412
3412 Hillview Avenue
Palo Alto, CA 94303

Electric Power Research Institute
Attn: J. Schaeffer
P.O. Box 10412
3412 Hillview Avenue
Palo Alto, CA 94303

Energy Concepts Co.
Attn: Don Erickson
627 Ridgely Ave.
Annapolis, MD 21401

Energy Division
Attn: Jimmy Johnston
320 6th Avenue North
6th Floor
Rachel Jackson Building
Nashville, TN 37243-0405

Energy Foundation
Attn: Bill Keepin
75 Federal Street
San Francisco, CA 94107

Environmental Technology & Education Center
(ETEC)
Attn: Jon Nimitz, Ph.D.
3300 Mountain Road NE
Albuquerque, NM 87106-1920

FAFCO
Attn: Freeman Ford
2690 Middlefield Road
Redwood City, CA 94063

Florida Energy Office
Attn: Michael Ashworth
Dept. of Community Affairs
2740 Centerview Drive
Tallahassee, FL 32399-2100

Florida Solar Energy Center
Attn: David Block
300 State Road, Suite 401
Cape Canaveral, FL 32920-4099

Florida Solar Energy Center
Attn: Library
300 State Road, Suite 401
Cape Canaveral, FL 32920-4099

Florida Solar Energy Center
Attn: Bruce Nimmo
300 State Road, Suite 401
Cape Canaveral, FL 32920

Florida Solar Energy Center
Attn: Mark Thornbloom
1679 Clearlake Road
Cocoa, FL 32922-5703

Georgia Institute of Technology
Attn: Sheldon Jeter
School of Mech. Engr.
Atlanta, GA 30332

Georgia Power Co.
Attn: D. Keebaugh
7 Solar Circle
Shenandoah, GA 30265

Gould Inc.
Attn: Greg Ringle
Foil Division
2929 W. Chandler Blvd.
P.O. Box 190
Chandler, AZ 85244-0190

Governor's Office of Economic Development
Attn: David M. O'Hara
711 E. Wells Avenue
Pierre, SD 57501-3369

Governor's Office of Energy/Comm Sys
Attn: Norwood Kenney, III
57 Regional Drive
Concord, NH 03301-8519

Governor's Office of Housing, Energy &
Intergovernment Rel
Attn: Joan Carbone
State House, Room 111
Providence, RI 22903

Harris Corporation
Attn: Byron F. Knight
P.O. Box 91000
Melbourne, FL 32902-9100

Hawaii Energy Extension Service
Attn: Andrea Beck
Dept. of Business & Economic Development
Hawaii Business Center
99 Aupuni Street #214
Hilo, HI 96720

Heliodyne, Inc.
Attn: Jurg H. Bieri, Ph.D.
4910 Seaport Avenue
Richmond, CA 94804

Heliotrope
Attn: Malcolm Herbert
3733 Kenora Drive
Spring Valley, CA 92077

Idaho Dept. of Water Resources
Attn: Joan Sipple
P.O. Box 83720
Boise, ID 83720-0098

Idaho Power
Attn: Jerry Young
P.O. Box 70
Boise, ID 83707

Indiana Dept.of Commerce
Attn: Sharon Storms
Energy Policy Division
One N. Capitol Avenue
Suite 700
Indianapolis, IN 46204

Industrial Solar Technology
Attn: Randy Gee (5)
4420 McIntyre Street
Golden, CO 80403

Inner Solar Roof Systems, Inc.
Attn: Joseph Allegro
731 NE 69th Street
Boca Raton, FL 33487

Institute of Gas Technology
Attn: Library
34245 State Street
Chicago, IL 60616

Instituto de Investigaciones Electricas
Attn: Jorge M. Huacuz Villamar
Interior Internado Palmira
Apartado Postal 475
62000 Cuernavaca, Mor., MEXICO

Inter-Island Solar Supply
Attn: Cully Judd
345 N. Nimitz Hwy
Honolulu, HI 96817

Iowa Dept. of Natural Resources
Attn: Ward Lenz
Energy Bureau - 4th Floor
Wallace State Office Building
Des Moines, IA 50319

JWK Associates, Inc.
Attn: J. Willard King
112 Cloister Drive
Peachtree City, GA 30269

Kearney & Associates
Attn: David W. Kearney (5)
14022 Condessa Drive
Del Mar, CA 92014

KJC Operating Company
Attn: Bob Cable
41100 Highway 395
Boron, CA 93516

KJC Operating Company
Attn: Gilbert E. Cohen
41100 Highway 395
Boron, CA 93516

Kramer Junction Company
Attn: Stuart Lawson
900 19th St. NW
Suite 600
Washington, DC 20006

LA Department of Natural Resources
Attn: Dionne Bordes
P.O. Box 44156
Baton Rouge, LA 70804-4156

Lawrence Berkeley Laboratory
Attn: Arlon Hunt
University of California
MS 90-2024
One Cyclotron Road
Berkeley, CA 94720

Los Alamos National Laboratory
Attn: Donald Neeper
Advanced Engineering Technology Group
P.O. Box 1663, MS F576
Los Alamos, NM 87545

Los Angeles Dept. of Water and Power
Attn: Daryl Yonamine
Alternate Energy Systems
111 North Hope Street, Rm. 661A
Los Angeles, CA 90012

Marine Corps Base Camp Pendleton
Attn: Steve Szorka
Assistant Chief of Staff Facilities
P.O. Box 555013
Camp Pendleton, CA 92055-5013

Maui Economic Opportunity, Inc.
Attn: Doreen M.K. Galam
Molokai Branch Office
P.O. Box 677
Kaunakakai, HI 96748

McDonnell-Douglas Astronautics Co.
Attn: Bob Drubka
5301 Bolsa Avenue
Huntington Beach, CA 92647-2048

Mechanical Technologies, Inc.
Attn: G.R. Dochat
968 Albany Shaker Road
Latham, NY 12110

Meridian Corporation
Attn: Anil Cabraal
4300 King Street
Suite 400
Alexandria, VA 22302-1508

Meridian Corporation
Attn: Chris Rovero
4300 King Street
Suite 400
Alexandria, VA 22302-1508

Ministry of Non-Conventional Energy Sources
Attn: S.K. Gupta
Block No. 14
CGO Complex
Lodhi Road
New Delhi, 110003 INDIA

Ministry of Non-Conventional Energy Sources
Attn: R.S. Sharma
Block No. 14
CGO Complex
Lodhi Road
New Delhi, 110003 INDIA

Ministry of Non-Conventional Energy Sources
Attn: Narendra Singh
Block No. 14
CGO Complex
Lodhi Road
New Delhi, 110003 INDIA

Mississippi Dept. of Economic & Community Development
Attn: Betty Norman
P.O. Box 850
Energy Division
Jackson, MS 39205-0850

Mississippi Technology Transfer Center
Attn: Clay Griffith
Stennis NASA Center
Bay St. Louis, MS 39529

Missouri Department of Natural Resources
Attn: Pam Barkhaus
P.O. Box 176
1500 Southridge
Jefferson City, MO 65102

Municipality of Anchorage
Attn: Larry Roetto
4831 Old Seward Highway #104
Anchorage, AK 99503

National Renewable Energy Laboratory
Attn: John Anderson
1617 Cole Blvd.
Branch 4710/133
Golden, CO 80401-3393

National Renewable Energy Laboratory
Attn: Mark Bohn
1617 Cole Blvd.
Branch 4710/132
Golden, CO 80401-3393

National Renewable Energy Laboratory
Attn: Mary Jane Hale
1617 Cole Blvd.
Branch 4710/105-03
Golden, CO 80401-3393

National Renewable Energy Laboratory
Attn: Steve Hauser
1617 Cole Blvd.
Branch 4700/217
Golden, CO 80401-3393

National Renewable Energy Laboratory
Attn: Russ Hewett
1617 Cole Blvd.
Branch 4710/122
Golden, CO 80401-3393

National Renewable Energy Laboratory
Attn: James G. Jones
1617 Cole Blvd.
Golden, CO 80401-3393

National Renewable Energy Laboratory
Attn: Chuck Kutscher, P.E.
1617 Cole Blvd.
Golden, CO 80401-3393

National Renewable Energy Laboratory
Attn: Allan Lewandowski
1617 Cole Blvd.
Branch 4710/130
Golden, CO 80401-3393

National Renewable Energy Laboratory
Attn: Hank Price (2)
1617 Cole Blvd.
Branch 4710/115
Golden, CO 80401-3393

National Renewable Energy Laboratory
Attn: Steve Rubin
1617 Cole Blvd.
Golden, CO 80401-3393

National Renewable Energy Laboratory
Attn: Tim Wendelin
1617 Cole Blvd.
Branch 4710/105-11
Golden, CO 80401-3393

National Renewable Energy Laboratory
Attn: Tom Williams
1617 Cole Blvd.
Branch 4700/118
Golden, CO 80401-3393

National Rural Electric Cooperative Association
Attn: Ron Orozco
5a. Avenida 16-28
Zona 10, 01010
Guatemala, C.A., GUATEMALA

National Technology Transfer Center
Attn: Sergio Lopes
Wheeling Jesuit College
316 Washington Ave.
Wheeling, WV 26003

Nature Conservancy
Attn: Will Murray
1815 N. Lynn Street
Arlington, VA 22209

NCAT
Attn: Jeff Birkby
P.O. Box 3838
Butt, MT 59702

Nebraska Dept. of Economic Development
Attn: Rex A. Martin
University of Nebraska at Lincoln
W191 Nebraska Hall
Lincoln, NE 68588-0535

Nebraska State Energy Office
Attn: Robert Harris
P.O. Box 95085
State Capitol Building, 9th Floor
Lincoln, NE 68509-5085

Nevada Energy Office
Attn: DeeAnn Parsons
1050 East Williams Street
Suite 435
Carson City, NV 89710

Nevada Power Co.
Attn: Eric Dominguez
P.O. Box 230
Las Vegas, NV 89151

New & Renewable Energy Authority
Attn: Adel Tawfik Soliman, Ph.D.
P.O. Box 39 El-Souk El-Togary
Maadi 11693 Cairo, EGYPT

New Mexico Manufacturing Extension Program
Attn: Ken Manicki
1009 Bradbury Drive, SE
Albuquerque, NM 87106

New Mexico Manufacturing Productivity Center
Attn: Graham Bartlett
1009 Bradbury Drive, SE
Albuquerque, NM 87106

New Mexico Natural Resources Dept.
Attn: Harold Trujillo
2040 South Pacheco
Santa Fe, NM 87503

New Mexico R&D Forum
Attn: Richard Cole
University of New Mexico
R&D Communication Office
Albuquerque, NM 87131-6076

New Mexico Solar Energy Industries Association
Attn:
C/O AAA Solar
2021 Zeoring NW
Albuquerque, NM 87102

New Mexico State University
Attn: Robert O. Coppedge, Ph.D.
Cooperative Extension Service
Box 3AE
Las Cruces, NM 88003-0001

New Mexico State University
Attn: Nick Deveraux
Astronomy Dept.
Box 30001
Dept. 4500
Las Cruces, NM 88003-0001

New Mexico State University
Attn: Steve Durand
Southwest Technology Development Institute
Box 30001, Dept. 3 SOL
Las Cruces, NM 88003-0001

New Mexico State University
Attn: G. Mulholland
New Mexico Solar Energy Institute
Box 3 SOL
Las Cruces, NM 88003

North Carolina Alternative Energy Corp.
Attn: Bob Weiss
P.O. Box 12699
Research Triangle Park, NC 27709

North Carolina Department of Commerce
Attn: David Smith
Energy Division
430 N Salisbury Street
Raleigh, NC 27611

North Dakota Energy Office
Attn: Kim Christianson
600 East Blvd., 14th Floor
Bismarck, ND 58505-0170

Northwest Power Planning Council
Attn: Tom Truelove
851 SW 6th Avenue
Suite 1100
Portland, OR 97204

Oak Ridge National Laboratory
Attn: Marilyn Brown
P.O. Box 2008
Oak Ridge, TN 37831-6070

Office of Energy Conservation
Attn: Tom Brotherton
1675 Broadway, #1300
Denver, CO 80202

Office of Policy and Management
Attn: David Lavine
Policy Development & Planning Div.
80 Washington Street
Hartford, CT 06106

Office of Technical Assessment
Attn: Sam Baldwin
U. S. Congress
Washington, DC 20510-8025

Ohio Department of Development
Attn: Robert Garrick
Office of Energy Efficiency
77 South High Street, 26th Floor
Columbus, OH 43266-0413

Oklahoma Department of Commerce
Attn: Sherwood Washington
Division of Community Affairs and Development
P.O. Box 26980
6601 North Broadway
Oklahoma City, OK 73126

Oregon Department of Energy
Attn: Suzanne Dillard
625 Marion Street NE
Salem, OR 97310-1313

Packerland Solar System
Attn: Richard Lane
P.O. Box 8262
Green Bay, WI 54308

Pennsylvania Energy Office
Attn: Joe Deklinski
116 Pine Street
Harrisburg, PA 17101-1227

Pennsylvania Energy Office
Attn: Phillip Schuller
116 Pine Street
Harrisburg, PA 17101-1227

Public Service Company of New Mexico
Attn: Becky Kilbourne
Alvarado Square
Retail Electric Marketing Center
Albuquerque, NM 87158

Public Service Electric & Gas
Attn: Harry Roman
P.O. Box 570
Newark, NJ 07101

Radco Products, Inc.
Attn: George O. Radford
2877 Industrial Parkway
Santa Maria, CA 93455

Reliable Inspection
Attn: Michael Weir
2429 South Shelton St.
Santa Ana, CA 92707

Renewable Energy Training Institute
Attn: Jeff Keas
122 C St. NW, Suite 520
Washington, DC 20001

Renewable Energy Training Institute
Attn: Jeffrey S. Ross
122 C St. NW, Suite 520
Washington, DC 20001

Research Triangle Institute
Attn: Carl Parker
P.O. Box 12194
Research Triangle Park, NC 27709

Roan Corporation
Attn: James L. Abolt
177 Bovet Road
Suite 520
San Mateo, CA 94402

Rockwell International Corp.
Attn: Bob Musica
Energy Technology Engineering Center
P.O. Box 1449
Canoga Park, CA 91304

Rockwell International Corp.
Attn: R. D. (Dale) Rogers
Rocketdyne Division
P.O. Box 7922
6633 Canoga Avenue
Canoga Park, CA 91309-7922

Rockwell International Corp.
Attn: Bill Wahl
Rocketdyne Division
P.O. Box 7922
6633 Canoga Avenue
Canoga Park, CA 91309-7922

Sacramento Municipal Utility District
Attn: Bud Beebe
Generation Systems Planning
Power Systems Dept.
6201 'S' St.
P.O. Box 15830
Sacramento, CA 95852-1830

Sacramento Municipal Utility District
Attn: Don Osborne
Generation Systems Planning
Power Systems Dept.
6201 'S' St.
P.O. Box 15830
Sacramento, CA 95852-1830

Salt River Project
Attn: Bob Hess
Generation Engineering
P.O. Box 52025
Mail Station PAB358
Phoenix, AZ 85072-2025

Salt River Project
Attn: Ernie Palomino
Research & Development
P. O. Box 52025
Mail Station ISB664
Phoenix, AZ 85072-2025

San Diego Gas & Electric Co.
Attn: Skip Fralick
P.O. Box 1831
San Diego, CA 92112

SBP - Schlaich, Bergermann und. Partner
Attn: Wolfgang Schiel
Hohenzollernstr. 1
D-70178 Stuttgart, GERMANY

Science Applications International Corp.
Attn: Kelly Beninga
15000 W. 6th Avenue
Suite 202
Golden, CO 80401

Science Applications International Corp.
Attn: Barry L. Butler
Room 2043, M/S C2J
10260 Campus Point Dr.
San Diego, CA 92121

Science Applications International Corp.
Attn: Dave Smith
15000 W. 6th Avenue
Suite 202
Golden, CO 80401

Scientific Information Service, Inc.
Attn: Patricia Gunkle
7 Woodland Ave.
Larchmont, NY 10538

Sloan Engineering
Attn: Michael Sloan
4306 Ramsey Ave.
Austin, TX 78756

Solar Energy Industries Association
Attn: Linda Ladas
122 C Street, NW
4th Floor
Washington, DC 20001-2109

Solar Energy Industries Association
Attn: Mac Moore
122 C Street, NW
4th Floor
Washington, DC 20001-2109

Solar Energy Industries Association
Attn: Ann Polansky
122 C Street, NW
4th Floor
Washington, DC 20001-2109

Solar Energy Industries Association
Attn: Ken Sheinkopf
122 C Street, NW
4th Floor
Washington, DC 20001-2109

Solar Energy Industries Association
Attn: Scott Sklar
122 C Street., NW
4th Floor
Washington, DC 20001-2109

Solar Kinetics, Inc.
Attn: Gus Hutchison
10635 King William Drive
P.O. Box 540636
Dallas, TX 75354-0636

Solar Steam
Attn: Doug E. Wood
P.O. Box 32
Fox Island, WA 98333

Solar Stirling Industries
Attn: Jack Stearns
2822 Highridge Road
La Crescenta, CA 91214

Solar Uno
Attn: Ellis Perez
Ave. Sarasota No. 54, Apto. 102
Santo Domingo, DOMINICAN REPUBLIC

Solel Solar Systems, Ltd.
Attn: Har Hotzvim
Science-Based Park
P.O. Box 23577
Jerusalem, 91234 ISRAEL

South Coast AQMD
Attn: Ranji George
21865 Copley Drive
Diamond Bar, CA 91765

Southern California Edison Co.
Attn: Mark Skowronski
P.O. Box 800
2244 Walnut Grove Avenue
Rosemead, CA 91770

Southern California Edison Co.
Attn: Paul Sutherland
6090 North Irwindale Avenue
Irwindale, CA 91702-3271

Spencer Management Associates
Attn: Byron J. Washom (5)
P.O. Box 724
Diablo, CA 94528-0724

State Energy Conservation Office
Attn: Michael Wiley
211 E. 11th Street
Austin, TX 78701

State of California
Attn: Harry Franey
Dept. of Corrections
3116 Pleasant Grove Rd.
Pleasant Grove, CA 95668

State of Colorado
Attn: Howard Andy Walker, Ph.D., M.E.
Office of Energy Conservation
1675 Broadway, Suite 1300
Denver, CO 80202-4613

State of Florida
Attn: Daryl O'Connor
Executive Office of the Governor
The Capitol
Tallahassee, FL 32399-0001

State of Hawaii
Attn: Maurice H. Kaya, P.E.
Dept. of Business and Economic Development
335 Merchant Street, Room 108
Honolulu, HI 96813

State of Hawaii
Attn: David A. Rezachek, Ph.D., P.E.
Dept. of Business and Economic Development
335 Merchant Street, Room 110
Honolulu, HI 96813

State of Hawaii
Attn: Carilyn Shon
Energy Division
335 Merchant Street, Room 110
Honolulu, HI 96813

State of New Mexico
Attn: Brian K. Johnson, P.E.
Energy Information Services
Energy, Minerals and Natural Resources Dept.
2040 S. Pacheco Street
Santa Fe, NM 87505

State of New Mexico
Attn: Ingrid Kelley
Energy Information Services
Energy, Minerals and Natural Resources Dept.
2040 S. Pacheco Street
Santa Fe, NM 87505

State of New Mexico
Attn: Harold Trujillo
Energy Information Services
Energy, Minerals and Natural Resources Dept.
2040 S. Pacheco Street
Santa Fe, NM 87505

State of Tennessee
Attn: David Edmunds
Department of General Services
312 8th Ave N
8th Floor
Nashville, TN 37243-0554

State of Texas
Attn: Charles Nichols
Dept. of Commerce
Office of Advanced Technology
P.O. Box 12728
Austin, TX 78711

State University of New York
Attn: R. Perez
Atmospheric Sciences Research Center
Albany, NY 12222

Sterling Grogan
Attn:
3128-2 Glenwood Drive
Albuquerque, NM 87107

Stirling Technology Co.
Attn: Jack Noble
2952 George Washington Way
Richland, WA 99352

Stirling Thermal Motors
Attn: Lennart Johansson
275 Metty Drive
Ann Arbor, MI 48103

Strategies Unlimited
Attn: R. Winegarner
201 San Antonio Circle
Suite 205
Mountain View, CA 94040

Sun Steam
Attn: Allen Bronstein
765 San Antonio
Palo Alto, CA 94303

Sun Utility Network, Inc.
Attn: Les Hamasaki
510 W. 6th Street
Suite 417
Los Angeles, CA 90014

Sustainable Energy Systems
Attn: David N. Borton, Ph.D.
Hilltop Road
Troy, NY 12180

Technology Ventures Corporation
Attn: W. Robert Gibson
1601 Randolph Road SE, Suite 220
Albuquerque, NM 87106

Ted Lewis & Associates
Attn: Edward G. Lewis
556 East Gill Way
Superior, CO 80027

Tennessee Dept.Economic & Comm Dev
Attn: Chyrall Dawson
320 Sixth Avenue North, 6th Floor
Energy Division
Nashville, TN 37243-0405

Texas State Energy Conservation Office
Attn: Terina Veasey
P.O. Box 13047
Austin, TX 78711-3047

The Solar Letter
Attn: Allan L. Frank
9124 Bradford Road
Silver Spring, MD 20901-4918

Trane Company
Attn: Lee Burgett
3600 Pammel Creek Road
LaCrosse, WI 54601

U.S. Army Corps of Engineers
Attn:
Mobile District
CESEAM-EM-CM
P.O. Box 2288
Mobile, AL 36628-0001

U.S. Army Corps of Engineers
Attn: Robert S. Gorham, Jr.
P.O. Box 9005
Champaign, IL 61826-9005

U.S. Army Corps of Engineers
Attn: Larry D. Lister
P.O. Box 4005
Champaign, IL 61820-1305

U.S. Army Engineering & Housing Support Center
Attn: Robert G. O'Brien, P.E.
Chief Utilities Engineering Division
CEHSC-FU
Ft. Belvoir, VA 22060-5580

U.S. Bureau of Reclamation
Attn: Stanley Hightower
Code D-3710
P.O. Box 205007
Denver, CO 80225

U.S. Department of Energy
Attn: Dan Alpert
2140 L Street, #709
Washington, DC 20037-1530

U.S. Department of Energy
Attn: Gary Burch
EE-132
Forrestal Building
1000 Independence Avenue, SW
Washington, DC 20585

U.S. Department of Energy
Attn: Ernie Chabot
Office of Grants' Management
EE-53
1000 Independence Avenue, SW
Washington, DC 20585

U.S. Department of Energy
Attn: Mark Ginsberg
Federal Energy Management Activities
EE-44
1000 Independence Avenue, SW
Washington, DC 20585

U.S. Department of Energy
Attn: Fred King
San Francisco Regional Support
1301 Clay Street
RM 1060-N
Oakland, CA 94612-5219

U.S. Department of Energy
Attn: Andrew Krantz
1000 Independence Avenue, SW
EE-10
Washington, DC 20585

U.S. Department of Energy
Attn: Bob Martin
Golden Field Office
1617 Cole Boulevard
Golden, CO 80401

U.S. Department of Energy
Attn: James Powell
Atlanta Support Office
730 Peachtree Street, NE, Suite 876
Atlanta, GA 30308

U.S. Department of Energy
Attn: D.A. Sanchez
Albuquerque Operations Office
P.O. Box 5400
Albuquerque, NM 87115

U.S. Department of Energy
Attn: Denise Swink
1000 Independence Avenue, SW
Washington, DC 20585

U.S. Department of Energy
Attn: Frank (Tex) Wilkins
Office of Industrial Technologies
Forrestal Building, MS EE-222, Room 5F-035
1000 Independence Avenue, SW
Washington, DC 20585

U.S. Environmental Protection Agency
Attn: Cindy Jacobs
401 M Street, SW
GCD 6202J
Washington, DC 20460

UC Operating Services
Attn: Jan Hansen
43880 Harper Lake Road
Hinkley, CA 92347

Union of Concerned Scientists
Attn: Donald Aitken
20100 Skyline Boulevard
Woodside, CA 94062

University of Arizona
Attn: George V. Mignon
Environmental Research Lab
Tucson, AZ 85706-6985

University of Central Florida
Attn: Gerard G. Ventre
Institute for Simulation and Training
12424 Research Parkway
Suite 300
Orlando, FL 32826

University of Chicago
Attn: Joe O'Gallagher
Enrico Fermi Institute
5640 Ellis Avenue
Chicago, IL 60637

University of Colorado at Boulder
Attn: Jan F. Kreider, P.E.
Dept. of Civil, Environ. & Arch. Engr.
Boulder, CO 80309

University of Houston
Attn: Lorin Vant-Hull
Physics Department 5506
4800 Calhoun Road
Houston, TX 77204-5506

University of Minnesota
Attn: E.A. Fletcher
1111 Church Street, SE
Dept. of Mech. Engr.
Minneapolis, MN 55455

University of Nevada at Las Vegas
Attn: Bob Boehm
Dept. of Mech. Engr.
4505 Maryland Parkway
P.O. Box 454027
Las Vegas, NV 89154-4027

University of New Mexico
Attn: M.W. Wildin
Dept. of Mech. Engr.
Albuquerque, NM 87131

Utah Dept. of Community & Economic Development
Attn: Michael Glenn
Office of Energy Services
Division of Comminity Development
324 South State Street, Suite 230
Salt Lake City, UT 84111

Vermont Dept. of Public Service
Attn: Scudder H. Parker
Energy Efficiency Division
120 State Street
Montpelier, VT 05602

Virgin Islands Energy Office
Attn: Claudette Young-Hinds
Old Customs House
Frederiksted
St. Croix, 00840 U.S. VIRGIN ISLANDS

Virginia Polytechnic Institute and State University
Attn: Saifur Rahman, Ph.D.
Dept. of Elec. Engr.
Blacksburg, VA 24061

Virginia Power Co.
Attn: Tim Bernadowski
Corp. Tech. Assess.
5000 Dominion Blvd.
Glen Allen, VA 23060

Wall Street Journal
Attn: David Stipp
10 Post Office Square
Suite 715
Boston, MA 02109

Weizmann Institute of Science
Attn: Michael Epstein
P.O. Box 26
IS-76100 Rehovot, ISRAEL

Weizmann Institute of Science
Attn: Doron Lieberman
P.O. Box 26
Rehovot, 76100 ISRAEL

Wyoming Energy Office
Attn: John F. Nunley, III
Barrett Building
4th Floor North
Dept. of Commerce
Cheyenne, WY 82002

Zentrum fur Sonnenenergie-und Wasserstoff-Forschung
Attn: Frank Lippke
P.O. Box 80 11 49
D-70511
Stuttgart, GERMANY

Zentrum fur Sonnenenergie-und Wasserstoff-Forschung
Attn: Jurgen Rheinlander
Hessbruhlstrasse 21 C
Postfach 80 11 49
D-70511 Stuttgart, GERMANY

Internal Distribution:

MS 0100	Document Proc. for DOE/OSTI, 7613-2 (2)
MS 0619	Technical Publications, 12613
MS 0702	D.E. Arvizu, 6200
MS 0703	J.R. Anderson, 6216
MS 0703	C.E. Andraka, 6216
MS 0703	R.B. Diver, 6216
MS 0703	D.R. Gallup, 6216
MS 0703	G.J. Kolb, 6216 (5)
MS 0703	T.R. Mancini, 6216
MS 0703	D.F. Menicucci, 6216 (15)
MS 0703	J.B. Moreno, 6216
MS 0703	T.A. Moss, 6216
MS 0703	J.E. Pacheco, 6216
MS 0703	M.R. Prairie, 6216
MS 0703	T.O. Reynolds, 6216
MS 0703	C.E. Tyner, 6216
MS 0704	C.J. Hanley, 6201
MS 0704	P.C. Klimas, 6201
MS 0704	E.H. Richards, 6201
MS 0752	M.L. Tatro, 6219
MS 0753	C.P. Cameron, 6218
MS 0753	H.N. Post, 6218
MS 0899	Technical Library, 13414 (5)
MS 1127	J.M. Chavez, 6215
MS 1127	V.E. Dudley, 6215 (5)
MS 1127	Library, 6215 (5)
MS 1127	A.R. Mahoney, 6215
MS 1127	E.E. Rush, 6215
MS 1127	J.W. Strachan, 6215
MS 9014	S. Faas, 5371
MS 9018	Central Technical Files, 8523-2
MS 9402	S. Goods, 8714
MS 9404	B. Bradshaw, 8716

• U.S. GOVERNMENT PRINTING OFFICE 1996-774-030/20015